

# **The Propulsive Small Expendable Deployer System (ProSEDS)**

**NASA Grant NAG8-1605**

## **Annual Report #2**

**For the period 1 August 2000 through 31 July 2001**

**Principal Investigator**

**Enrico C. Lorenzini**

**July 2001**

**Prepared for**

**National Aeronautics and Space Administration**

**Marshall Space Flight Center, Alabama 35812**

**Smithsonian Institution**

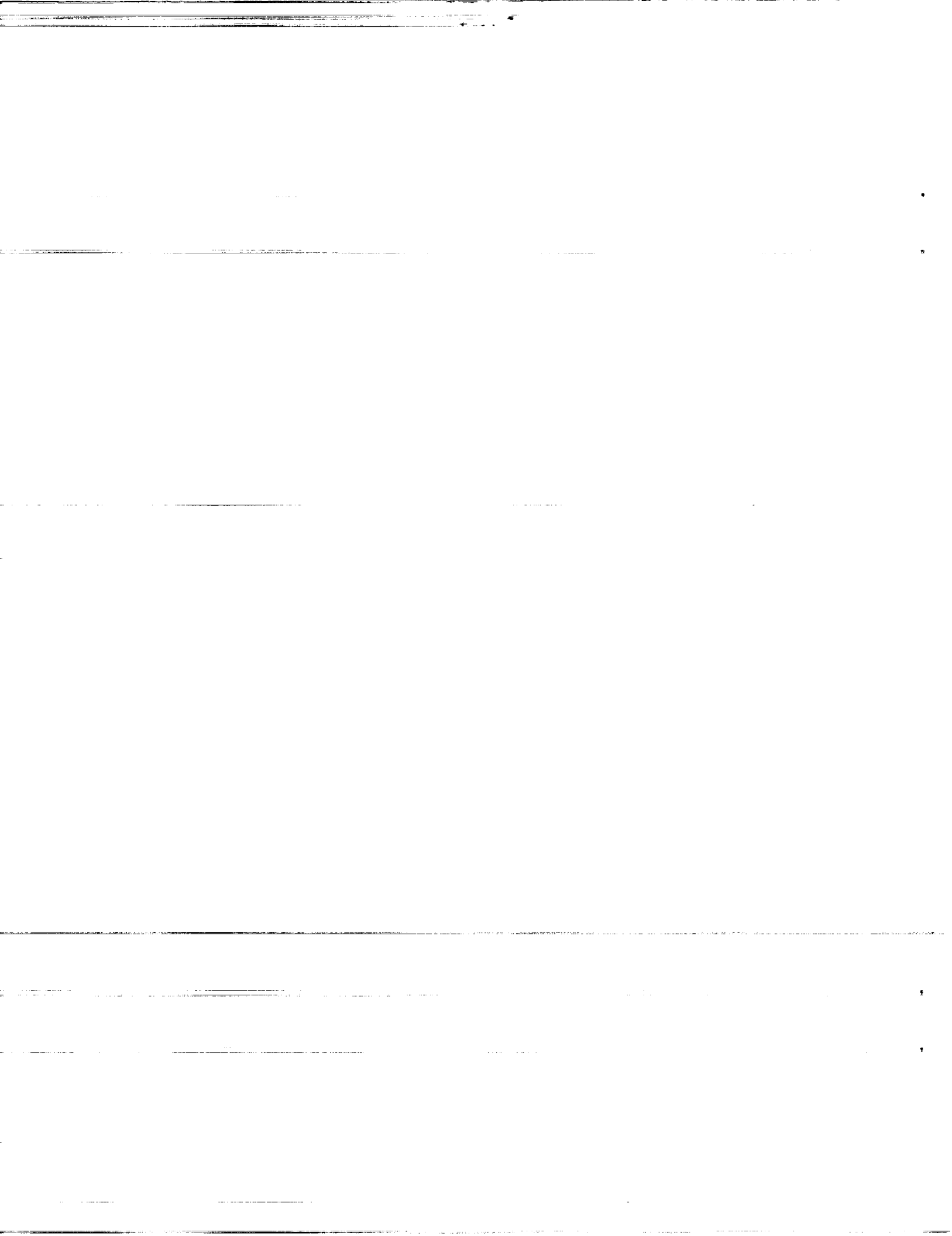
**Astrophysical Observatory**

**Cambridge, Massachusetts 02138**

**The Smithsonian Astrophysical Observatory**

**is a member of the**

**Harvard-Smithsonian Center for Astrophysics**



## **The Propulsive Small Expendable Deployer System (ProSEDS)**

NASA Grant NAG8-1605

### **Annual Report #2**

For the period 1 August 2000 through 31 July 2001

#### Principal Investigator

Enrico C. Lorenzini

#### Co-Investigators

Robert D. Estes

Mario L. Cosmo

#### Collaborators

Juan Sanmartin

Jesus Peláez

July 2001

Prepared for

National Aeronautics and Space Administration  
Marshall Space Flight Center, Alabama 35812

Smithsonian Institution  
Astrophysical Observatory  
Cambridge, Massachusetts 02138

The Smithsonian Astrophysical Observatory  
is a member of the  
Harvard-Smithsonian Center for Astrophysics

## TABLE OF CONTENTS

<b>LIST OF FIGURES.....</b>	<b>4</b>
<b>LIST OF TABLES .....</b>	<b>6</b>
<b>SCOPE.....</b>	<b>7</b>
<b>SUMMARY .....</b>	<b>8</b>
<b>1. UPDATED SYSTEM PERFORMANCE.....</b>	<b>9</b>
1.1 INTRODUCTION.....	9
1.2 UPDATED VALUES OF DECAY RATES.....	10
<b>2. MISSION ANALYSIS.....</b>	<b>12</b>
2.1 EFFECTS OF A LOWER ORBIT.....	12
2.1 ATOMIC OXYGEN TETHER EROSION.....	14
<b>3. DYNAMIC REFERENCE MISSION.....</b>	<b>17</b>
3.1 REFERENCE MISSION SIMULATION.....	17
3.1 EXTREME CASES.....	26
3.4 CONCLUDING REMARKS.....	29
<b>4. UPDATED DEPLOYMENT CONTROL PROFILES AND SIMULATIONS.....</b>	<b>30</b>
4.1 INTRODUCTION.....	30
4.2 FRICTION PARAMETERS .....	31
4.3 CONTROL PARAMETERS.....	33
4.4 REFERENCE TABLES.....	34
4.5 VALIDATION PROCESS.....	43
4.4 CONCLUDING REMARKS.....	70
<b>5. KALMAN FILTERS FOR MISSION ESTIMATION.....</b>	<b>71</b>
5.1 INTRODUCTION.....	71
5.2 MAGNETOMETER DATA KALMAN FILTER.....	71
5.3 POSITION/CURRENT DATA KALMAN FILTER.....	75
<b>6. COMPARISON OF ED TETHERS AND ELECTRICAL THRUSTERS.....</b>	<b>78</b>
6.1 INTRODUCTION.....	78
6.2 COMPARISONS.....	79
6.3 CONCLUSIONS.....	81
<b>7. DELIVERY OF INTERACTIVE SOFTWARE FOR ED TETHERS.....</b>	<b>82</b>
7.1 DELIVERED SOFTWARE.....	82
7.2 BRIEF DESCRIPTION .....	82
<b>APPENDIX A.....</b>	<b>85</b>
<b>REFERENCES.....</b>	<b>101</b>

## LIST OF FIGURES

Figure 1 Schematic of ProSEDS on Delta 2 <sup>nd</sup> stage.....	9
Figure 2 13-month smoothed F10.7 radio flux [from MSAFE NASA/MSFC].....	10
Figure 3 Decay rates of ProSEDS for various altitude and operational scenarios with a launch in August 2001 .....	13
Figure 4 Ratio of average electro/aero forces vs. altitude .....	14
Figure 5 Atomic oxygen density (number-of-atoms/m <sup>3</sup> ) vs. mission time for nominal atmospheric conditions.....	15
Figure 6 AO mass flux integrated over mission time (start altitude = 400 km).....	15
Figure 7 Ground trace of preliminary Delta 7925 Block IIR trajectory [adapted from The Boeing Company] .....	20
Figure 8 Results for day-launch with launch date on 16 August 2001. ....	21
Figure 9 Results for day-launch with launch date on 16 August 2001. ....	22
Figure 10 Results for day-launch with launch date on 16 August 2001.....	23
Figure 11 Results for day-launch with launch date on 16 August 2001.....	24
Figure 12 Results for day-launch with launch date on 16 August 2001.....	25
Figure 13 System decay and geographic position (latitude and longitude) for double the nominal plasma density on 16 August 2001.....	27
Figure 14 System decay and geographic position (latitude and longitude) without any electrodynamic forces for a launch on 16 August 2001.....	28
Figure 15 Reference profile Ref#47 (without slow down maneuver).....	36
Figure 16 Reference profile Ref#55 (without slow down maneuver) .....	37
Figure 17 Deployment dynamics for Ref#55 for $T_0 = 0$ mN .....	39
Figure 18 Deployment dynamics for Ref#55 for $T_0 = 10$ mN (nominal).....	40
Figure 19 Deployment dynamics for Ref#55 for $T_0 = 20$ mN.....	41
Figure 20 Final libration amplitude vs. $T_0$ for selected deployment profiles.....	42
Figure 21 Nominal minimum tension $T_0 = 10$ mN.....	44
Figure 22 Nominal minimum tension $T_0 = 10$ mN (MASTER vs. DUMBELL).....	45
Figure 23 Nominal minimum tension $T_0 = 10$ mN.....	46
Figure 24 Nominal minimum tension $T_0 = 10$ mN.....	47
Figure 25 Nominal minimum tension $T_0 = 10$ mN .....	48
Figure 26 Nominal minimum tension $T_0 = 10$ mN .....	49
Figure 27 Nominal minimum tension $T_0 = 10$ mN .....	50
Figure 28 Minimum tension $T_0 = 5$ mN (MASTER vs. DUMBELL).....	51

Figure 29 Minimum tension $T_0 = 5$ mN.....	52
Figure 30 Minimum tension $T_0 = 5$ mN.....	53
Figure 31 Minimum tension $T_0 = 20$ mN.....	54
Figure 32 Minimum tension $T_0 = 20$ mN (MASTER vs. DUMBELL) .....	55
Figure 33 Minimum tension $T_0 = 20$ mN.....	56
Figure 34 Minimum tension $T_0 = 20$ mN.....	57
Figure 35 No brake is activated throughout deployment.....	58
Figure 36 No brake is activated throughout deployment.....	59
Figure 37 Wire inertia multiplier = 2.5.....	61
Figure 38 Wire inertia multiplier = 2.5.....	62
Figure 39 Wire inertia multiplier = 2.5.....	63
Figure 40 Wire inertia multiplier = 2.5.....	64
Figure 41 Wire inertia multiplier = 2.5.....	65
Figure 42 Wire inertia multiplier = 3.5.....	66
Figure 43 Wire inertia multiplier = 3.5.....	67
Figure 44 Wire inertia multiplier = 3.5.....	68
Figure 45 Wire inertia multiplier = 3.5.....	69
Figure 46 Wire inertia multiplier = 3.5.....	70
Figure 47 Estimated Bias Components (SEDS-1 Flight Data) .....	73
Figure 48 Magnetometer Y Component - Estimated vs. Measured (SEDS-I Flight Data) .	74
Figure 49 Estimated vs. Actual Proseds Semi-major Axis (MASTER simulation) .....	76
Figure 50 Estimated Average vs. Current Measured at Delta (MASTER simulation) .....	76
Figure 51 Estimated Proseds EMF (MASTER simulation).....	77
Figure 52 Comparison of EDT (a, b) and Electrical Thrusters (c, d) With Dedicated Solar Power System.....	79
Figure 53 Comparison of EDT (a, b) and Electrical Thrusters (c, d) Without Dedicated Solar Power System.....	80
Figure 54 The simulation setup window for defining the system. ....	83
Figure 55 Starting orbit setup window with boost system setup in background. ....	84

## LIST OF TABLES

Table 1 Decay rates for different launch dates .....	11
Table 2 ProSEDS position errors after 24 hours .....	26
Table 3 Characteristics of selected reference profiles .....	38

## SCOPE

This is the Annual Report #2 for Grant NAG8-1605 entitled "The Propulsive Small Expendable Deployer System (ProSEDS)" prepared by the Smithsonian Astrophysical Observatory for NASA Marshall Space Flight Center. The technical officer for this grant is Randy Baggett; the Program Manager for the ProSEDS project is Leslie Curtis. This report covers the period of activity from 1 August 2000 through 30 July 2001.

## SUMMARY

This Annual Report covers the following main topics:

### *1. Updated System Performance*

Comparative analysis of the decay rate expected for ProSEDS for various launch dates.

### *2. Mission Analysis*

Analysis to define the effect of a lower orbital altitude on the environmental forces acting on ProSEDS. Evaluation of the altitude at which the atomic oxygen is expected to damage the Dyneema tether.

### *3. Updated Dynamics Reference Mission*

The reference ProSEDS mission is evaluated for the updated launch date. Simulations are run for nominal solar activity condition at the time of launch. Simulations include the dynamics of the system, the electrodynamics of the bare tether, the neutral atmosphere and the thermal response of the tether.

### *4. Updated Deployment Control Profiles and Simulations*

Selected deployment profiles are compared in terms of their deployment performance. The flight profile is derived based on the latest friction characteristics obtained from deployment tests.

### *5. Comparison of ED tethers and electrical thrusters*

A comparison between electrical thrusters and electrodynamic bare tethers which takes into account the energy conversion efficiency and the mass of the hardware involved.

### *6. Kalman filters for mission estimation*

Development of two Kalman filters for estimation of position from GPS data and attitude from magnetometer data.

### *7. Delivery of interactive software for ED tethers*

The features of the software delivered to NASA are briefly described.

## 1. UPDATED SYSTEM PERFORMANCE

### 1.1 Introduction

The Propulsive Small Expendable Deployment System (ProSEDS) will carry out a demonstration of a bare electrodynamic tether for propulsion. ProSEDS will fly as a secondary payload on a Delta II stage. The electrodynamic system will be deployed from the stage (see Fig. 1). The electrodynamic forces generated by the current flowing in the conductive tether are expected to strongly increase the decay rate of the Delta stage. The reader should consult references<sup>1 2 3 4 5</sup> for a more detailed description of ProSEDS and the principles of operation of bare-tether anodes.

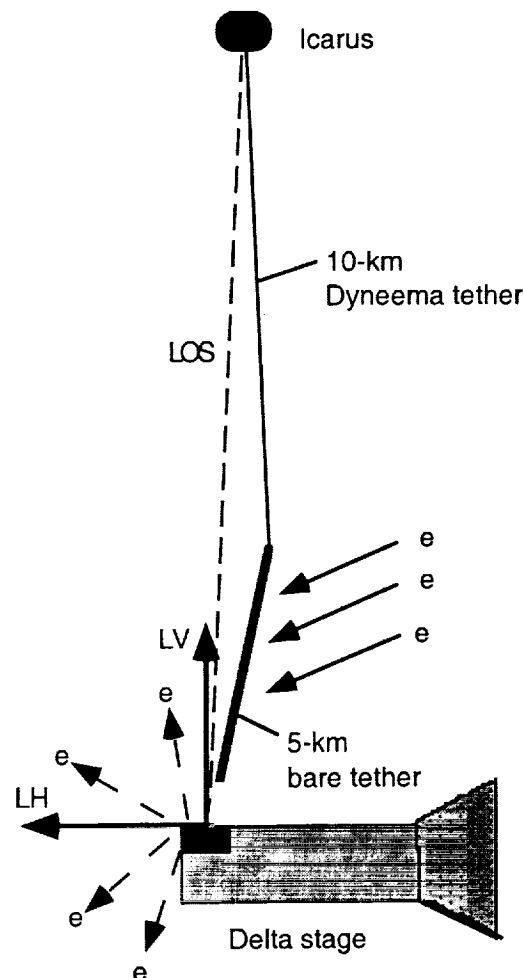


**Figure 1** Schematic of ProSEDS on Delta 2<sup>nd</sup> stage

The performance of ProSEDS will be assessed on the basis of the decay rate of the Delta stage which is affected mostly by the plasma conditions at the time of launch. The launch date of ProSEDS has changed with respect to the performance analysis carried out in the Annual Report #1 for this grant. For this reason it is important to update the analysis and to compare those results.

## 1.2 Updated Values of Decay Rates

We are presently in the solar cycle 23 during which the solar activity peaked in April-June 2000. Consequently, the solar activity and the plasma density (that is a function of the solar activity) will likely decrease over the next few years (see Fig. 2).

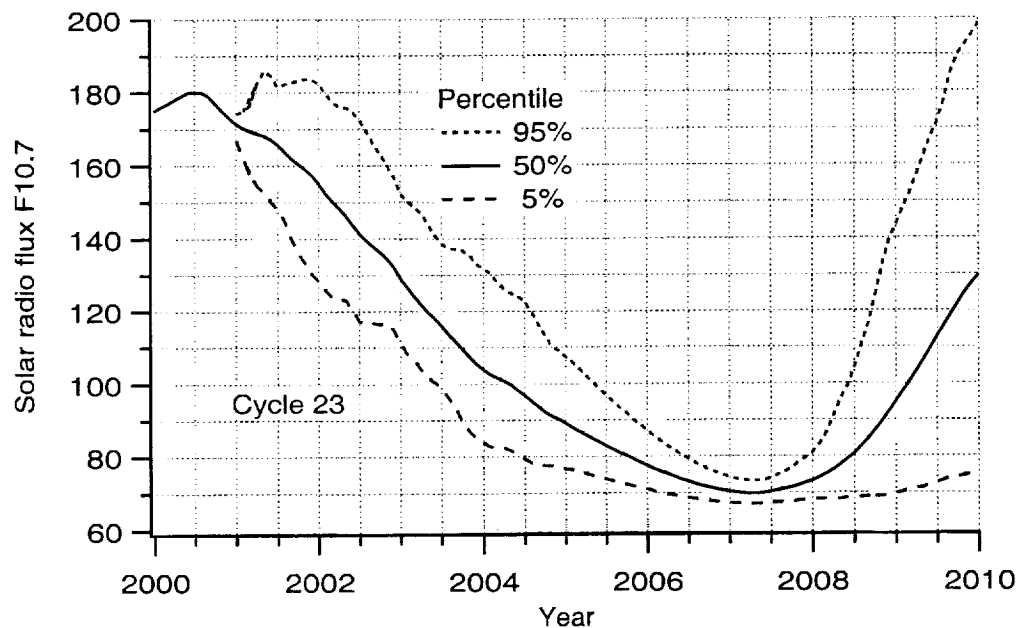


**Figure 2** 13-month smoothed F10.7 radio flux [from MSAFE NASA/MSFC]

In other words, we should expect that a mission launched in August 2001 or later will exhibit a slower decay rate than a mission launched in August 2000. The later the mission will take place during the next few years, the slower the decay rate because of the reduced plasma density.

We have produced an updated reference mission for nominal (50% percentile) solar activity and according to the updated mission sequence with 7 orbits (instead of the previous 3) operating under the primary operating cycle. The goal of this analysis is to

estimate the orbital decay rate during the first day (primary mission phase) and the first week (extended mission phase). The launch time (not yet known) influences the position of the plasma field with respect to the magnetic field and, hence, affects the decay rate because of the phase of the maxima of the magnetic field with respect to the maxima of the plasma density. If we consider two mission start times, one close to local noon and after to midnight, the difference in decay rates is less than 10% in favor of the night launch.

**Table 1** Decay rates for different launch dates

Launch date	Orbit (kmxkm)	1 <sup>st</sup> day decay rate (km/day)	1 <sup>st</sup> week decay rate (km/day)
April 2000 <sup>o</sup>	400x400	12.5 <sup>*</sup>	14.3
August 2000 <sup>#</sup>	400x400	10.6 <sup>*</sup>	12.0
August 2001 <sup>#</sup>	400x400	9.4	11.8

\* The primary cycle was limited to 3 orbits in 2000 as opposed to 7 in 2001 resulting in a first-day decay rate which is closer to the weekly decay rate than in the 2001 scenario

<sup>o</sup> night launch

<sup>#</sup> day launch

The main measure of ProSEDS success will be the decay rate of the Delta stage which is increased by more than an order of magnitude with respect to the Delta stage natural decay. The success criteria for ProSEDS specify a decay rate of at least 5 km/day. Assuming the worst possible condition that ProSEDS will operate only for the primary mission phase of 1 day, it is clear from Table 1 that the margin on the success criteria (now slightly less than two) is decreasing and it will decrease a bit more if the launch is postponed further<sup>&</sup>.

---

<sup>&</sup> At the time of writing of this report, ProSEDS launch date has been moved to June 2002. The mission profile and decay rate for this new launch date have not been analyzed yet.

## 2. MISSION ANALYSIS

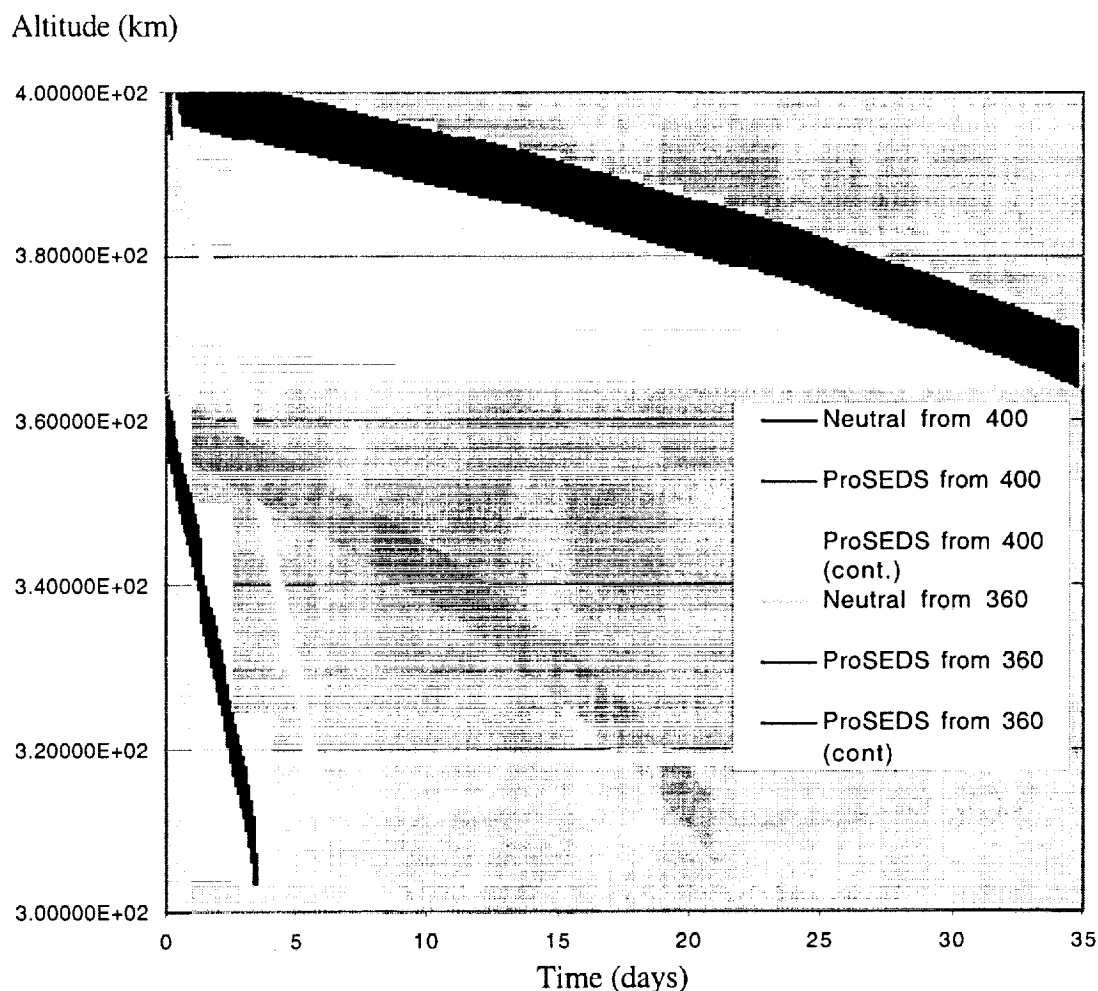
### 2.1 Effects of a lower orbit

Another issue that is essential for the success of ProSEDS is that the decay rate must be dominated by the electrodynamic forces rather than the drag due to the neutral density. In other words, the ratio of the electrodynamic forces over the atmospheric forces must be large. One related problem is, however, the determination of the (neutral) drag area of ProSEDS. We have to consider that the Delta stage is not 3-axis stabilized and the 10-km-long, non-conductive tether is flat and likely randomly twisted. The 5-km-long conductive tether is cylindrical and, consequently, unaffected by the twist.

The Delta stage will be hanging from the tether with a torque equilibrium angle (TEA) of about  $35^\circ$ . The stage will be fairly close to the local vertical and rotating about the tether axis, that is, its drag area will be  $A_{\text{Delta}} = A_{\text{max}} \cos(\text{TEA})$  where  $A_{\text{max}}$  is the lateral drag area of the Delta. For  $A_{\text{max}} \approx 12 \text{ m}^2$  and  $\text{TEA} = 35^\circ$ ,  $A_{\text{Delta}} \approx 10 \text{ m}^2$ . However, later during the mission the Delta stage develops large attitude oscillation and its effective drag area can not be estimated accurately.

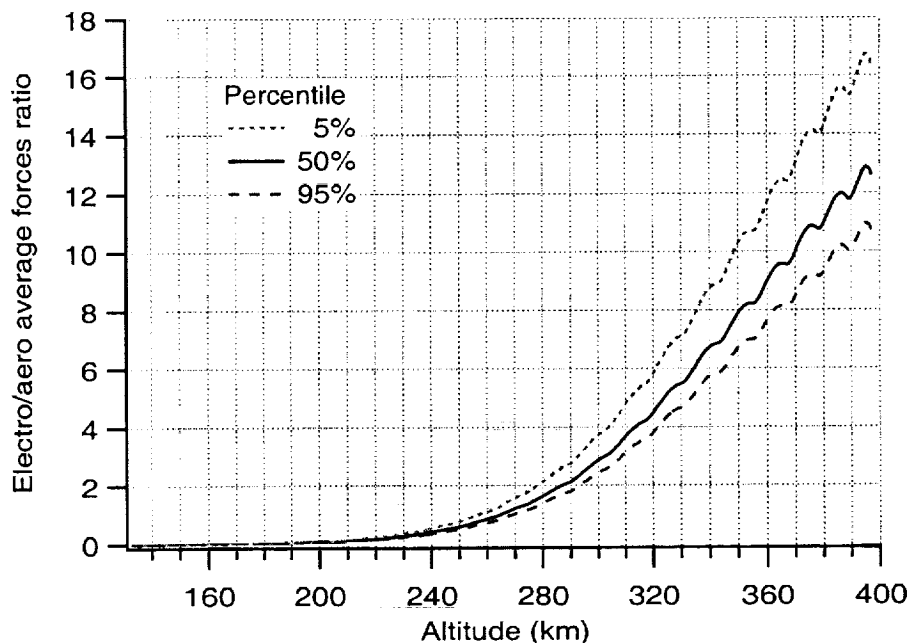
The flat tether has a close to rectangular cross section of  $0.2\text{mm} \times 1.2\text{mm}$ . If we assume that the tether will have many twists so that its orientation with respect to the ram follows an 'ABS(cosine)' law we can estimate the drag area as  $A_{\text{ncTether}} = (2/\pi) \times W \times L$  where  $W$  and  $L$  are the width and length of the non-conductive tether. For  $L = 10 \text{ km}$  and  $W = 1.2 \text{ mm}$ ,  $A_{\text{ncTether}} \approx 7.7 \text{ m}^2$ . Finally, after adding the cross section of the  $1.2\text{mm} \times 5\text{km}$  conductive tether, we obtain  $A_{\text{Drag}} \approx 23.7 \text{ m}^2$  for the total drag area of the system.

Figure 3 shows estimated deorbit rates for ProSEDS assuming nominal operating cycle starting from 400 km and 360 km compared with those from neutral drag on ProSEDS system with no current. Neutral drag is included in all cases. Actual ProSEDS deorbit rate would likely be greater than what is shown due to extended periods of battery charging. Simulations assume OML current collection and constant 220 ohm resistance for tether. A satellite without a tether would deorbit more slowly than a tethered system without current.



**Figure 3** Decay rates of ProSEDS for various altitude and operational scenarios with a launch in August 2001

The ratio of electrodynamic forces to atmospheric (i.e., neutral density) drag forces was estimated by computing the orbit-average magnitude of those forces acting on ProSEDS at various altitudes for a launch in August 2001. An error band on the ratio between electrodynamic and neutral drag forces was also computed based on estimates of the variability of the plasma and neutral densities for 5 and 95 percentile probabilities as shown in Fig. 4.



**Figure 4** Ratio of average electro/aero forces vs. altitude

In summary, the electrodynamic forces overpower the neutral drag forces under nominal conditions (at 50% percentile probability) by a factor of 13 at 400-km of altitude and a factor of 9 at 360 km of altitude. Under the most conservative conditions (at 95% percentile probability), the ratio of the two forces is approximately equal to 11 and 8 at 400 km and 360 km of altitude, respectively.

## 2.1 Atomic Oxygen Tether Erosion

The lifetime of the ProSEDS tether is affected by two major factors: (1) micrometeoroids and orbital debris (M/OD) impacts and (2) erosion by atomic oxygen (AO). It was computed by NASA/MSFC that the tether of ProSEDS has about a 82% probability of surviving M/OD hits over a period of 14 days<sup>6</sup>. Conversely, the probability of a fatal hit over 14 days is about 18%

The rate of erosion of the Dyneema by AO is more deterministic than the M/OD impact risk. This rate can be computed by integrating the flux of AO impinging on the tether over the altitude profile during the orbital decay. The AO density is derived from the MSIS'86 atmospheric model that is part of the SAO tether dynamic simulator. The critical value of the integrated AO mass flux that makes the tether fails depends on the tether design and internal structure.

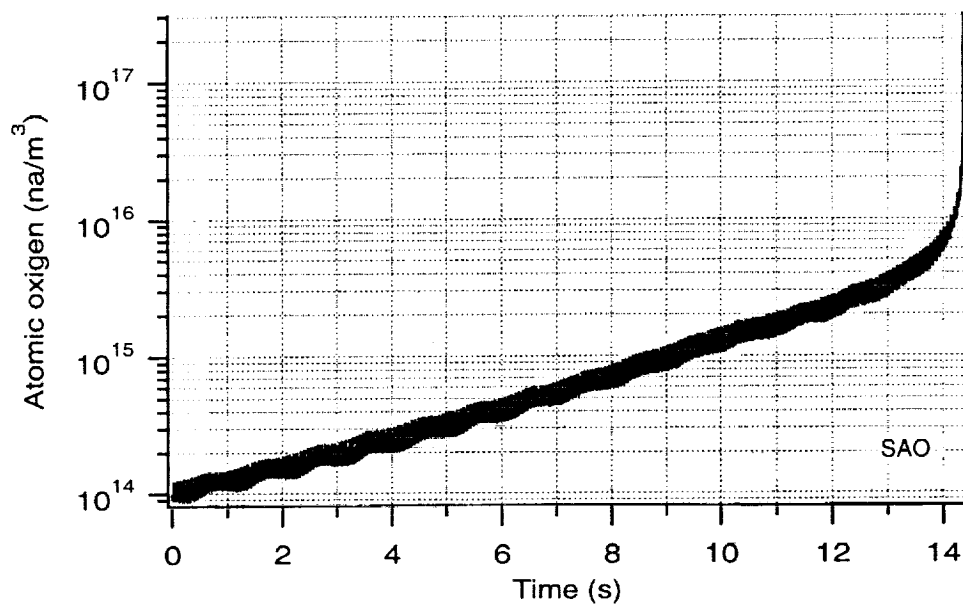


**Figure 5** Atomic oxygen density (number-of-atoms/m<sup>3</sup>) vs. mission time for nominal atmospheric conditions.

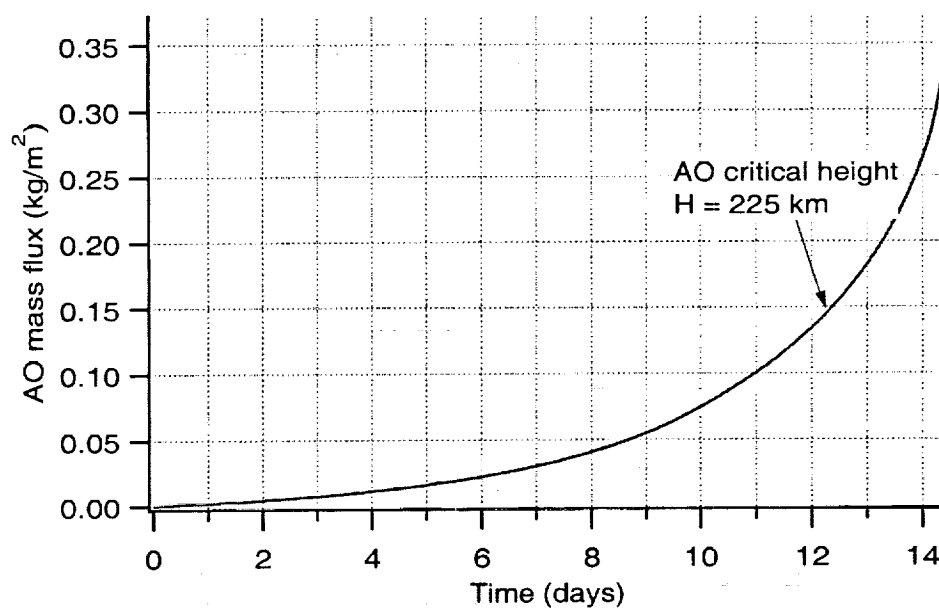


**Figure 6** AO mass flux integrated over mission time (start altitude = 400 km)

For a flat braided tether like ProSEDS, it is reasonable to assume that the tether fails once the AO has chewed away a layer of tether as thick as the fibers that constitute the braided tether. With this assumption, the critical value of the integrated AO mass flux is =

0.15 kg/m<sup>2</sup>. Figure 5 shows the AO density which increases as the orbit of ProSEDS moves lower. Figure 6 shows the AO mass flux (vs. time) integrated over the trajectory spanned by ProSEDS.

If we assume nominal atmospheric density conditions (at 50% probability), a launch date in August 2001 and a starting altitude of 400 km, the critical altitude where the Dyneema tether fails due to AO is equal to 225 km, which occurs (for simulated conditions) after about 12 days from the mission start.

### 3. DYNAMIC REFERENCE MISSION

#### 3.1 Reference Mission Simulation

The orbital and system parameters for the reference mission are as follows:

Orbit: 400 km circular

Inclination: 36 deg

Launch date: 16 August 2001

Ascending node for: (a) day launch at about 10:00AM EST and (b) night launch at about 10:00PM EST

Ionosphere/Atmosphere: nominal (50 percentile) solar activity at time of launch

Delta mass: 994 kg

Endmass: 21.4 kg

Tether linear densities: 0.15 kg/km (Dyneema); 2 kg/km (wire).

Tether optical properties:

Dyneema -  $\alpha_s = 0.1$ ,  $\epsilon_{IR} = 0.5$ ;

C-COR coated wire -  $\alpha_s = 0.9$ ,  $\epsilon_{IR} = 0.8$ .

Tether mechanical properties:  $EA = 15,000$  N;  $E'A \approx 2000$  Ns.

Tether electrical resistance: 265 ohm at 20 °C.

Operating modes<sup>7</sup>: 7 orbits according to the primary mode and the remainder according to the secondary mode. The first operating cycle starts approximately when the Delta stage crosses the Atlantic coast of South America (see Fig. 7).

The time of launch affects the phasing between the magnetic field (corotating with the Earth) and the plasma field which is mostly driven by the position of the Sun. Because the time of launch is not yet known for the Delta rocket, simulation have been run for a day

launch which sets the deployment of ProSEDS close to midday EST and a night launch which sets the deployment close to midnight EST. The ground trace of the orbit is unaffected by the time of launch. The preliminary trajectory ground trace (computed by The Boeing Company) is shown in Fig. 7.

The results of the day-launch simulation August 2001 are shown in Figs. 6-9 over the extended mission duration of over 2 weeks. The system response (not show here) for a night launch is similar to the day launch with the notable difference of a 6% increase in the decay rate and average current with respect to the day-launch case.

The main conclusions from the analysis of the reference mission are as follows:

The decay rate during the first day (primary mission) is about 9.4 km/day and 10 km/day for the day and night launches, respectively. These values exceed the minimum value of 5 km/day established as a success criteria for ProSEDS but the margin for errors has been reduced substantially with respect to the cases with a launch in August 2000.

The orbit-average current produced by the tether and the decay rates are as follows:

*Day launch:*

Orbit-average current = 0.8 Amp (over entire current cycle)

Orbit-average current = 1.5 Amp (during battery charging)

1<sup>st</sup> day decay rate = 9.4 km/day

1<sup>st</sup> week decay rate = 11.8 km/day

*Night launch*

Orbit-average current = 0.85 Amp (over entire current cycle)

Orbit-average current = 1.6 Amp (during battery charging)

1<sup>st</sup> day decay rate = 10 km/day

1<sup>st</sup> week decay rate = 12.4 km/day

The minimum and maximum tether temperatures for the Spectra tether and the C-COR wire are:

Spectra: from  $-90^{\circ}\text{C}$  to  $-45^{\circ}\text{C}$ ;

C-COR: from  $-86^{\circ}\text{C}$  to  $+53^{\circ}\text{C}$ .

The tether temperatures are within the allowable limits for the two tether types.

The system dynamics is stable and rather well-behaved over the extended mission lifetime of over two weeks. Because of the relatively low ratio of absorptivity/emissivity ( $\alpha/\epsilon \approx 1.1$ ) provided by the latest formulation of C-COR, the wire temperature is rather low as it ranges from  $-86^{\circ}\text{C}$  to  $+53^{\circ}\text{C}$ . Consequently, the electrical resistance of the wire ranges from 150 ohm to 300 ohm.

It is worth reminding that a purely-bare aluminum tether would have an  $\alpha/\epsilon \approx 8$  which would reduce the decay rate by approximately 40%. A purely-bare copper wire of the same resistance would fare even more poorly.

( ESTAR Min. for T/M Sites = 2.00 deg )

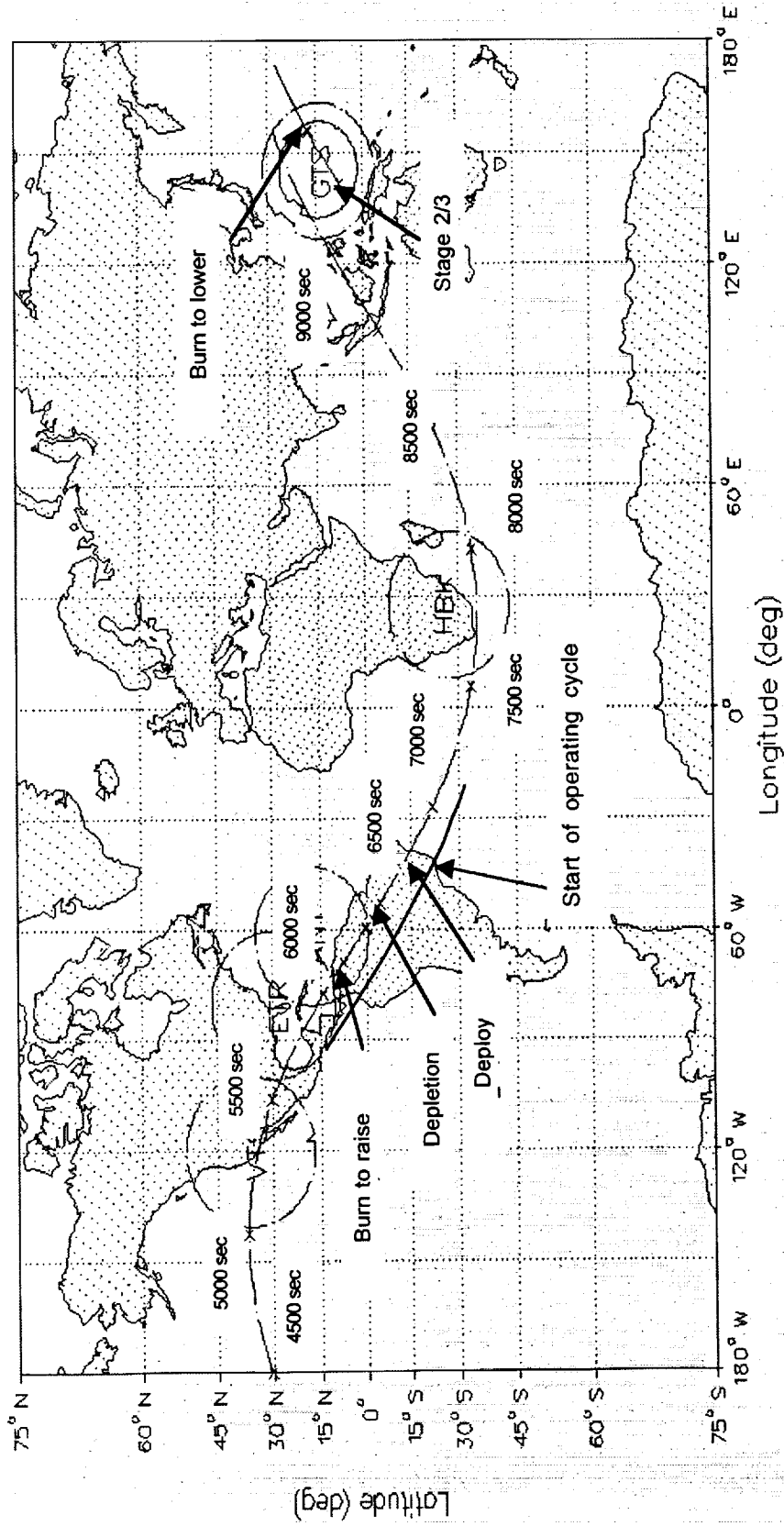


**Figure 7** Ground trace of preliminary Delta 7925 Block IIR trajectory [adapted from The Boeing Company]

ProSEDS 265 ohm@20 C, 400x400km, nom. solar, day launch, Antigua burn, 16 August 2001

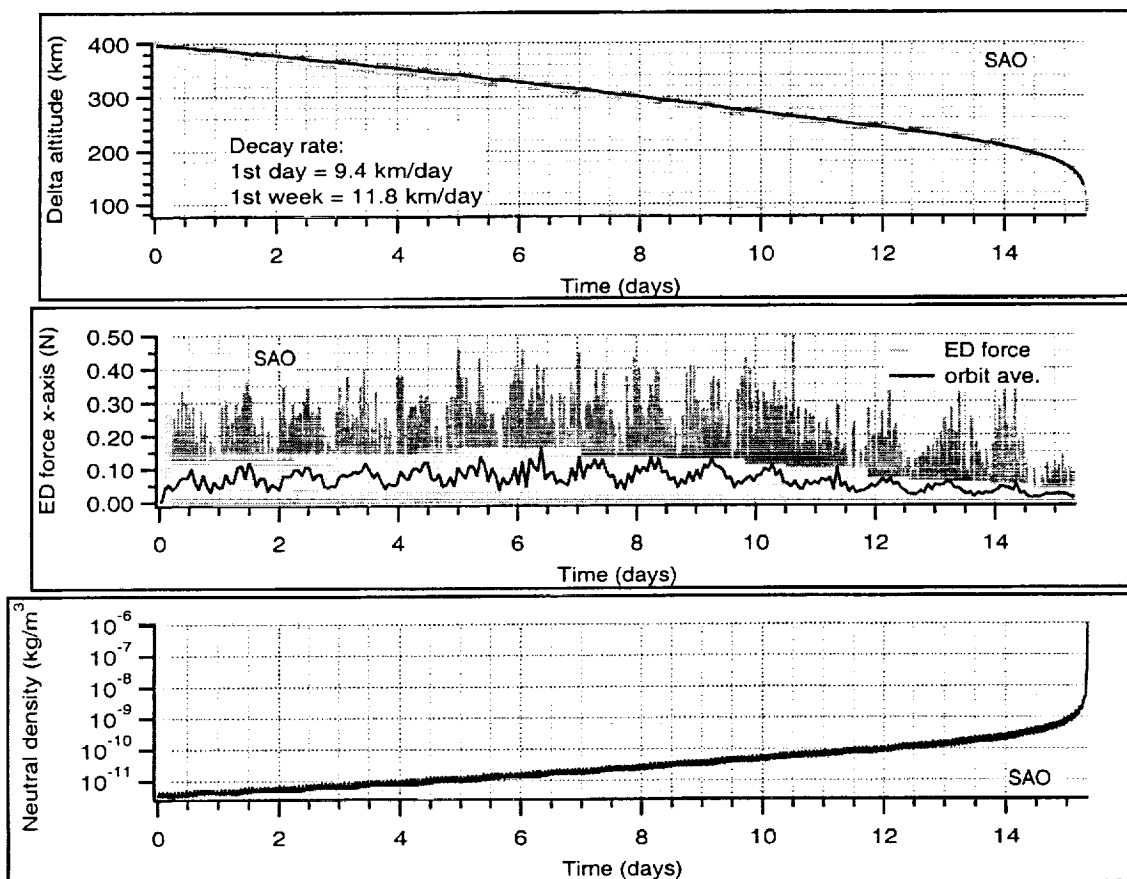


**Figure 8** Results for day-launch with launch date on 16 August 2001.

ProSEDS 265 ohm@20 C, 400x400km, nom. solar, day launch, Antigua burn, 16 August 2001

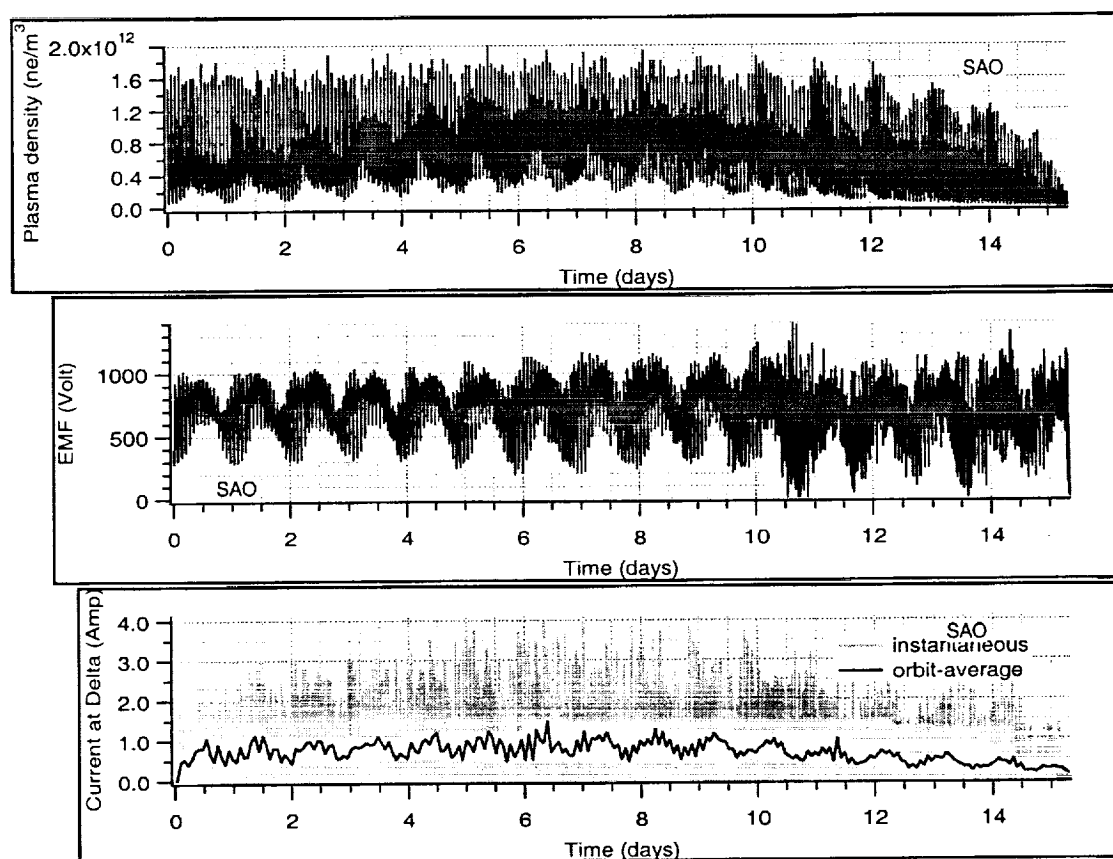


**Figure 9** Results for day-launch with launch date on 16 August 2001.

ProSEDS 265 ohm@20 C, 400x400km, nom. solar, day launch, Antigua burn, 16 August 2001

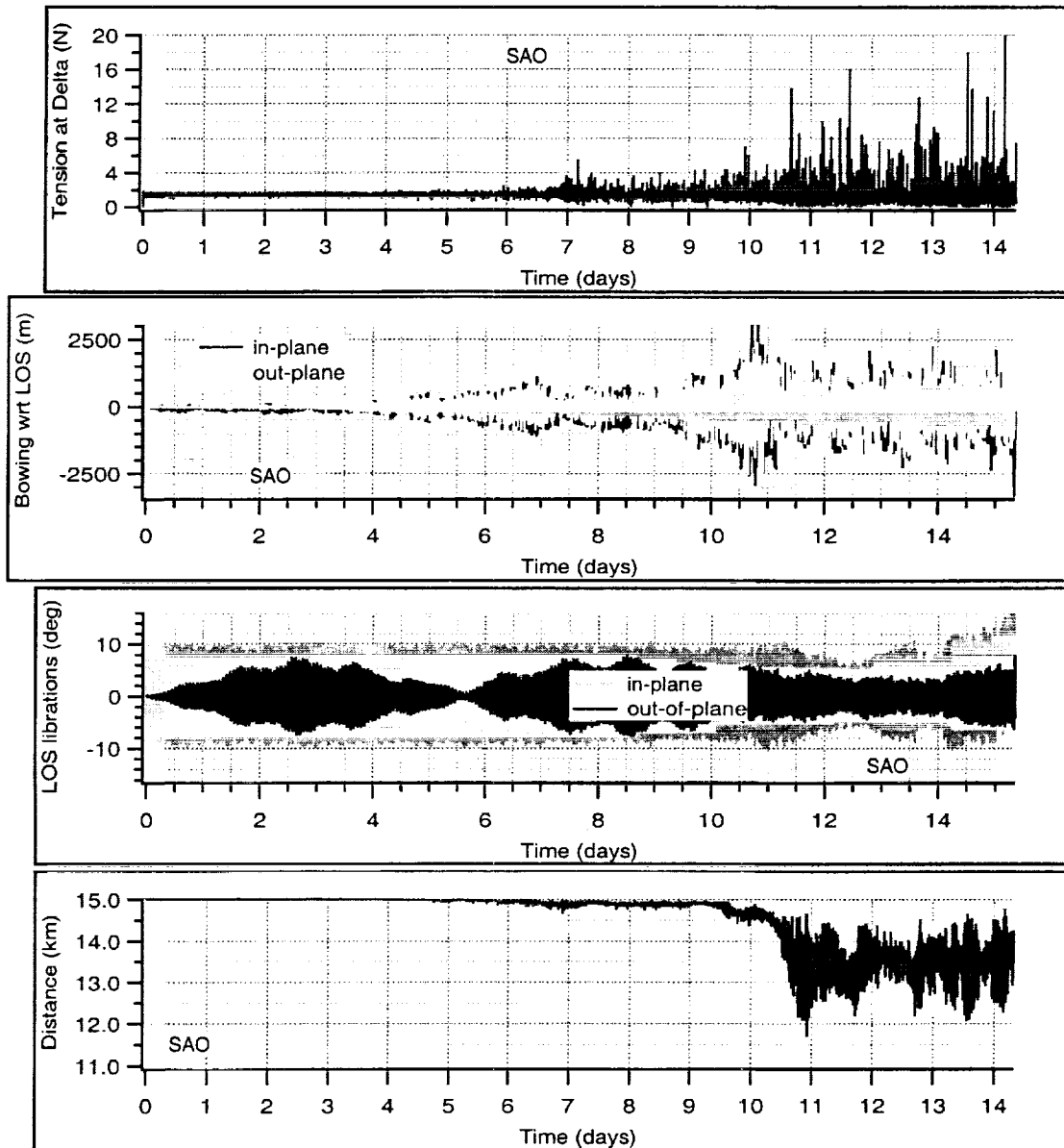


**Figure 10** Results for day-launch with launch date on 16 August 2001

ProSEDS 265 ohm@20 C, 400x400km, nom. solar, day launch, Antigua burn, 16 August 2001

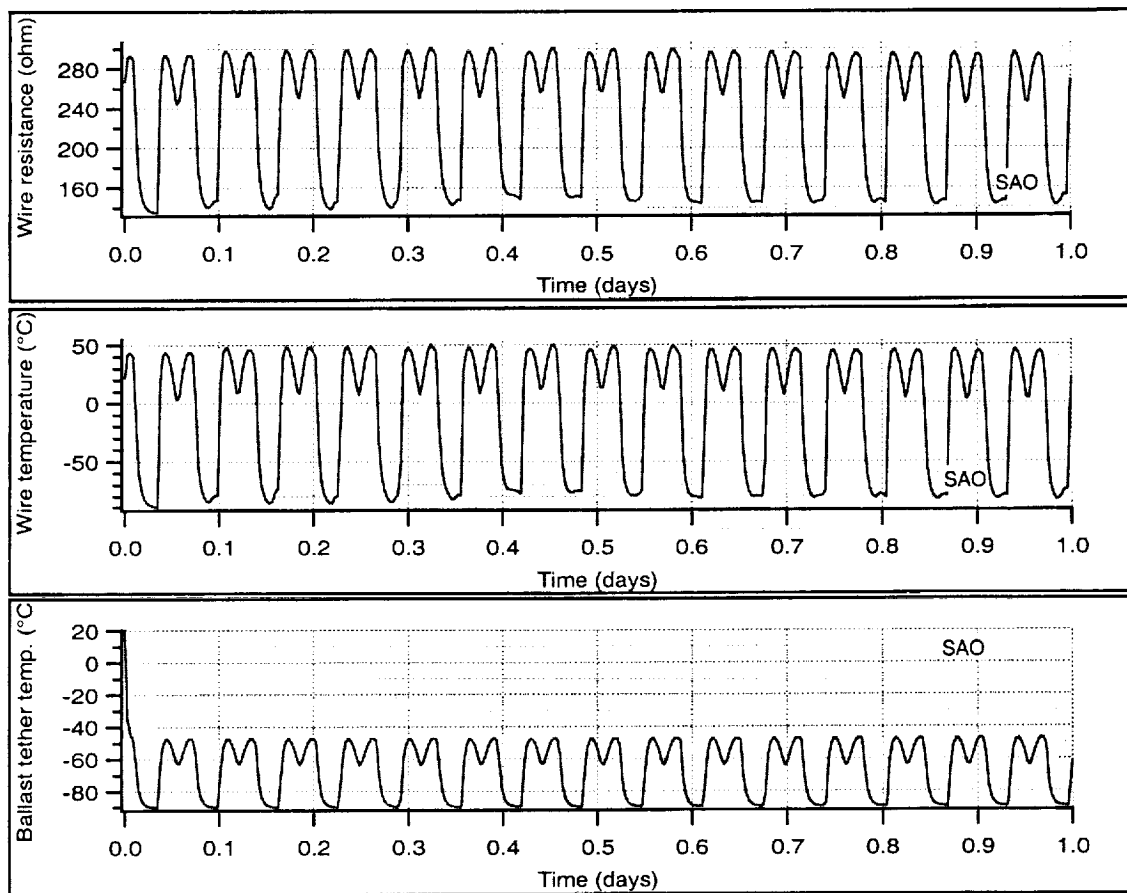


**Figure 11** Results for day-launch with launch date on 16 August 2001

ProSEDS 265 ohm@20 C, 400x400km, nom. solar, day launch, Antigua burn, 16 August 2001

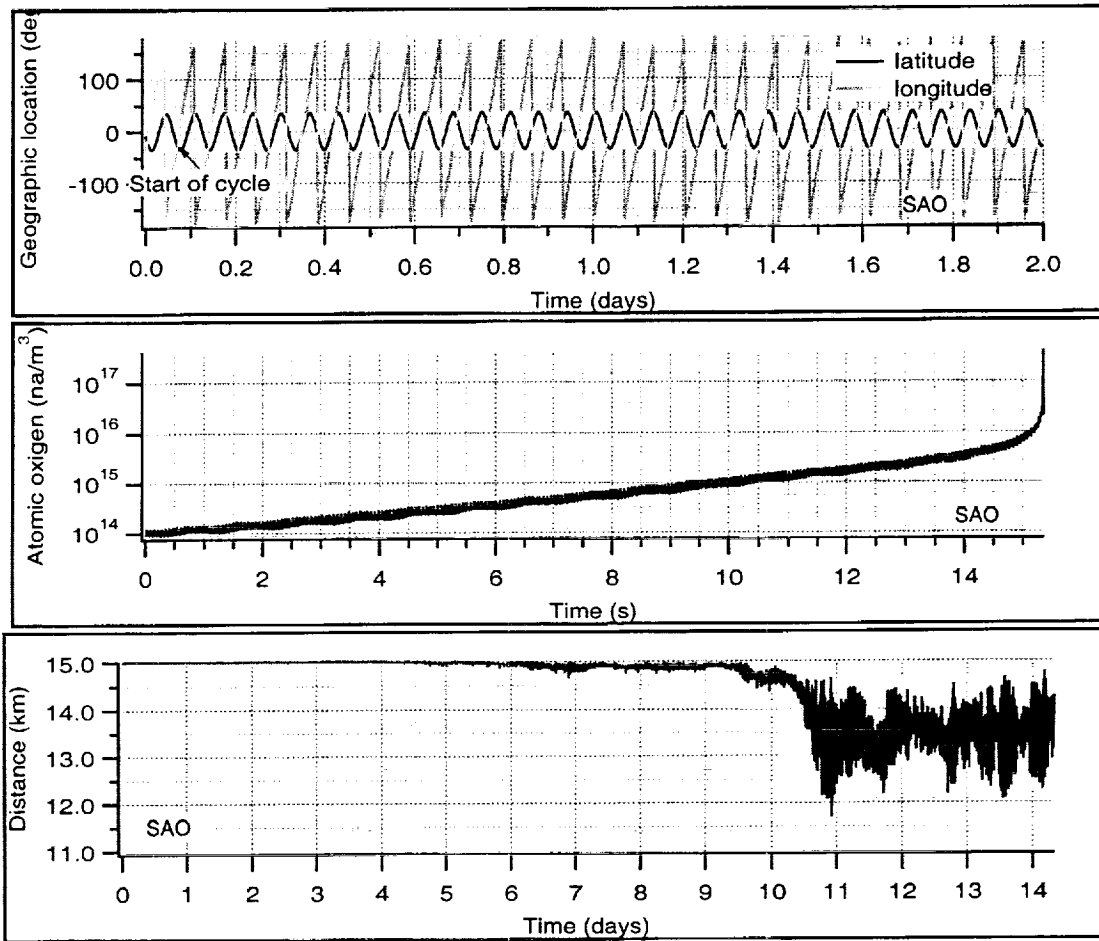


**Figure 12** Results for day-launch with launch date on 16 August 2001

### 3.1 Extreme Cases

For the purpose of evaluating the system behavior under extreme conditions, cases were also run for: (1) a plasma density that is (artificially) twice the plasma density under nominal conditions and (2) without any electrodynamic force. These simulations were run for a 5 day mission duration as MSFC personnel was interested in estimating ProSEDS position under worst case scenarios and, hence, evaluating the risk posed by ProSEDS to other spacecraft operating at the same altitude.

The double plasma density increases the decay rate to 16.5 km/day averaged over a week (and hence the error in the pre-flight estimate of the position). Fig. 13 shows the plasma density, altitude and geographic position (latitude and longitude) of the system. The latitude and longitude are shown over a period of only 2 days for increasing the display clarity. It is notable that the decay rate does not double with respect to the baseline case thanks to ability of the bare tether to adjust in part to changing plasma conditions.

The case without electrodynamic forces provides the largest difference in ProSEDS position with respect to the nominal estimate because the decay rate is reduced by more than a factor of 10 with respect to the baseline case (with nominal electrodynamic forces) when the electrodynamic forces vanish. Figure 14 shows the plasma density, altitude and geographic position of the system. The latitude and longitude are shown over a period of only 2 days for increasing the display clarity.

The position errors after 1 day of mission elapsed time are shown in Table 2. The latitude and longitude angular errors have been converted to kilometers assuming an orbital altitude of 400 km. The distance is the magnitude of the position error vector. The errors grow approximately linearly with mission time.

**Table 2** ProSEDS position errors after 24 hours

	Altitude error (km)	Latitude error (km)	Longitude error (km)	Mag. distance (km)
No current	+7.3	-208	-614	648
Double plasma	-2.3	+68	+222	232

ProSEDS 265 ohm@20 C, 400x400km, 2xnominal plasma density, day launch, 16 August 2001

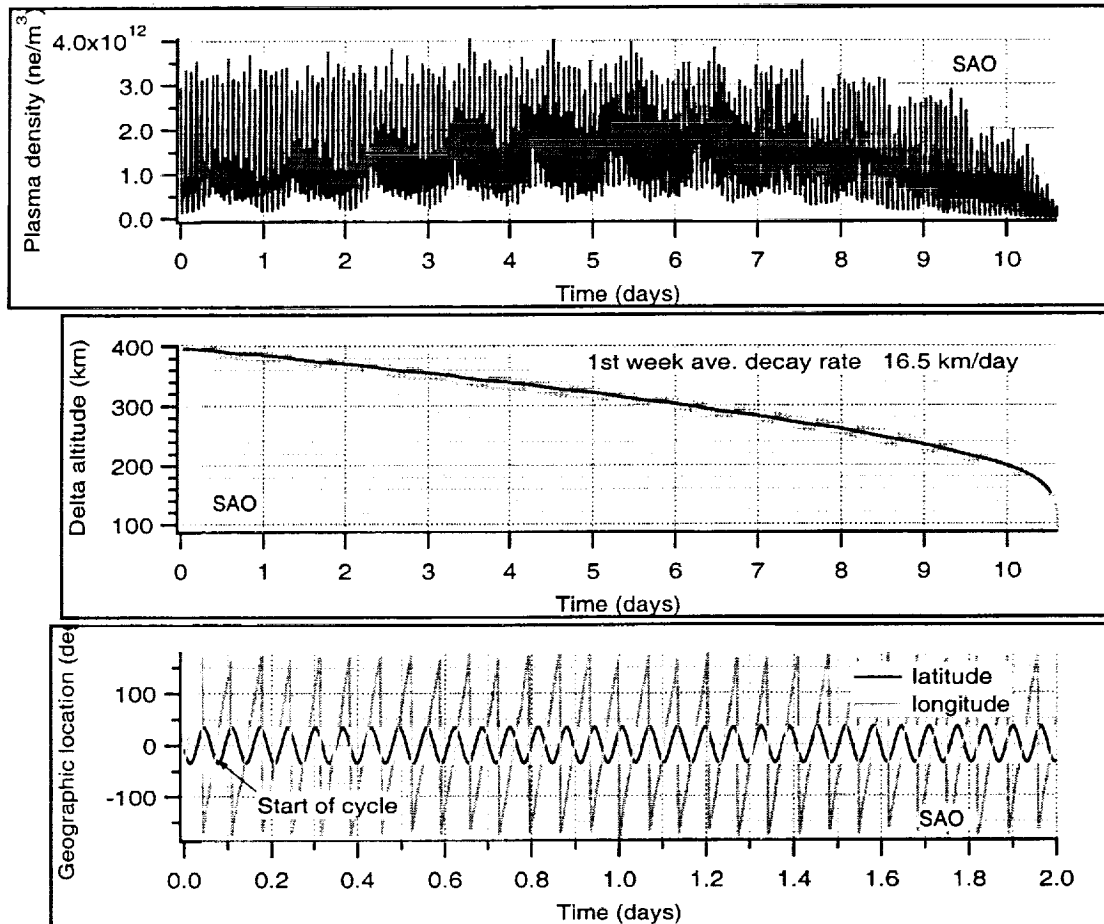


**Figure 13** System decay and geographic position (latitude and longitude) for double the nominal plasma density on 16 August 2001.

ProSEDS 265 ohm@20 C, 400x400km, no plasma, day launch, 16 August 2001

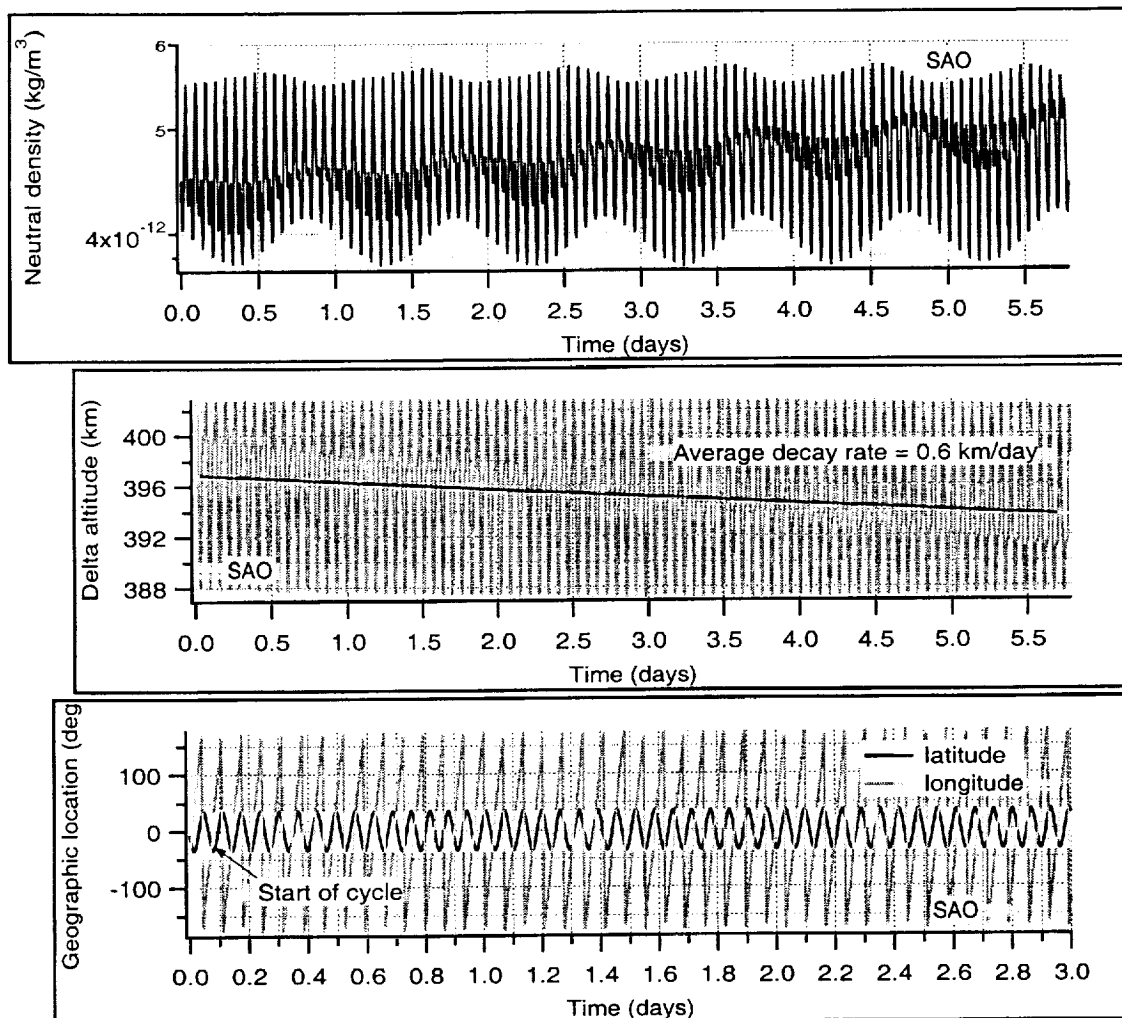


**Figure 14** System decay and geographic position (latitude and longitude) without any electrodynamic forces for a launch on 16 August 2001.

### 3.4 Concluding Remarks

The postponement of the mission to August 2001 does not change substantially the dynamics of ProSEDS with respect to the cases with earlier launch dates. The 1st day decay rate, however, is reduced by about 11% (with respect to a launch in August 2000) due to the reduced plasma density and the increase in the number of orbits on the primary operating cycle. The reduced plasma density is a consequence of the launch date moving away from the peak of the solar cycle 23 that occurred in April-June 2000. With the launch date being postponed even further, the decay rate and the average current available for recharging the secondary batteries will be further reduced.

The present estimates of the orbital decay rate during the 1st day of the mission are 9.4 km/day and 10 km/day for day and night launch, respectively. The estimates of the average current, for ProSEDS is operating on the secondary cycle, are 0.8 Amp and 0.85 Amp for a day and night launch respectively with the average computed over the entire secondary cycle. When the average is computed over the battery charging portion only of the secondary cycle, then the average current values are 1.5 Amp and 1.6 Amp for a day and a night launch, respectively.

Conservative estimates of ProSEDS position error with respect to the nominal trajectory were also computed for two extreme cases of no current and excessive current due to an (artificial) doubling of the plasma density. After one day of mission elapsed time, the magnitude of the position errors are about 648 km (lag) and 232 km (lead), for the two case above, with respect to the nominal position. The position errors grow approximately linearly with time.

## 1. UPDATED DEPLOYMENT CONTROL PROFILES AND SIMULATIONS

### 4.1 Introduction

The ProSEDS control law consists of three distinct modes of operations which are activated during the deployment of the three different tether sections. The non-conductive 10-km-long Dyneema tether is deployed according to the SEDS-II feedback-feed-forward control law. During the deployment of the 4.9-km conductive wire, the brake is simply kept at a constant, low value (typically a fraction of a turn) in order to limit the deployment velocity. During the deployment of the 200-m insulated tether section, the brake is commanded to follow a time-based profile to slow down the deployment velocity at the end of the tether.

As explained in details in the Annual Report #1, the control law utilizes a set of control parameters and a reference table that provides the feedforward information to the first portion of the control law. The reference table provides the control law with the nominal deployed length, speed (in terms of turn counts and turn count rate) and brake profiles that the system should follow under ideal conditions. The feedback, then, adjust the nominal fed forwarded brake profile based on the errors of the actual length and speed with respect to the nominal length and speed profiles.

The second and third portions (for the CCOR wire and insulated section deployment) are open-loop control. The second portion is a tension-offset control in which the brake is kept constant at a low value of turns simply for increasing the tether tension and reduce the maximum exit velocity. The wire is coated with a fairly delicate coating that can be rubbed off by excessive friction. Consequently, it is not possible to utilize a feedback control that ramps the brake up and down. The offset value of the brake utilized during this portion is a constant value in the range 0.5-0.8 brake turns.

In the third portion of the control law, the brake is made to follow an open loop rampup-constant-rampdown profile. This control law acts on a 205-m-long section of the tether with a quick rampup phase. Because of the absence of a sensor that measure the exit velocity directly in the SEDS hardware, the velocity must be computed numerically from a noisy signal and then filtered to make it usable for a feedback control law. This process is actually used in the first portion of the control law where a delay in the computation of the velocity does not affect the performance of the controller. Due to the shortness of the reaction time in the third portion of the control law, there is not enough time to obtain a

filtered value of the velocity especially at a time when the noise from the tether length information is very high. Consequently, we opted for an open-loop control during this phase and we shaped the slow down profile in such a way that it is rather tolerant of changes in the friction characteristics of the tether (see Ref. # for more details).

## 4.2 Friction parameters

We rewrite in the following the frictional tension model (derived by J. Carroll and best explained in Ref 8 of the tether and its parameters for the reader's convenience:

$$T = \left( T_0 + I \cdot \rho \cdot \dot{L}^2 \cdot A_{rel}^E \right) \cdot e^{2\pi f n^{effe}} \cdot e^{f|\theta_0 - \theta|} \quad (1)$$

In equation (1), the term in round parenthesis is the frictional model of the tether/deployer. The first exponential function is the model of the brake and the second exponential function is the model of the tether exit guide. The model parameters are:

$A_{rel}$	$= 1 - A_{sol} \cdot L / L_{fin}$
$A_{sol}$	= annulus solidity of tether
$L$	= length of tether deployed
$L_{fin}$	= final length of tether
$B$	$= 2\pi f n$ ( $n$ is the number of tether turns wrapped around the brake post)
$T_0$	= minimum tension
$\rho$	= linear density of tether
$I$	= inertia multiplier
$\dot{L}$	= tether exit speed
$\theta$	= tether's exit angle with respect to the local vertical
$\theta_0$	= tether deployment null angle (orientation of the longitudinal axis of deployer with respect to the local vertical)
$f$	= friction coefficient
$n$	= number of brake turns
$effe$	= brake effectiveness coefficient

The values of the parameters resulting from the deployment tests on ground of a development tether and two prototype flight tethers (MAO Tether, Tether-A and Tether-B) resulted in the following values of the friction parameters:

**Dyneema (cleaned)**

$T_{min}$	= spectra minimum tension	= $4 + 15L/L_F$ mN
$\rho$	= spectra linear density	= 0.15 kg/km
I	= inertia multiplier	= 2.5
f	= spectra friction coeff	= 0.19
E	= area exponent	= -0.4
effe	= brake effectiveness	= 0.8
AnSol	= annulus solidity	= 0.2 (for $L_F = 10\text{km}$ )

**Wire (CCOR)**

$T_{min}$	= wire minimum tension	= 75 mN
$\rho$	= wire linear density	= 2.0 kg/km
I	= inertia multiplier	= 3.3
f	= friction coeff	= 0.25
E	= area exponent	= -0.6
effe	= brake effectiveness	= 1.2
AnSol	= annulus solidity	= 0.947 (from 1.25km -> 6.25km)

**Insulated (Kevlar overbraided)**

$T_{min}$	= insulated minimum tension	= 350 mN
$\rho$	= insulated linear density	= 3.17 kg/km
f	= friction coeff	= 0.22
I	= inertia multiplier	= 2.5
E	= area exponent	= -0.6
Effe	= brake effectiveness	= 0.9
AnSol	= annulus solidity	= 0.947

The friction parameters of the entire tether (with the three different sections) are utilized to derive the reference table, that is, the reference deployment profile and a brake profile for the entire tether. The brake actuation is then adjusted by the feedback control law during

the deployment of 10-km Dyneema portion while the reference brake profile is followed (without adjustments) during the wire and insulated portions of the tether.

### 4.3 Control parameters

Extensive simulations (numbering in the few hundreds) with a simplified yet accurate computer code are utilized to define and check the control parameters set with the goals of reducing the system libration and the exit speed at the end of deployment and making the control law fairly robust with respect to changes in the friction coefficients.

The present values of the control parameters for ProSEDS are shown in the following. These values may be updated if new results from the deployment tests require it.

----- CONTROL PARAMETERS (Ref#55) -----		
No.	PARAMETER	VALUE (Units) Type
1.	c	0.125 Filter coefficient
2.	K1	0.002 (1/Turn) TurnCount Gain
3.	DZTC	5 (Turn) TurnCount Deadzone
4.	TCELIM	3000 (Turn) Max. TurnCount Error
5.	K2	0.4 (s/Turn) TurnCountRate Gain
6.	DZTCR	0.1* (Turn/s) TurnCountRate Deadzone
7.	TCRELIM	5 (Turn/s) Max. TurnCountRate Error
8.	WAILP	3 WrapIncrement UpperLimit
9.	TBD s	65535 (s) Time after which BIAS is applied
10.	BIAS	0 (Turn) BrakePost Bias
11.	WACLP	6 (Turn) WrapAdjustment UpperLimit
12.	TCBS	18000 (Turn) Turns Count Brake Stop (pertinent to SEDS-II)
13.	A1	0.724 Coeff_1 in Variable Gains
14.	A2	2.82E-6 Coeff_2 in Variable Gains
15.	STOPDEPLOY	65535 (s) Time for brake ramping up at end of deployment (pertinent to SEDS-II)

16. TCDUTY	13900 (turns)	End of 50% duty cycle
17. TURNBRAKE0	14160* (turns)	ramp down brake to WIREBRAKE
18. WIREBRAKE	0.5 (BrakeTurn)	BrakeTurns during CCOR deployment
19. RAMPUP	25890 (turns)	Start of slowdown procedure
20. QUITLAWBACKUP	14320 (turns)	ramp down brake in case of Counter-A or -B failure
21. BRSD	1.5 (BrakeTurns)	Max brake turns during slow down
22. TBD(15)	14.2 (sec)	Time to rampup brake from WIREBRAKE to BRSD
23. TIMECFAIL	120 (sec)	Time of no update of Counter-C to declare the Counter-C failed
24. TIMEDUTY	3300 (sec)	time-based equivalent of TCDUTY
25. TIMEQUERY	4170 (sec)	the software interrogates the BES** if Counter-C had failed
26. TIMERAMPNOBES	4230 (sec)	Time-based start of slowdown procedure if the BES was declared failed

-----  
 \*Values per ECR SAO-001  
 \*\*BES = brake enable switch  
 -----

#### 4.4 Reference tables

The desired final state at the end of deployment is for the system to be aligned and swingless with respect to the local vertical with a residual longitudinal velocity greater than 3 m/s before the beginning of the insulated portion of the wire (last 205 m of tether). The residual velocity is then reduced by a final activation of the brake immediately after the exiting of the insulated wire is sensed.

Several constraints are imposed to the minimization routine used to derive the reference profile mostly aimed at obtaining a reference brake profile that does not force undesired situations during deployment. The exit velocity is constrained to be above about 2 m/s during deployment of the non-conductive tether and above 3 m/s during deployment of the wire. The velocity limitations ensure that the satellite has enough kinetic energy to overcome unexpected discontinuities along the tether. A constraint function that penalizes

the trajectories with rate values smaller than the predetermined minimal rate values is used in the minimization process to achieve this goal.

Because of the constraints imposed on the minimization routine, the process of deriving a good reference profile that meets all the requirements is tedious. The process requires a large number of trials. In many of them the routine is unable to converge properly to a cost function which is within the specified accuracy. In many other cases, the process produce a reference profile but some characteristics of the reference profile are not desirable such as sharp gradients in the brake actuation or in the exit velocity profile. Many attempts must be made and once a good reference profile is found it must be tested in the simulator for assessing its robustness vs. variations in the tension model parameters.

All in all, 55 valid profiles (out of a much larger number of trials) have been derived for ProSEDS. Some of these profiles differ in the selection of reference values of the tension model. In others, the same reference values have produced substantially different reference profiles depending on the different initialization of the minimization routine. The final selection of a flight control profile is then made on the basis of: (1) meeting its performance goals and (2) its robustness to variations of the parameters of the tension model.

The most uncertain and also influential parameter (during the early and critical phase of deployment) of the tension model is  $T_{\min}$ . The minimum tension of the ProSEDS non-conductive tether (which dominates the final state at the end of deployment) has already been measured in deployment tests on the ground under different temperatures to vary between 5 mN and 20 mN depending on the cleanliness of the tether. Consequently, the control law must provide a residual libration at the end of deployment of less than  $20^\circ$  (as specified by the mission requirements) within the measured range of variability of the minimum tension.

The control law can tolerate without a significant decay in performance a value of the non-conductive tether minimum tension between 5 mN and 20 mN. For  $20 \text{ mN} < T_0 < 50 \text{ mN}$ , the libration at end of deployment increases rapidly. For  $T_0 \geq 80 \text{ mN}$ , the deployment stops at a distance of about 500 m because of excessive friction and without any role being played by the control law. The critical value of 80 mN for the minimum tension is determined by the ejection velocity which with the present ejection system is equal to 2.74 m/s. It is, therefore, very important that the 10-km Dyneema tether satisfies the critical tension constraint. The two reference profiles that have been thoroughly developed and analyzed in details are the Ref#47 and Ref#55 as follows:

Ref#47 is based on the friction characteristics and spooling of the development tether and it is for an orbital altitude of 400 km.

Ref#55 is based on the friction characteristics of the MAO tether and spooling characteristics expected of the F-2 tether (which were extrapolated by Tether Applications from the spooling of the F-1 tether) and it is for an orbital altitude of 360 km.

Reference Profile #47

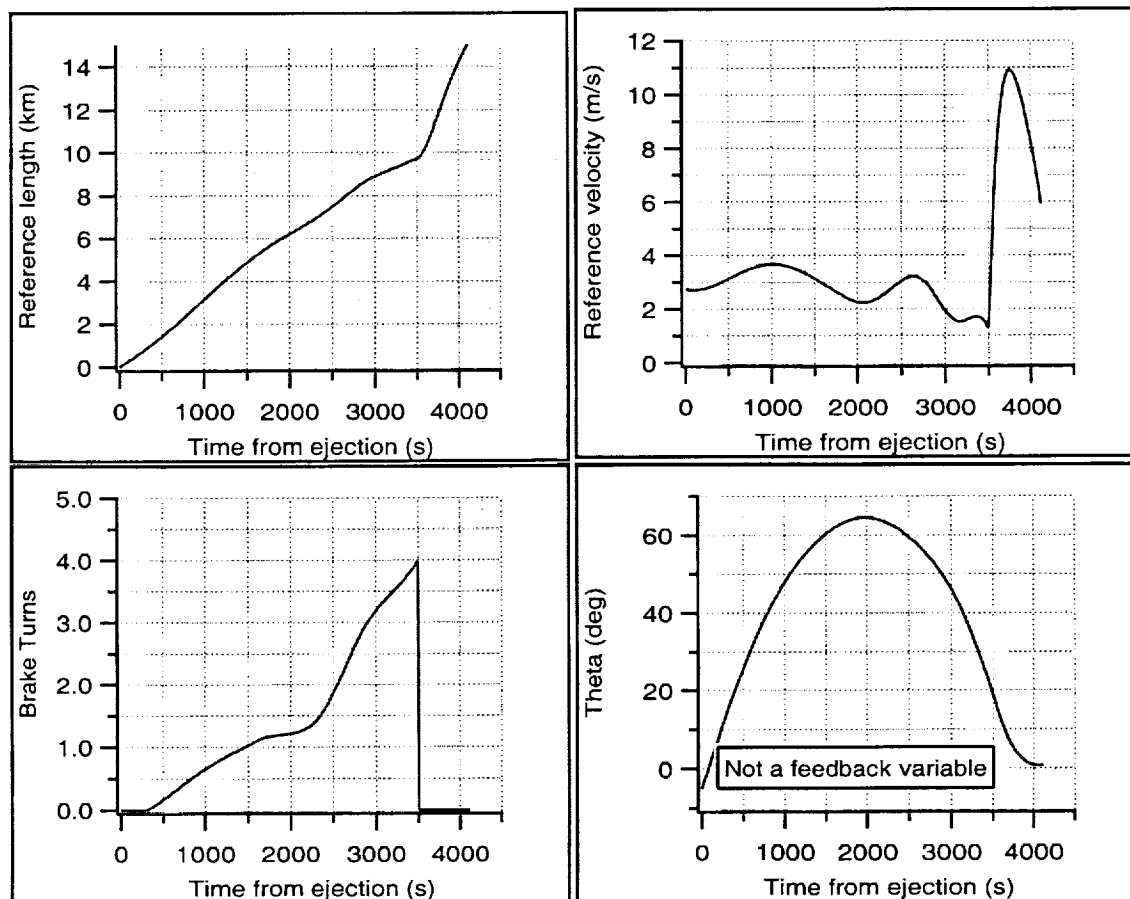


**Figure 15** Reference profile Ref#47 (without slow down maneuver)

Reference Profile #55

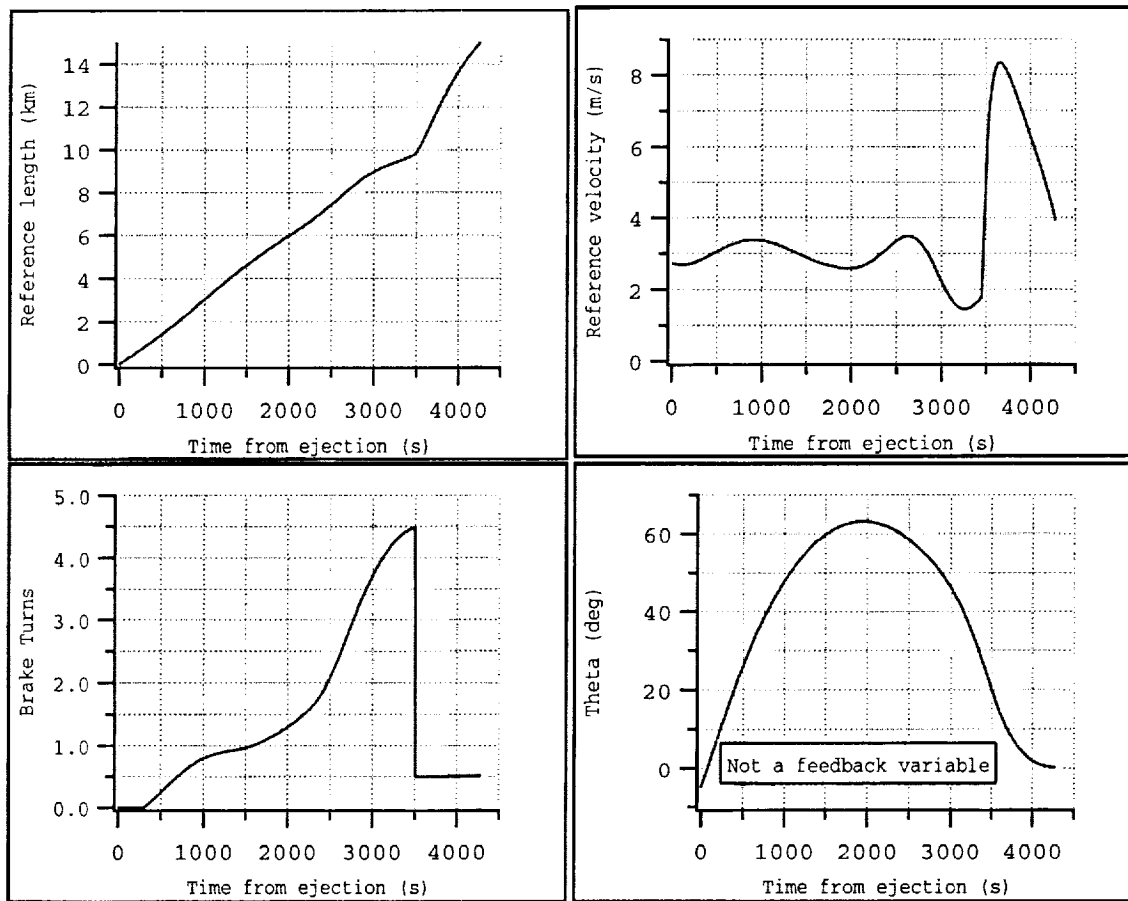


**Figure 16** Reference profile Ref#55 (without slow down maneuver)

The most recent parameters adopted for deriving the latest reference profiles are as follows

*Orbital and ejection parameters*

Orbit: 400x400 km (for Ref#47)

Orbit: 360x360 km (for Ref#55)

Orbital inclination: 36 deg

Ejection velocity = 2.74 m/s

Ejection angle = 5 deg (forward of LV with an upward deployment)

*System parameters*

Satellite mass = 21.4 kg

Delta-II Mass = 994 kg

Tether lengths: 10 km Dyneema, 4.85 km CCOR and 205-m insulated

**Table 3** Characteristics of selected reference profiles

Profile	$\Delta V$ (m/s)	$T_0/T_{\text{wire}}$ (mN)	Orbit (kmXkm)	Friction characteristics	Spooling
#47	2.8	10/100	400x400	Dev. tether	Dev. tether
#55	2.8	10/75	360x360	MAO	F-2 (estim.)

Table 3 shows key characteristics of the two reference profiles discussed in this Annual Report. Simulation results of ProSEDS deployment for Ref. #55 are shown in Figs. 17-19 for different values of the minimum tension of the Dyneema tether. The dynamic response is well within the required 20 deg maximum residual amplitude required for ProSEDS.

Ref#55,  $T_{ref} = 10\text{mN}$ ,  $T_{min} = 0\text{mN}/100\text{mN}$ ,  $\Delta V = 2.74\text{ m/s}$ , Brake 1.5V/0.07v-Ins205m

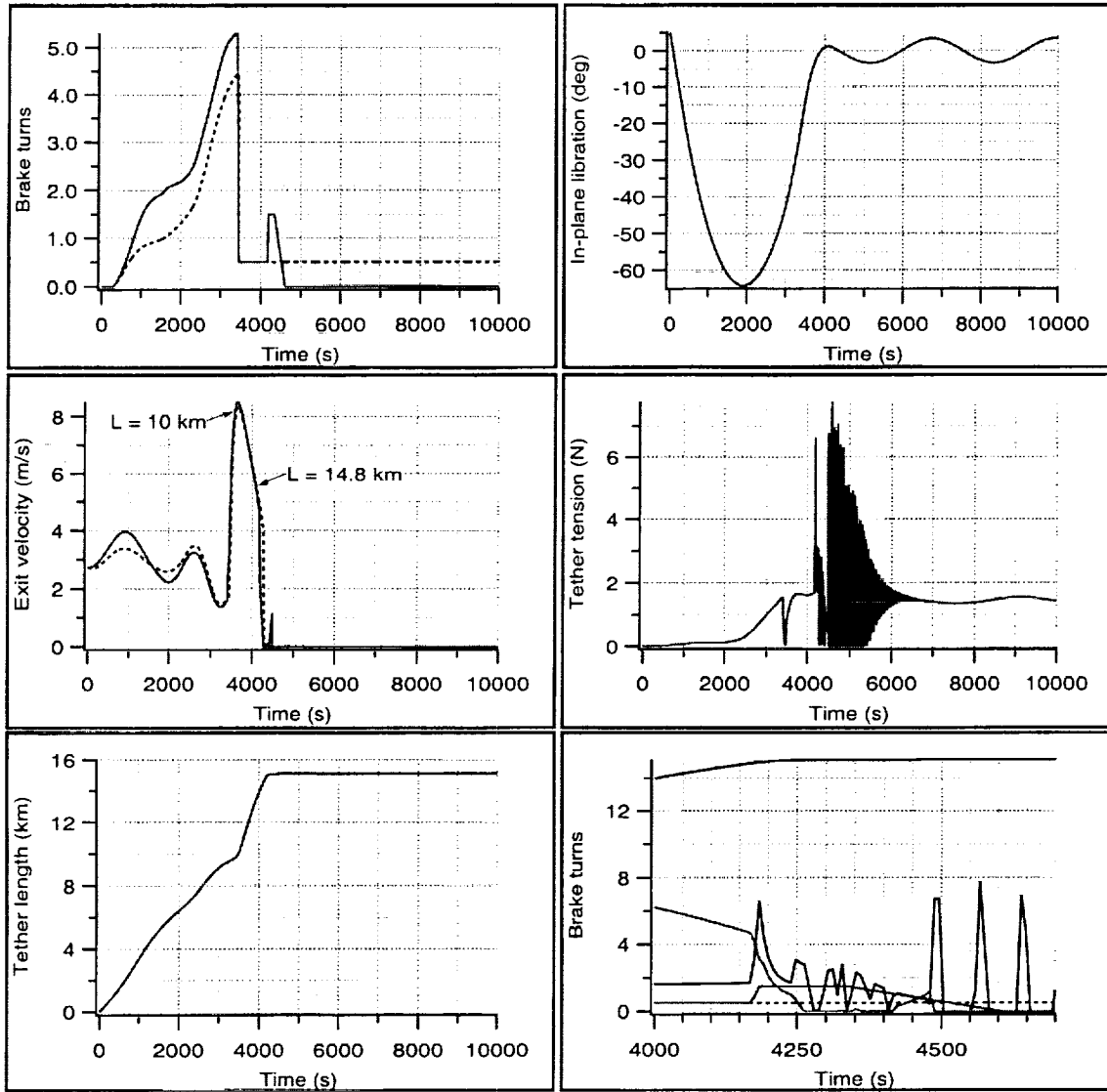
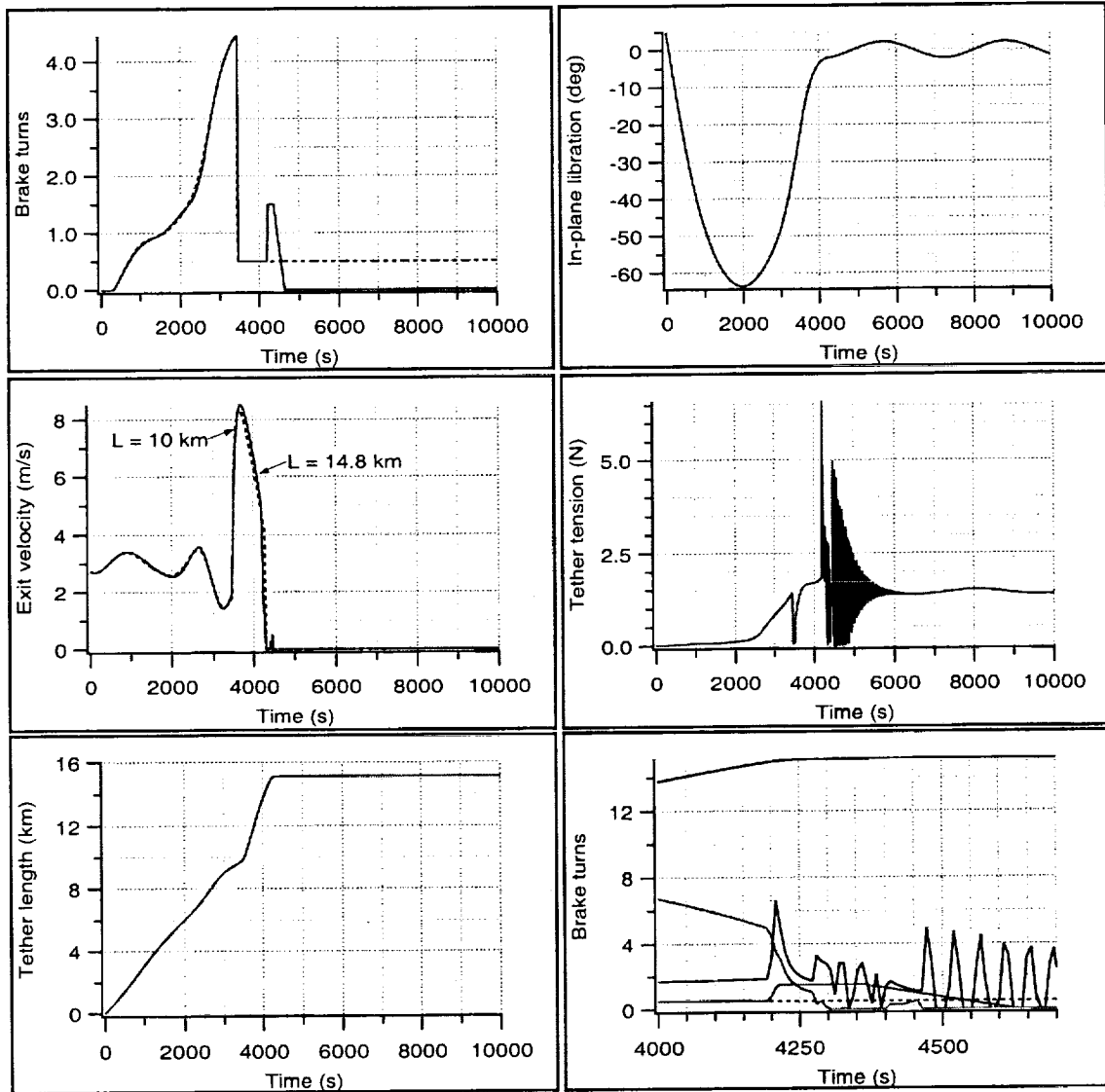


Figure 17 Deployment dynamics for Ref#55 for  $T_0 = 0\text{ mN}$

Ref#55,  $T_{ref} = 10\text{mN}$ ,  $T_{min} = 10\text{mN}/100\text{mN}$ ,  $\Delta V = 2.74\text{ m/s}$ , Brake  $1.5/0.07\text{v-Ins205m}$



**Figure 18** Deployment dynamics for Ref#55 for  $T_0 = 10\text{ mN}$  (nominal)

Ref#55,  $T_{ref} = 10\text{mN}$ ,  $T_{min} = 20\text{mN}/100\text{mN}$ ,  $\Delta V = 2.74\text{ m/s}$ , Brake 1.5/0.07v-Ins205m

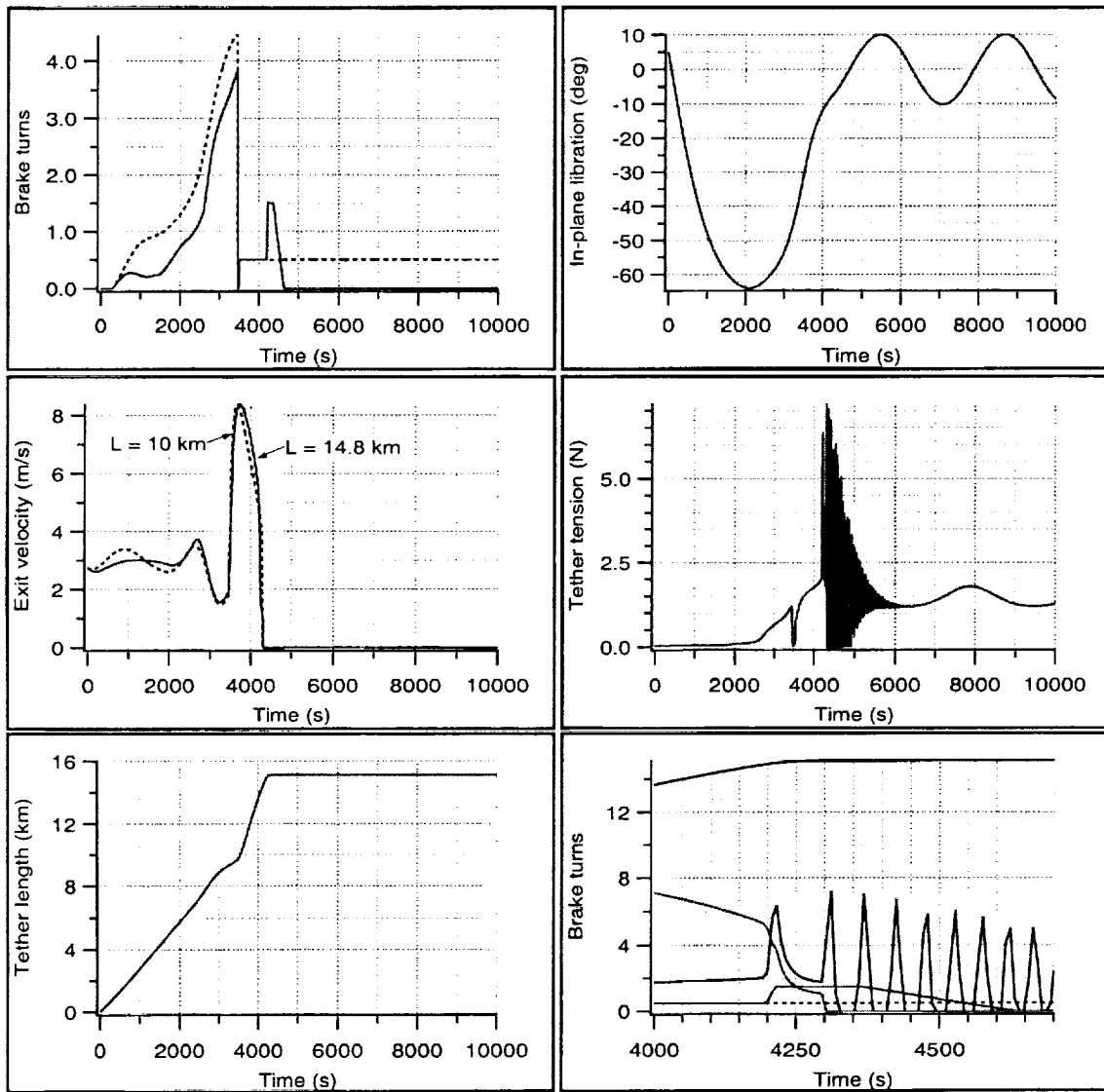


**Figure 19** Deployment dynamics for Ref#55 for  $T_0 = 20\text{ mN}$

Figure 20 shows the amplitude of the residual libration at the end of deployment vs. the minimum tension  $T_0$  of the Dyneema tether for the selected profiles. The final libration amplitude is very sensitive to the leader tether  $T_0$  and it is quite insensitive to the value of the wire  $T_{\text{wire}}$ . Values of  $T_{\text{wire}}$  of 50-300 mN have been explored with very good deployment dynamics. Values as high as 500 mN are tolerable for the minimum tension of the wire.

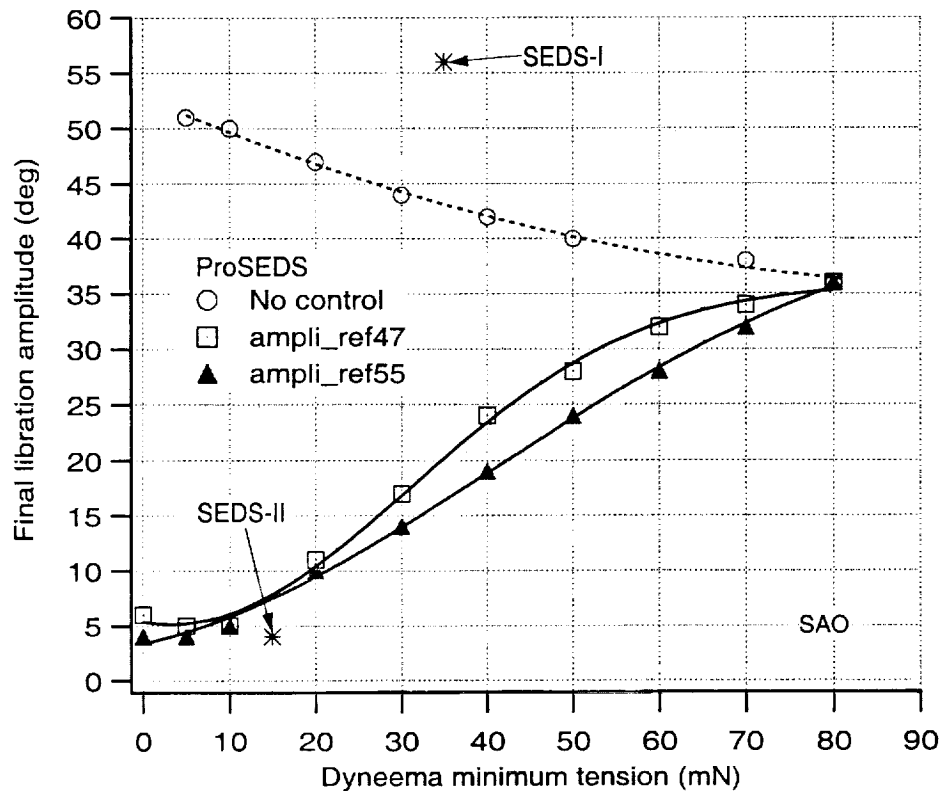


**Figure 20** Final libration amplitude vs.  $T_0$  for selected deployment profiles

## 4.5 Validation process

### Hi-Fi ProSEDS deployment verification

The numerical simulations of ProSEDS deployment (Ref#47) were run using SAO's high-fidelity code MASTERDEP. The results were compared to the DUMBBELL numerical code and generally agree. Noticeable differences were found when the dynamics of the wire, not simulated by dumbbell, was a driver. Namely the lateral modes excited by the deployment (e.g. Coriolis) caused the tether to bow and the pre-selected brake was too low to be able to control the final velocity. The problem, however, was solved by applying a moderate brake during the CCOR wire deployment and the results are presented in the following.

The reference deployment profile is ProSEDS Ref#47. MASTERDEP simulates the two end-platforms and tether with nine lumps. The system is acted by gravity ( $J_0 + J_2$ ), aerodynamic drag and tether tensions (Spring-dashpot system). The system orbits the earth at 400 Km of altitude.

The following simulations will be presented:

- a. Nominal Deployment (ProSEDS Ref#47 assumes 10 mN as minimum tension)
- b. Minimum tension = 5 mN
- c. Minimum tension = 20 mN

**Case a:** Nominal Dyneema minimum tension,  $T_0 = 10$  mN. Unlike for the reference profile, the brake is set to 0.5 turns during wire deployment

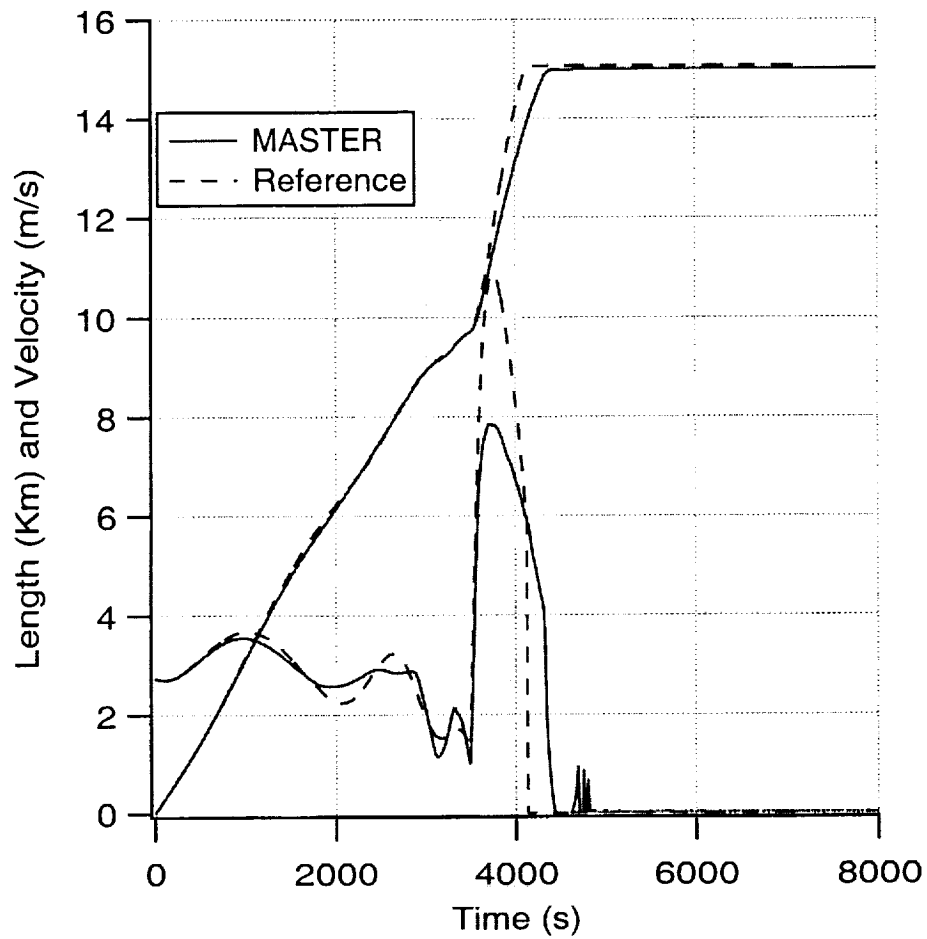


**Figure 21** Nominal minimum tension  $T_0 = 10$  mN

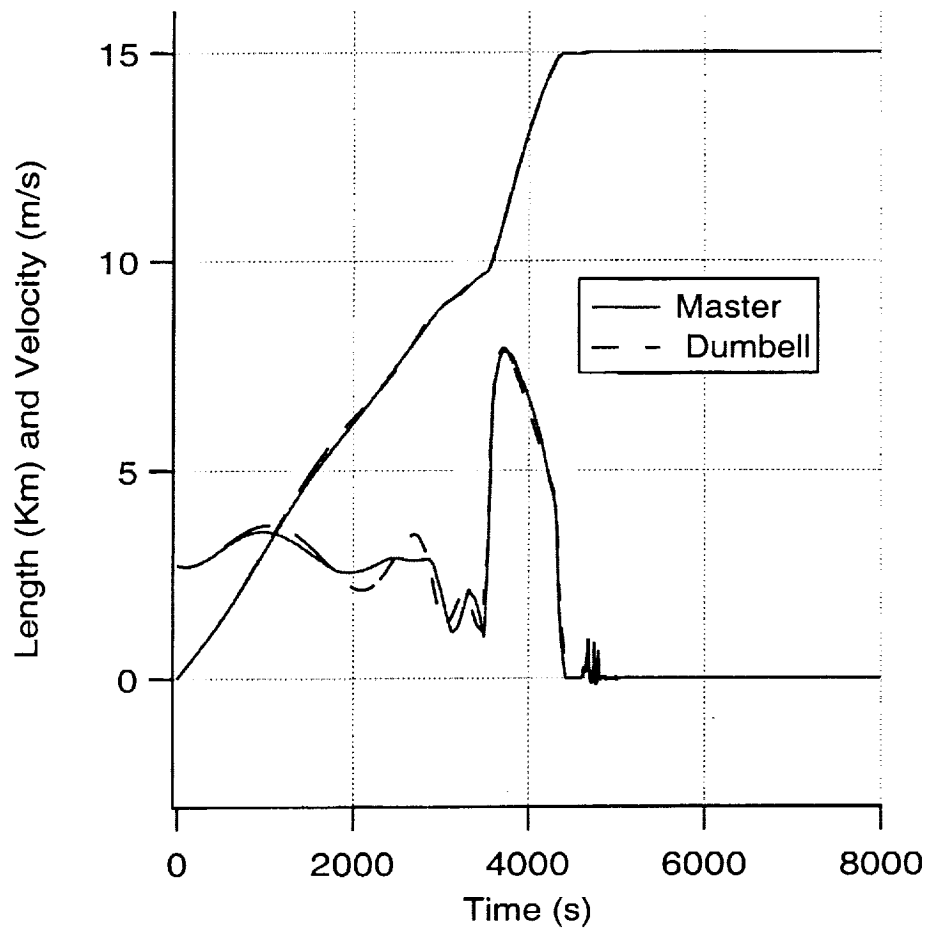


**Figure 22** Nominal minimum tension  $T_0 = 10$  mN (MASTER vs. DUMBELL)

The agreement between dumbbell and multimass MASTER simulations is quite good. The lateral dynamics however plays a role in the differences between the results of the programs. Large bowing produces travelling waves along the tether when braking is applied. The bowing can be minimized (as done here) by applying a moderate brake during wire deployment.

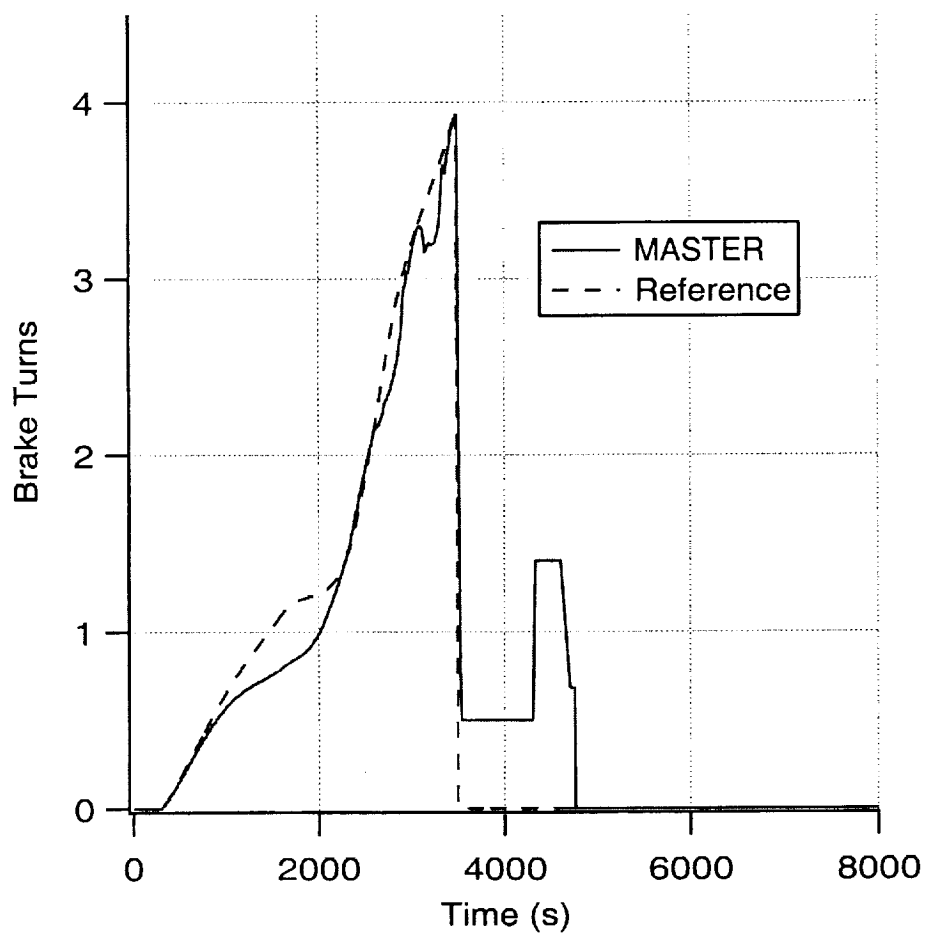


**Figure 23** Nominal minimum tension  $T_0 = 10$  mN

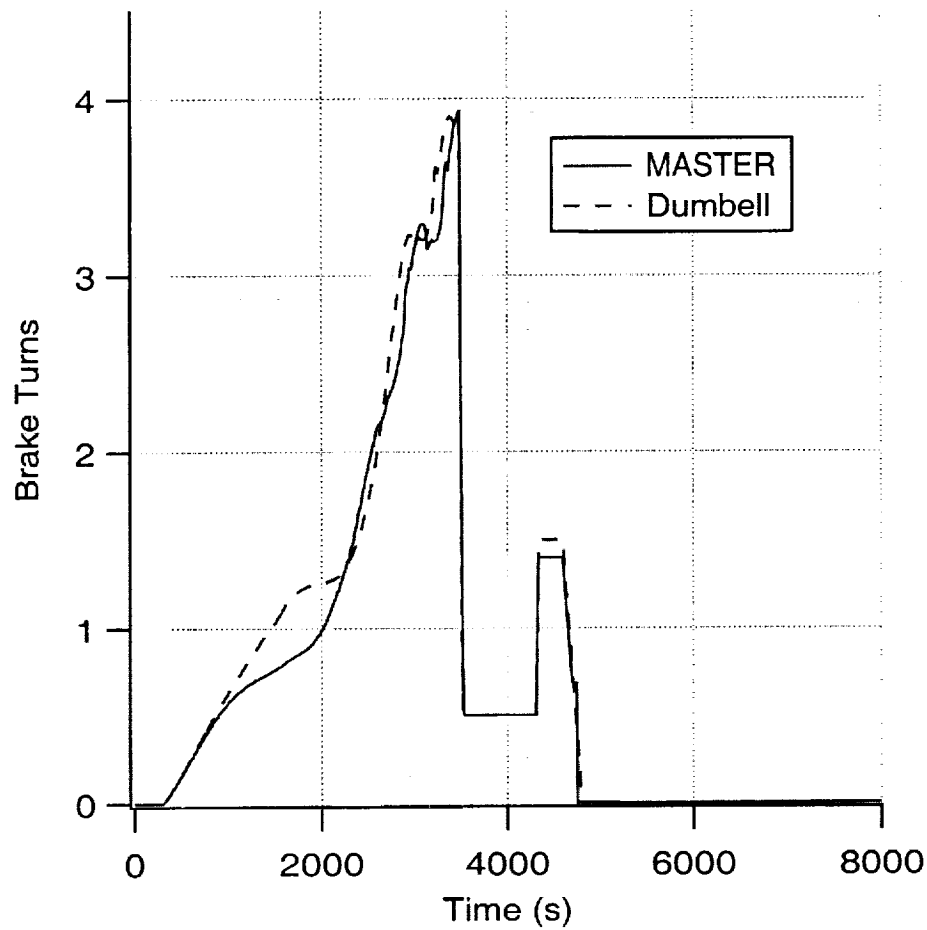


**Figure 24** Nominal minimum tension  $T_0 = 10$  mN

We applied a 0.5 turns of brake during wire deployment (starting at about 4000 s) to limit the magnitude of the bowing caused by the Coriolis force. The last portion of the control law (during deployment of the insulated wire) is used to bring the end-mass to a smooth stop. Values between 1.2 and 1.7 brake turns (for the constant-brake plateau) have been used without noticeable differences. A value of 1.4 turns was adopted for Ref#47.

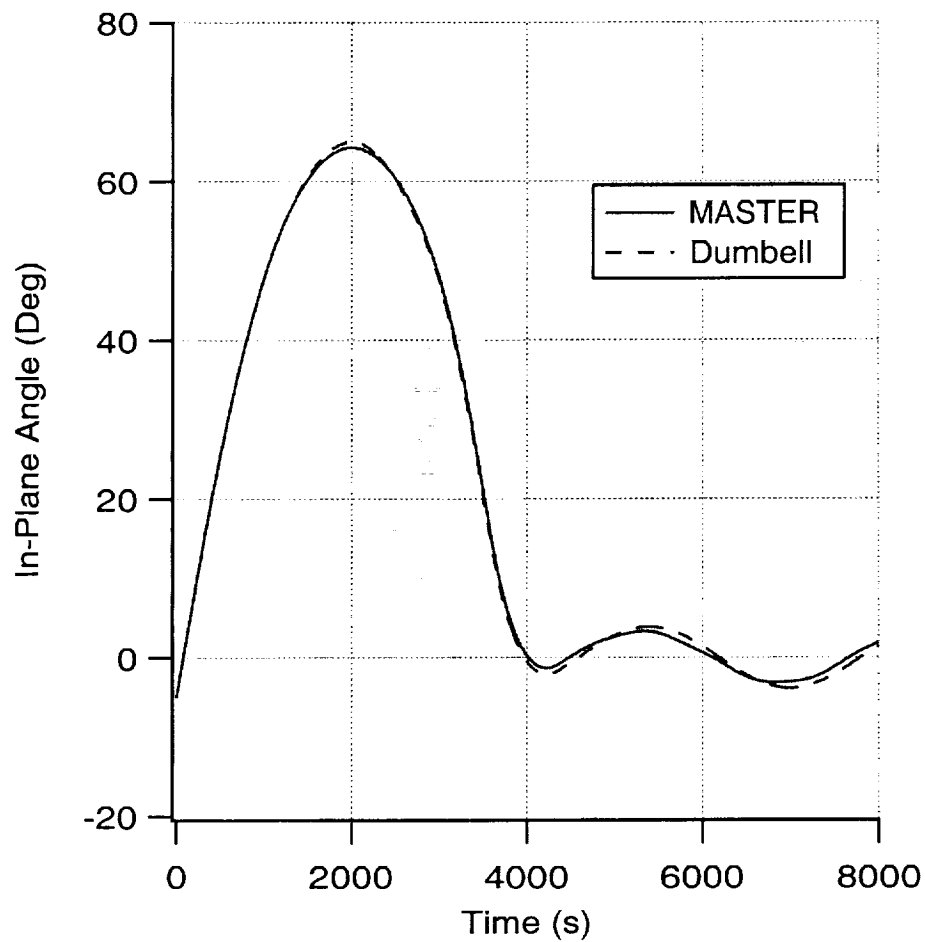


**Figure 25** Nominal minimum tension  $T_0 = 10$  mN

The in-plane angle is similar both in amplitude and in phase to the simplified simulation (DUMBELL). A final libration amplitude of less hat 10 deg has been reached.

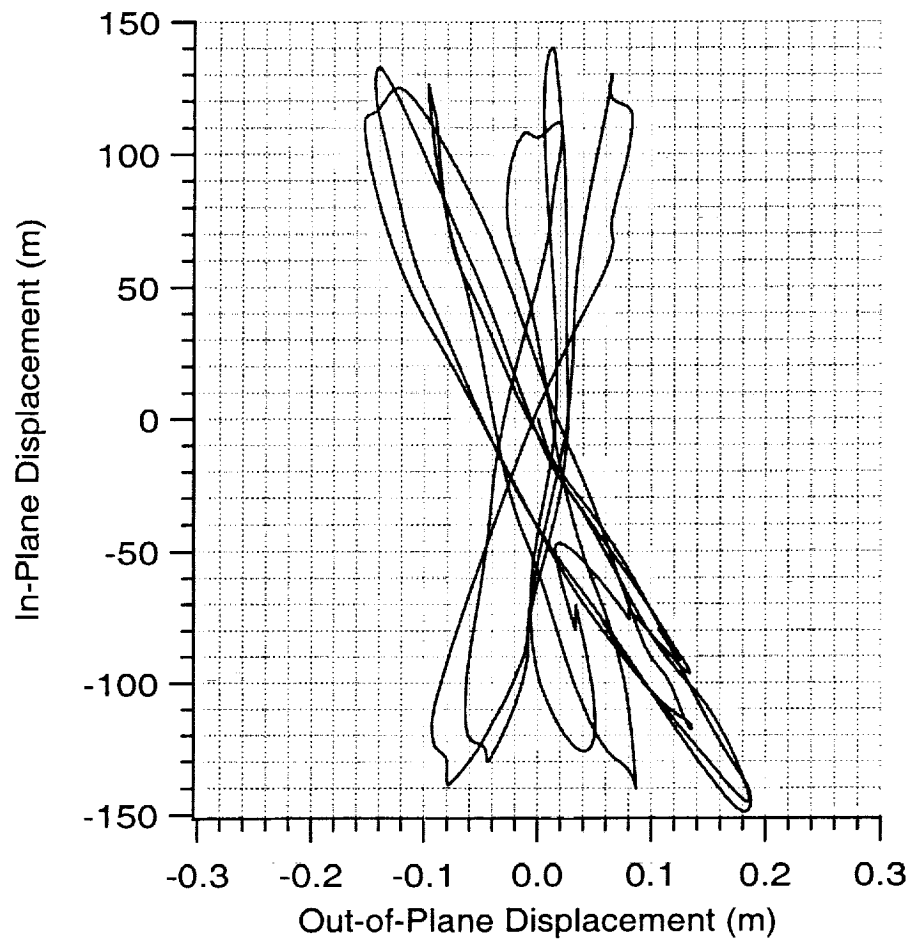


**Figure 26** Nominal minimum tension  $T_0 = 10$  mN

The lateral dynamics is mainly in-plane and it is limited to a few hundred meters. The out-of-plane dynamics is almost negligible during deployment.

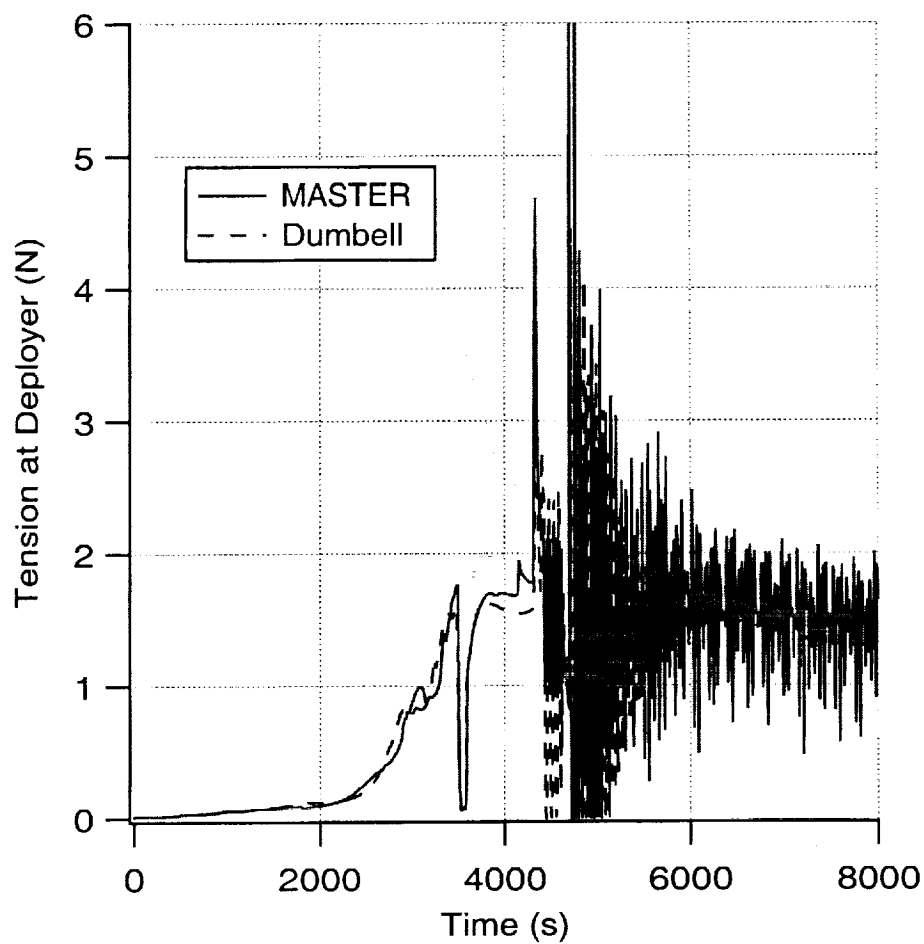


**Figure 27** Nominal minimum tension  $T_0 = 10$  mN

The tether tension is similar during deployment. The rebound phase differs in variations because of the tether's higher longitudinal modes.

**Case b:** Dyneema minimum tension = 5 mN

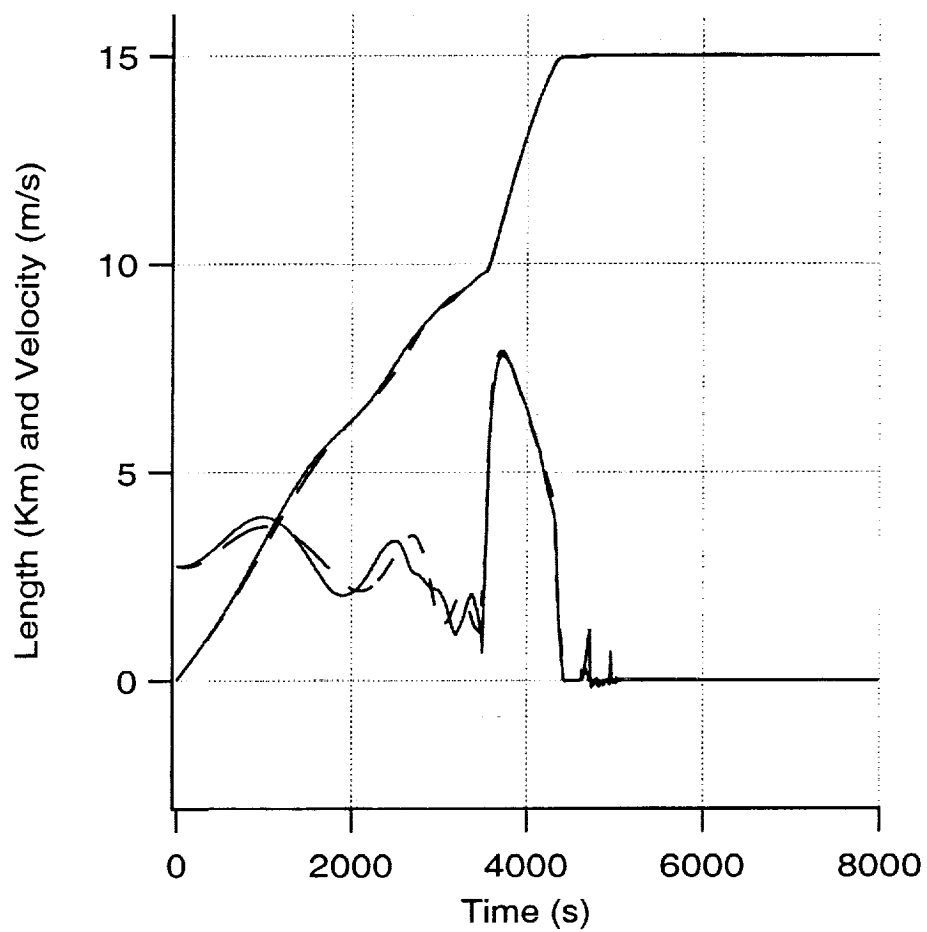


**Figure 28** Minimum tension  $T_0 = 5$  mN (MASTER vs. DUMBELL)

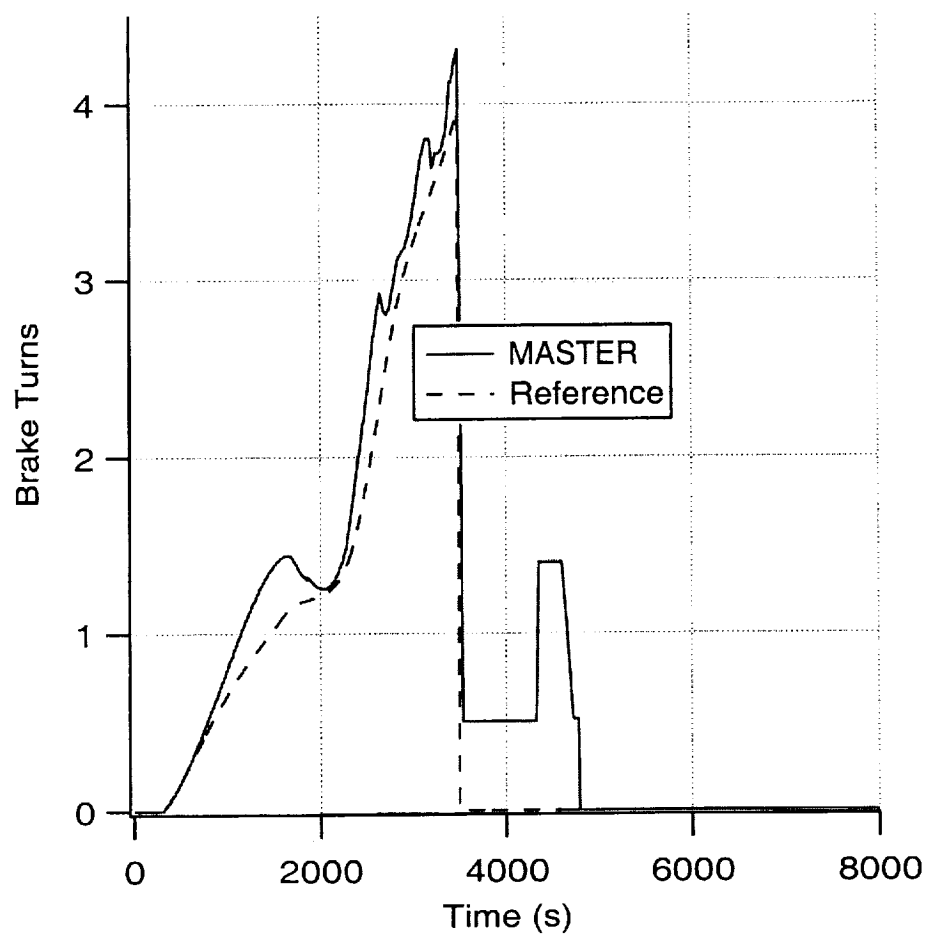


**Figure 29** Minimum tension  $T_0 = 5$  mN

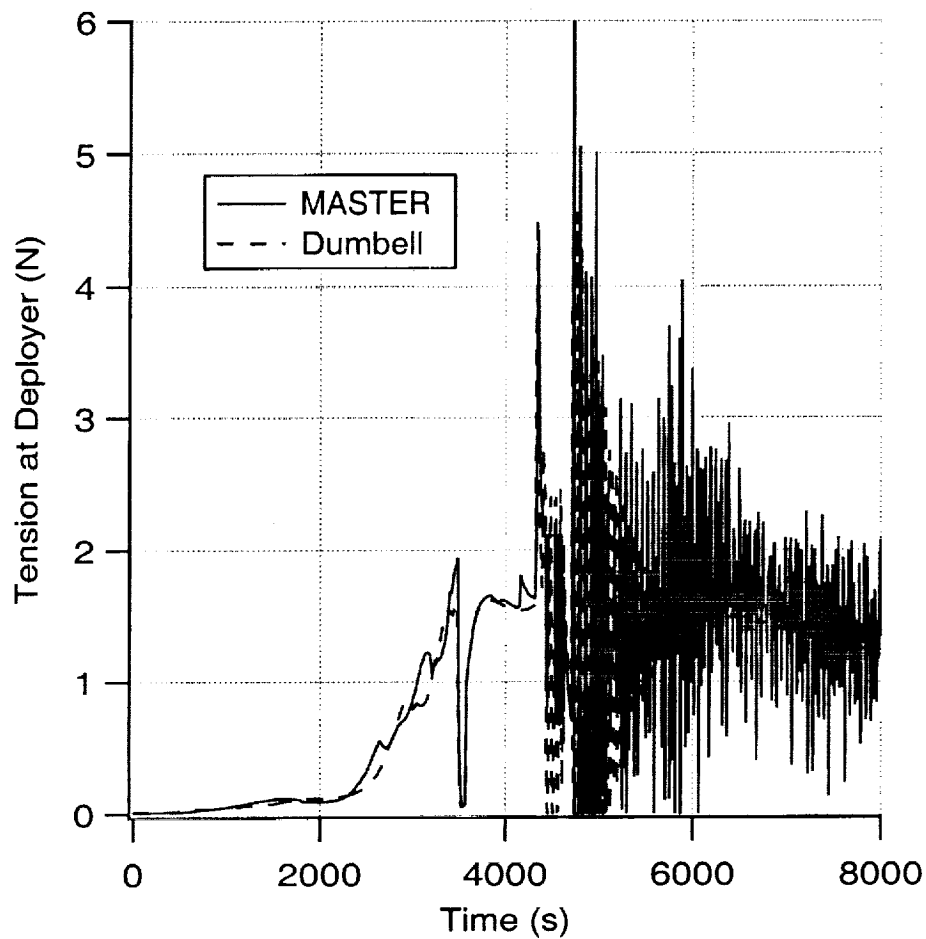


**Figure 30** Minimum tension  $T_0 = 5$  mN

No dramatic changes can be noticed from case a. However, given a smaller tension in the deployment, the brake is about 1/2 turn larger than for the DUMBELL simulations. The in-plane libration (not shown here) has the same amplitude of the simplified simulations with a slight change of phase. Tension and lateral displacement are not reported for the sake of brevity and they do not show any peculiarities.

Case c: Dyneema minimum tension = 20 mN

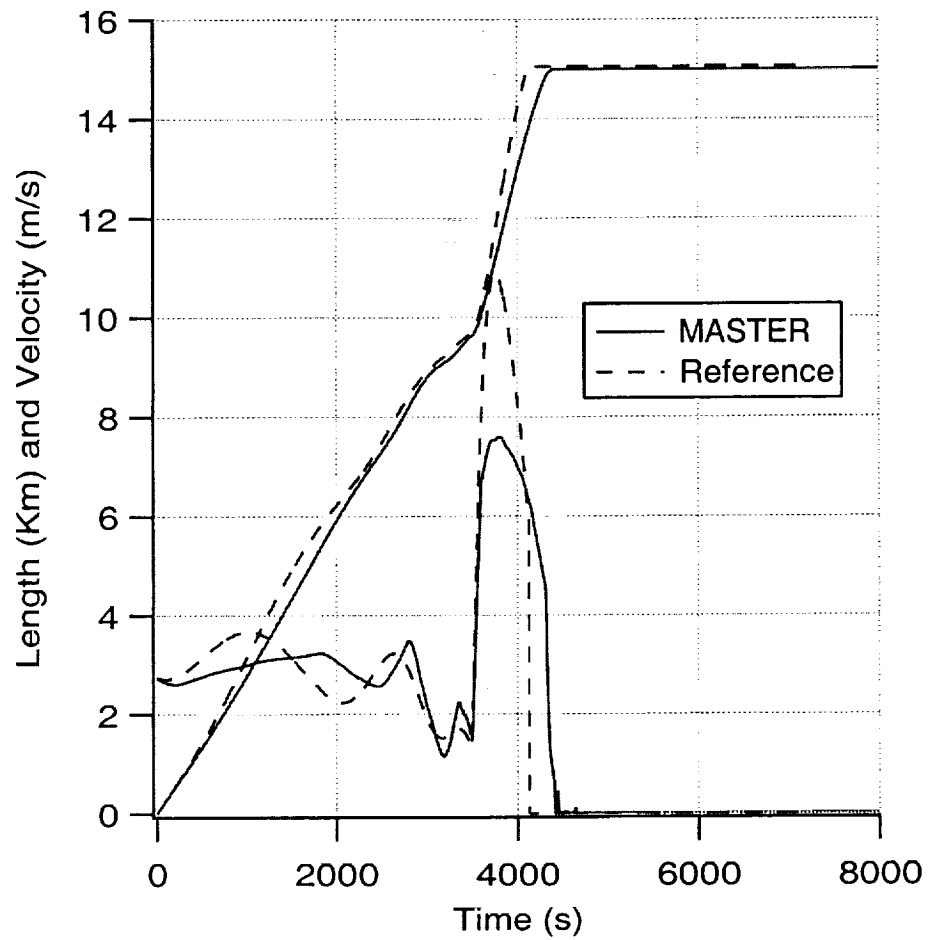
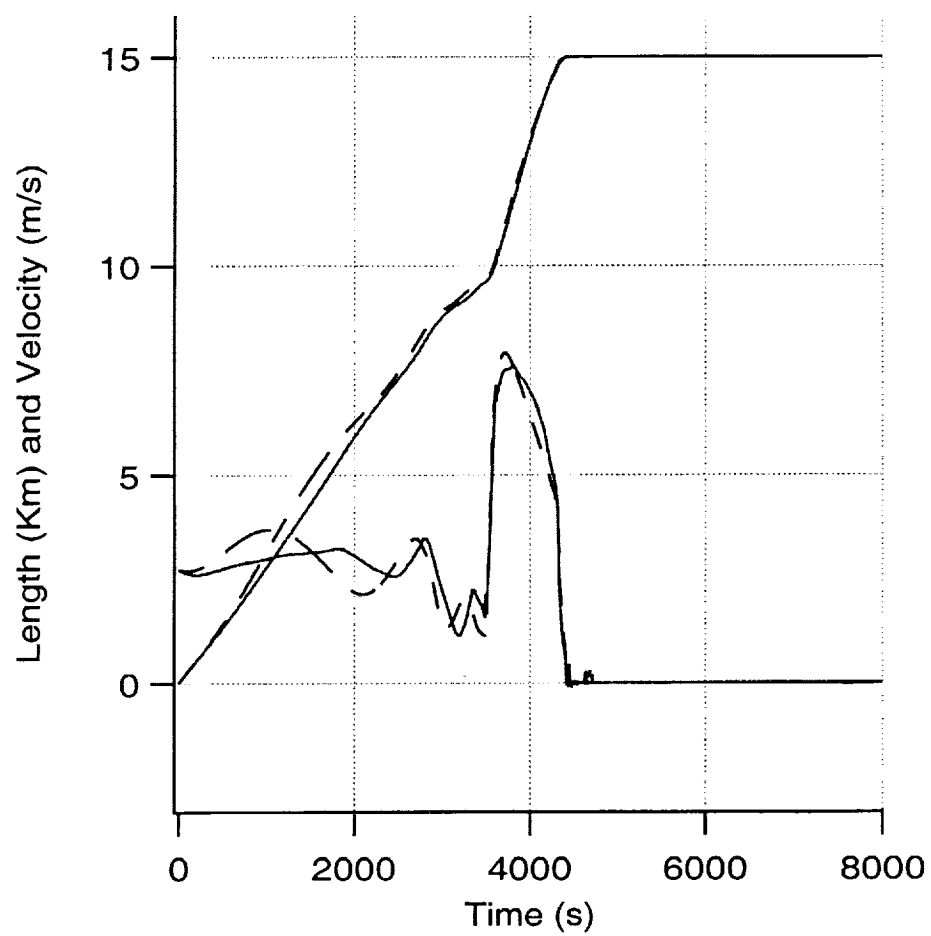
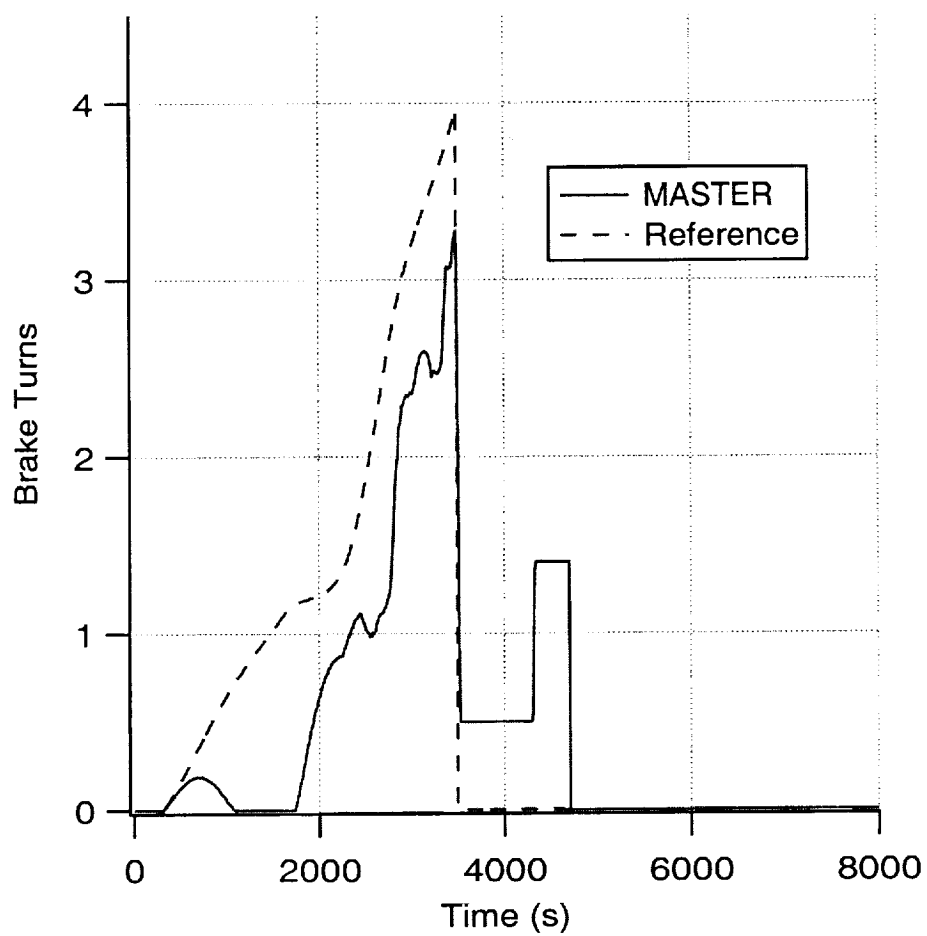


Figure 31 Minimum tension  $T_0 = 20$  mN



**Figure 32** Minimum tension  $T_0 = 20$  mN (MASTER vs. DUMBELL)



**Figure 33** Minimum tension  $T_0 = 20$  mN

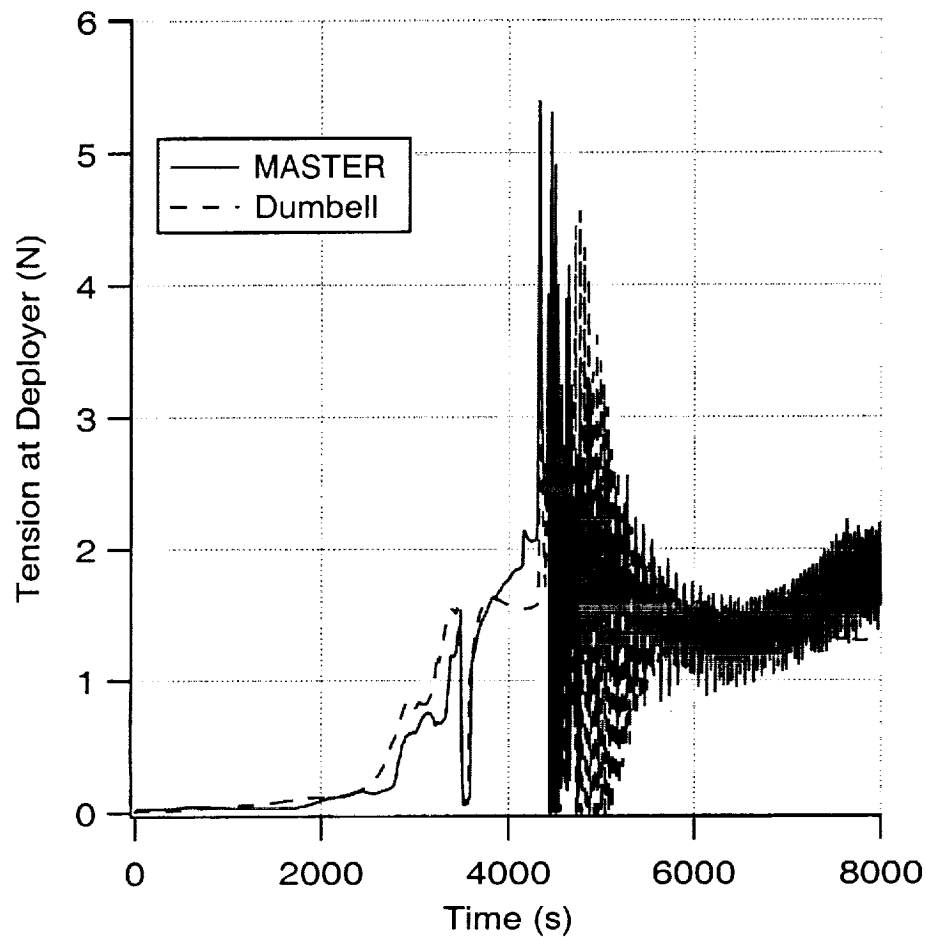


**Figure 34** Minimum tension  $T_0 = 20$  mN

Also in this case no noticeable changes can be seen from case a. The libration is a few degrees higher with a more pronounced change in the phase angle. Tension and lateral displacement are not reported for the sake of brevity and do not show any peculiarities.

In all three cases the control law has shown robustness to deploy 15 Km of tether and bring the endmass to a smooth stop with small tension variations and rebound velocity. In all three cases the lateral dynamics has been limited by the brake action. The final libration is about 10 degrees or less in the minimum tension range of  $5 \text{ mN} < T_0 \leq 20 \text{ mN}$ .

Deployment without braking

This run simulates ProSEDS dynamics when the brake is not activated. The tether is fully deployed but the rebound is quite significant ( $\sim 5$  m/s final deployment velocity).

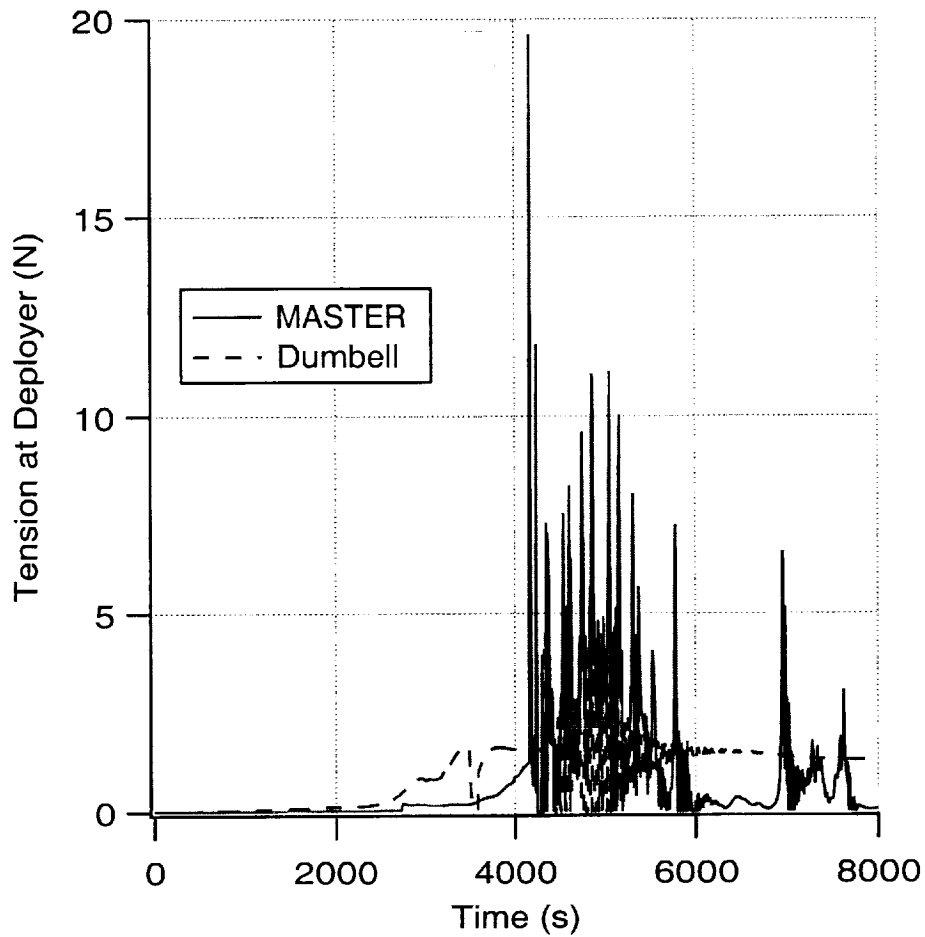


**Figure 35** No brake is activated throughout deployment

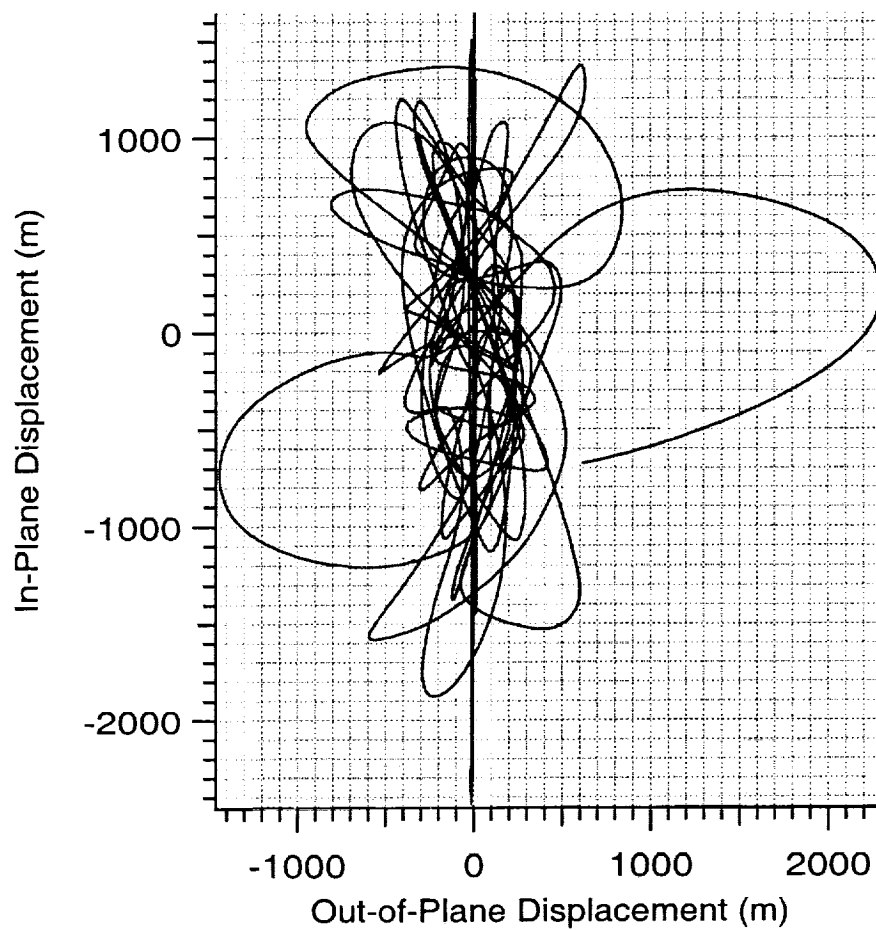


**Figure 36** No brake is activated throughout deployment

The final libration is about 60 degrees since the brake was not activated. The tension reaches a limit of 20 N during rebound and the lateral dynamics is highly excited increasing in time and it of the order of the kilometer both in-plane and out-of-plane.

Off-nominal Inertial Multiplier of Conductive Wire

No significant differences have been found from the baseline case when the inertia multiplier of tether conductive part is changed from 3 (nominal) to 2.5 and 3.5.

A final in-plane angle slightly less than the baseline is reached when the multiplier is 2.5. Tension and in-plane motion of the mid-tether point are similar to the baseline.

On the other hand when the multiplier is 3.5, the deployment is similar to the baseline, though larger tension variations at the end suggest a larger final velocity. These variations and the associated peaks are within the desired bounds.

*Inertial Multiplier of Conductive Wire = 2.5*

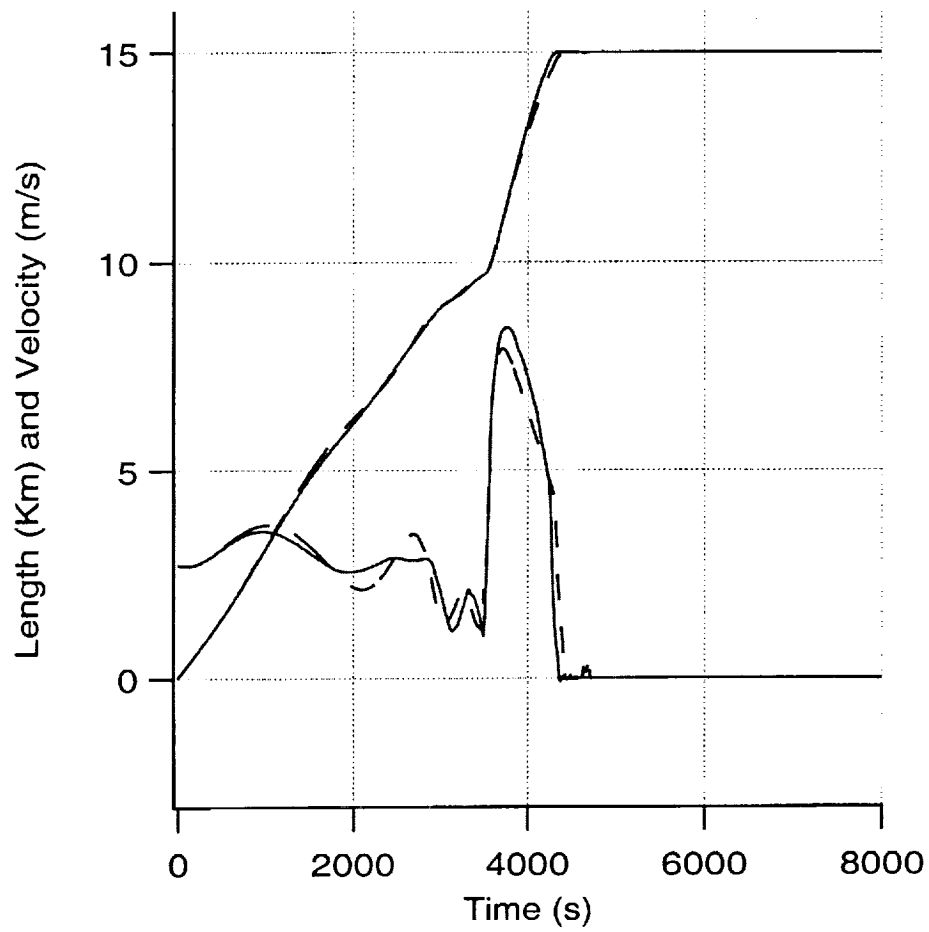


**Figure 37** Wire inertia multiplier = 2.5

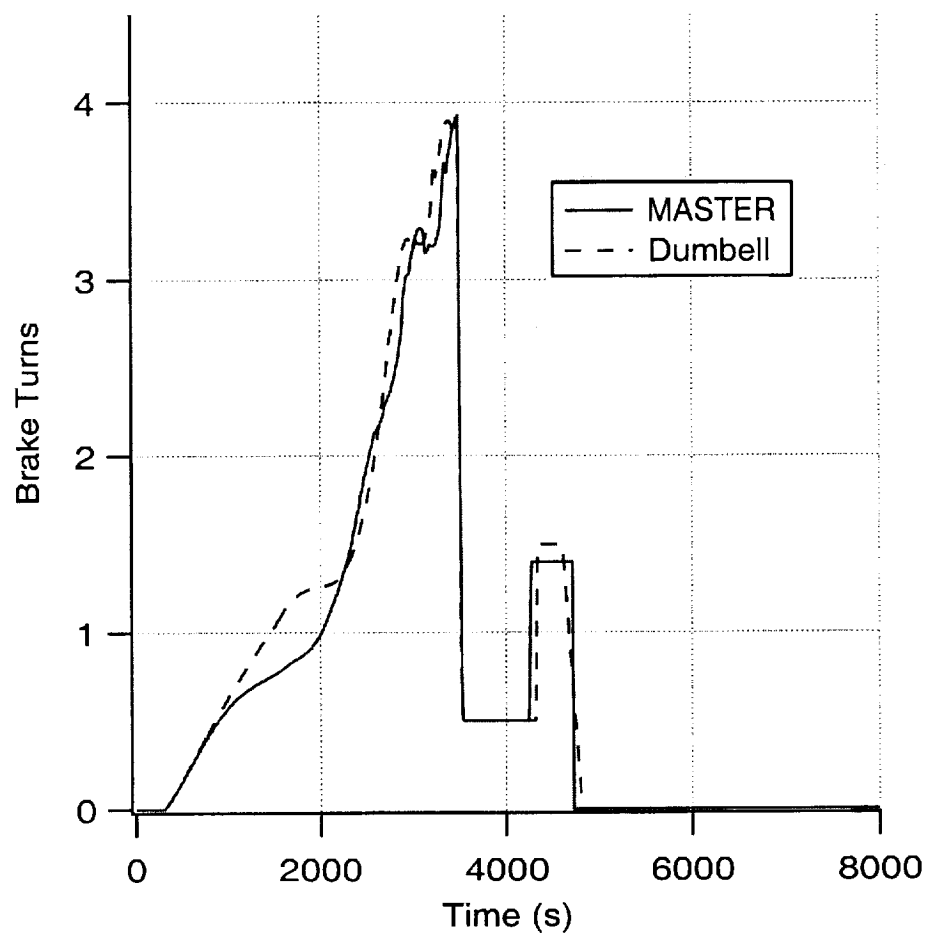
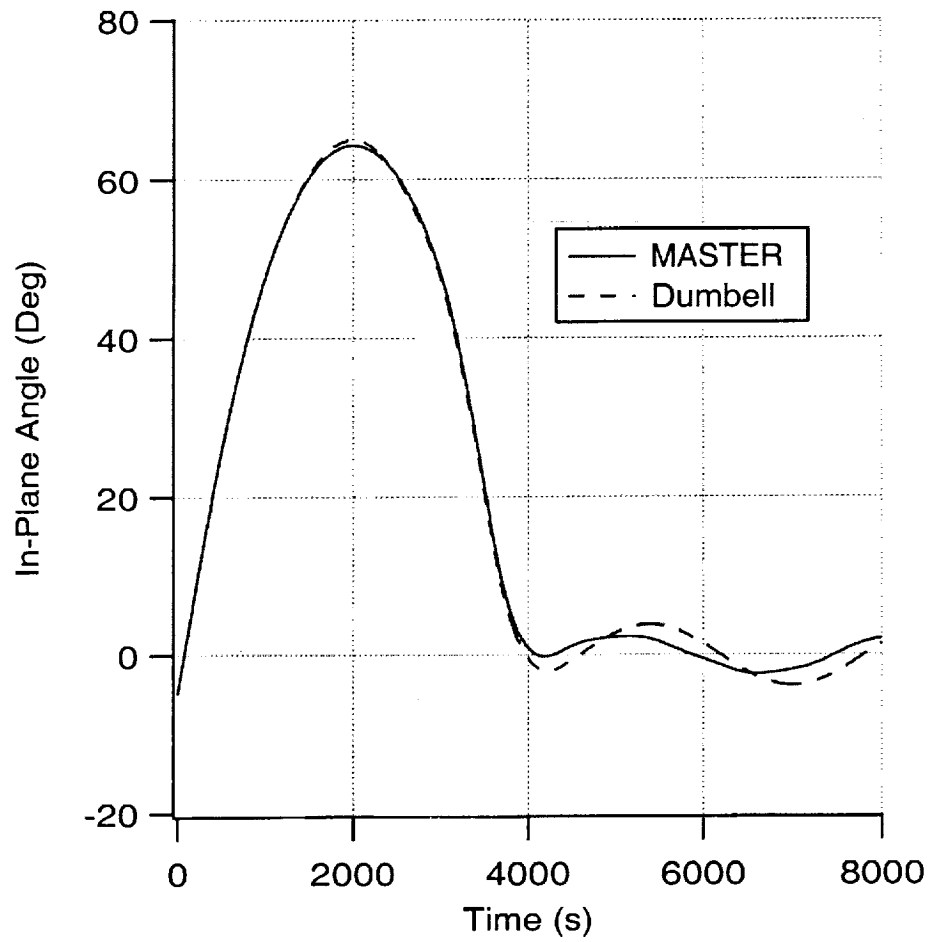
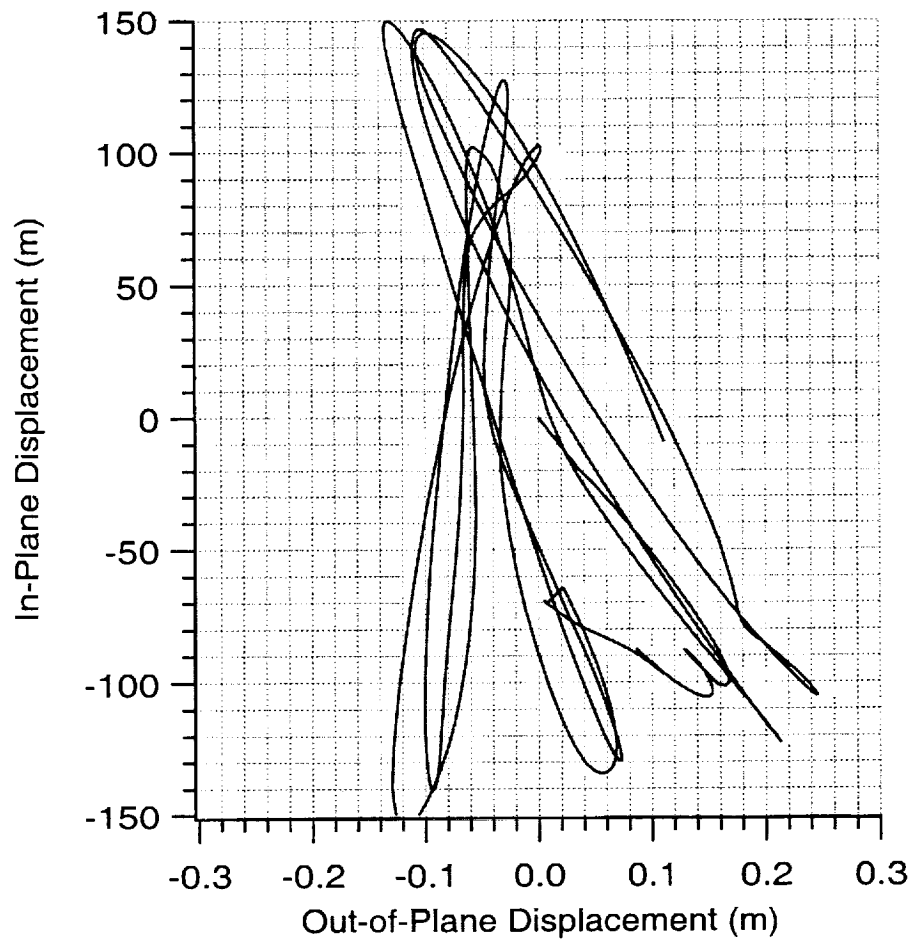


Figure 38 Wire inertia multiplier = 2.5



**Figure 39** Wire inertia multiplier = 2.5



**Figure 40** Wire inertia multiplier = 2.5

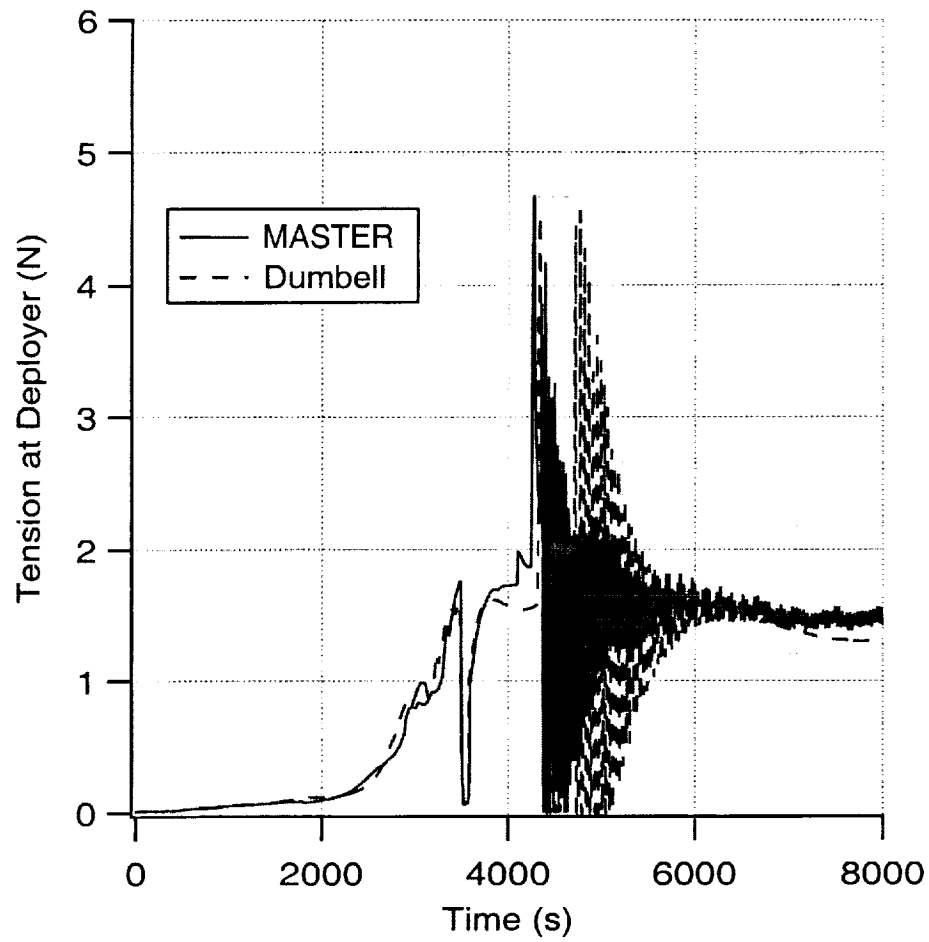


**Figure 41** Wire inertia multiplier = 2.5

*Inertial Multiplier of Conductive Wire = 3.5*

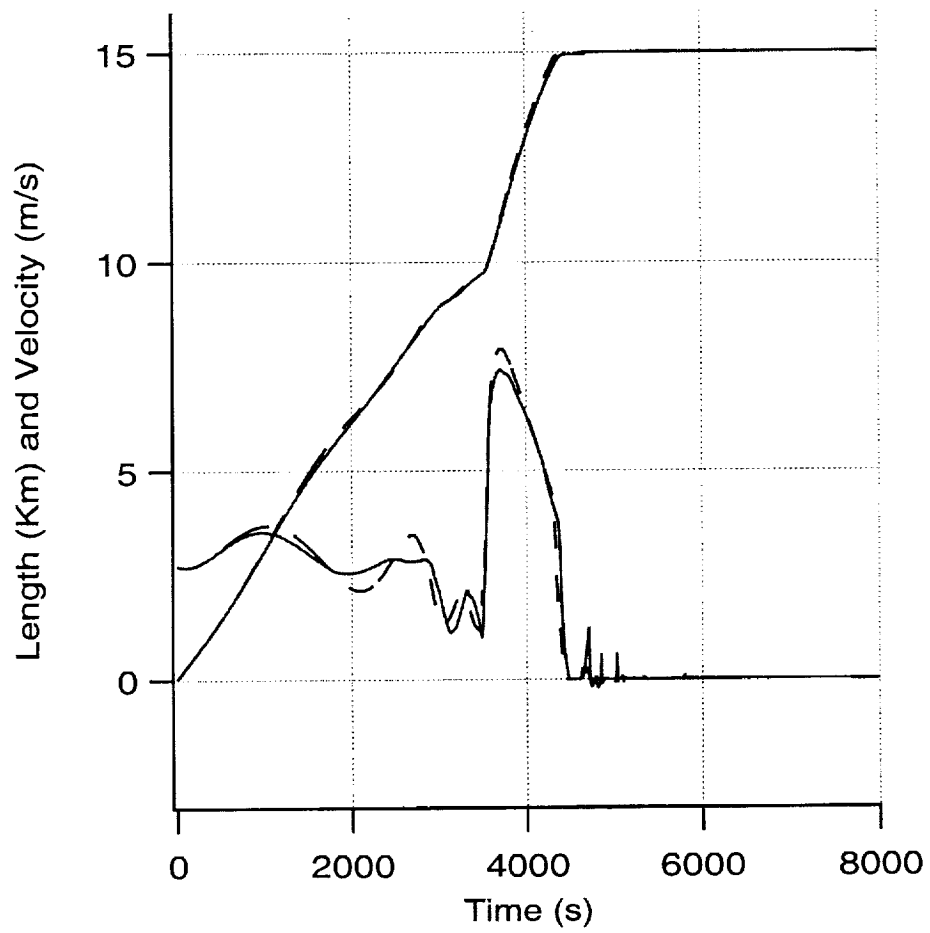


**Figure 42** Wire inertia multiplier = 3.5

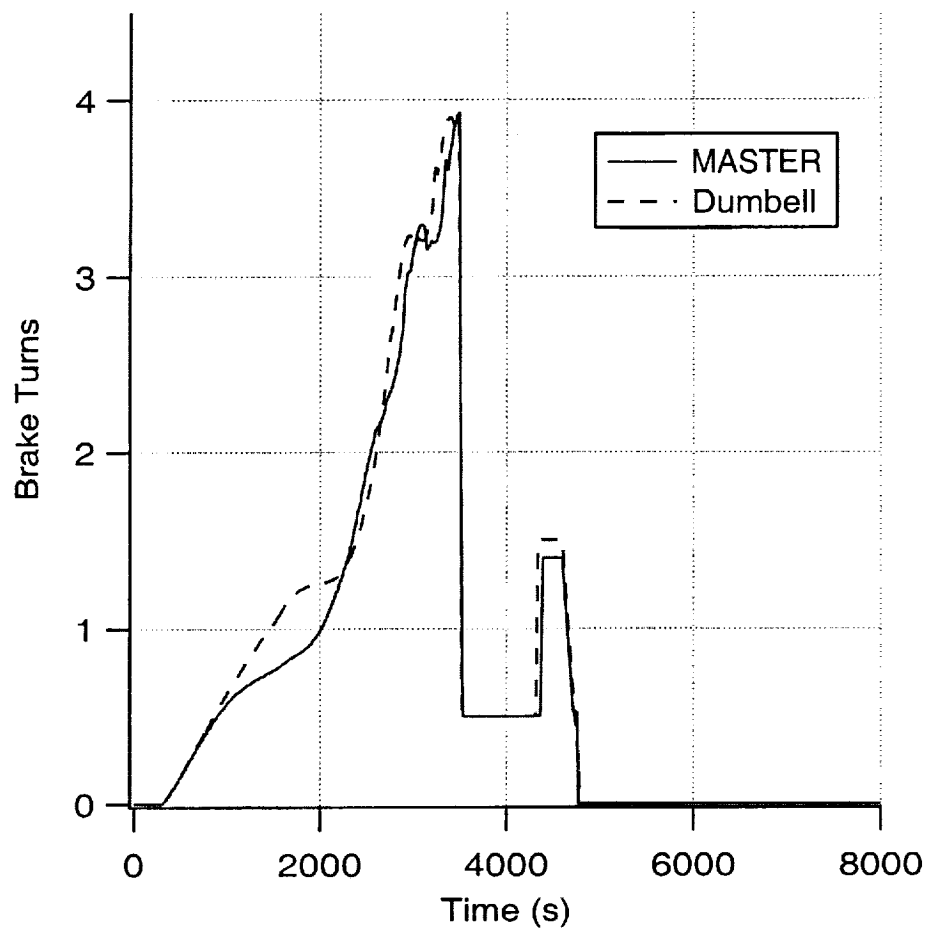


**Figure 43** Wire inertia multiplier = 3.5

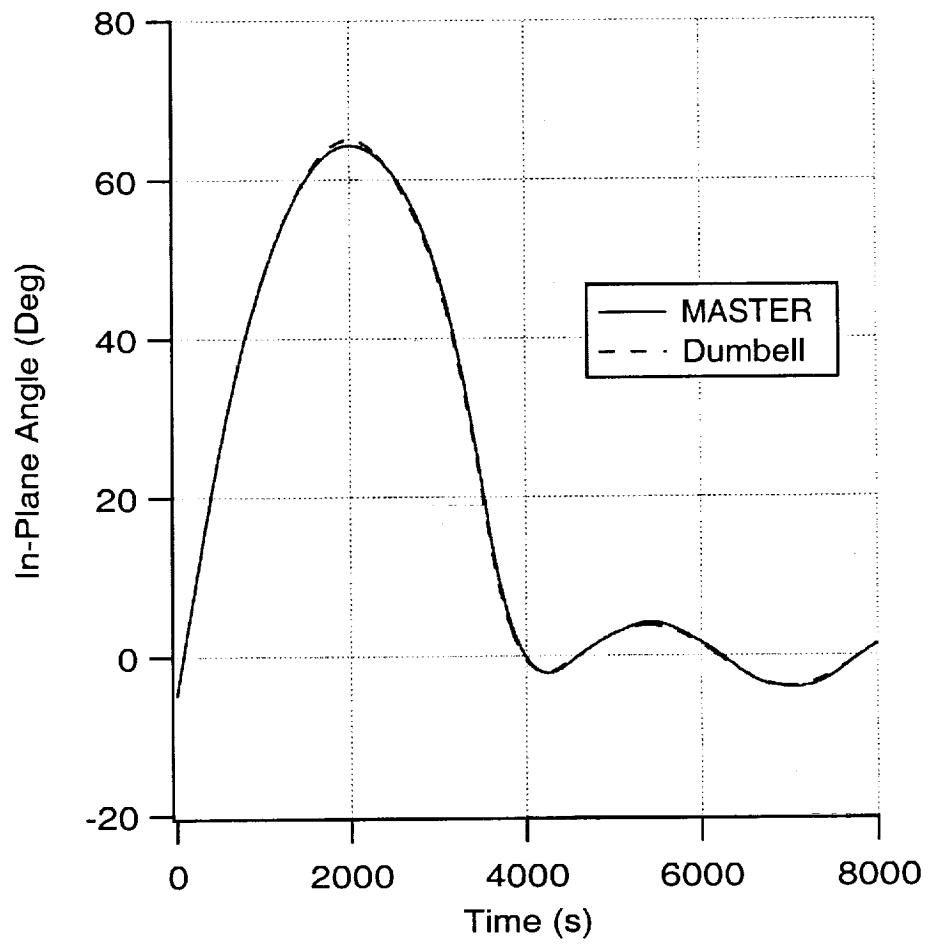


**Figure 44** Wire inertia multiplier = 3.5

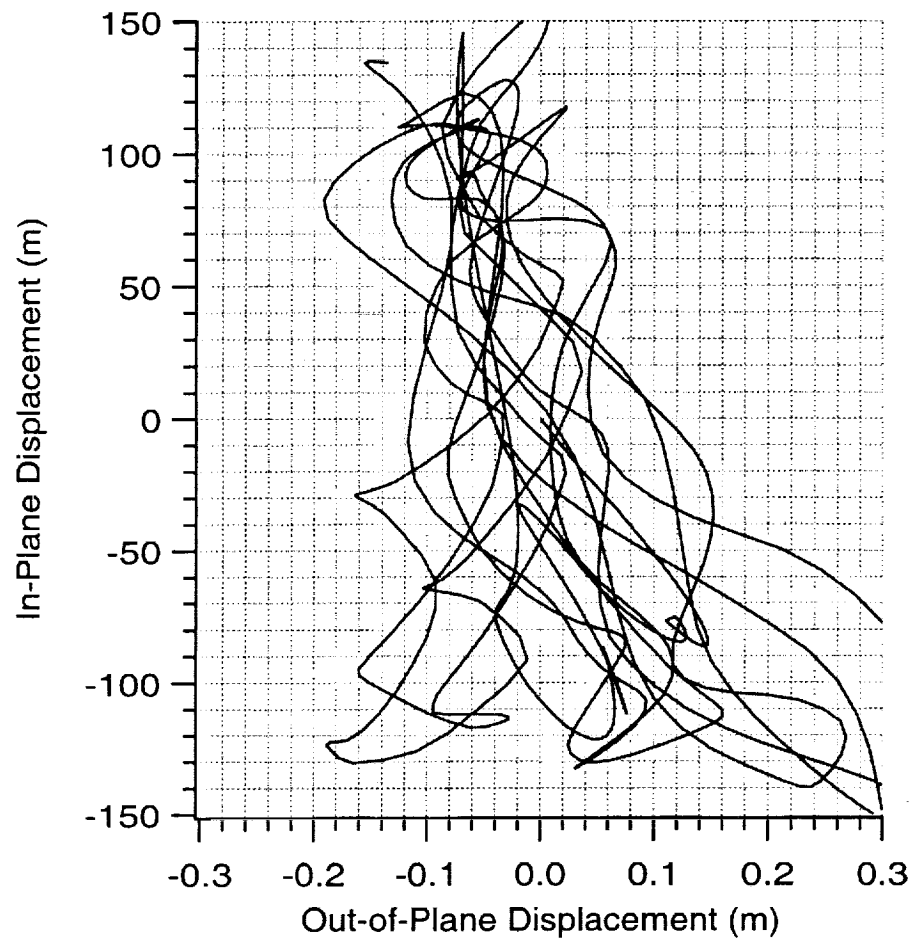


**Figure 45** Wire inertia multiplier = 3.5

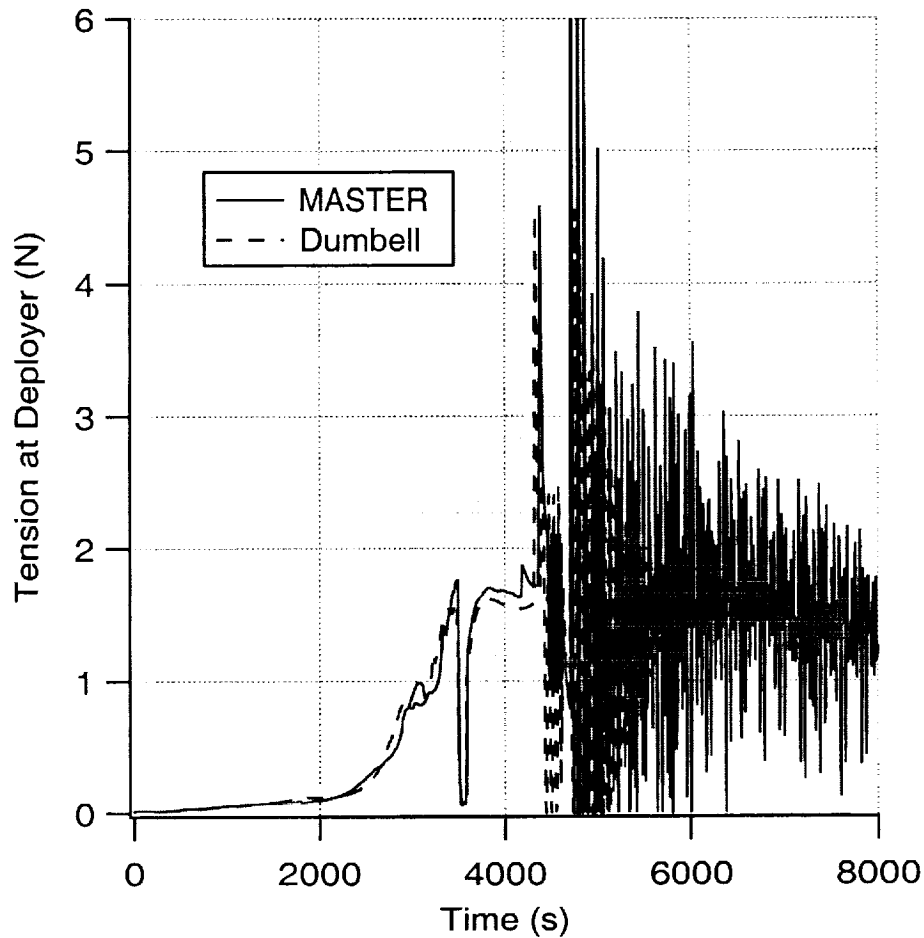


Figure 46 Wire inertia multiplier = 3.5

#### 4.4 Concluding Remarks

The simplified simulation code DUMBELL is adequate to describe the overall dynamics of ProSEDS during deployment. The more refined (and much more CPU intensive) MASTER code is strictly necessary to analyze particular features like the lateral (string-like) dynamics of the tether. Examples are deployment of the wire at very high velocity with consequent large bowing of the tether and the damping of the oscillations at the end of deployment due to tether rebounds and transfer of energy from the well-damped longitudinal modes to the lightly-damped lateral modes.

## **5. KALMAN FILTERS FOR MISSION ESTIMATION**

### **5.1 Introduction**

As part of the data analysis effort, SAO has focused on the following objectives:

- a. Characterization of the system Reentry (semi-major axis and rates)
- b. Estimation of the Average Current (for reentry and EM modeling)
- c. Estimation of Delta Rotation Rates (Magnetometer calibration and Instrument Readings)
- d. Estimation of Skip Rope Motion (produced by deployment and built up during mission)

Two extended Kalman Filter estimators have been developed to address the objectives.

### **5.2 Magnetometer data Kalman filter**

KAL Mag - Uses magnetometer data and a reference magnetic field (IGRF) to estimate:

- a. Bias, on each axis, due to uncalibrated residual magnetic fields and those generated during the flight from currents.
- b. Rotation rates of Delta stage (yaw rotation about the tether axis)
- c. Skip-rope motion (Frequency analysis and estimation of amplitude)

An FFT pre-processor estimates the yaw rate (highest amplitude) and one user-defined frequency (e.g. skip-rope frequency). A pre-calculated IGRF field data, inertial components and modulus, is supplied for the time readings of the magnetometer.

Each magnetometer component is decomposed into a constant bias and a series of sinusoids with known frequency and unknown random-walk amplitudes.

The software works in conjunction with the IGOR data analysis and display software package. It has been designed to process data in real-time, making it suitable during the ProSEDS flight. The program can also be run backwards in order to provide a smoothed estimate of the parameters in the post-processing phase.

The software is very robust and has been tested with SEDS-I data, where the constant bias affecting the magnetometer was calculated after the flight with a least-squares estimator. Moreover, SEDS-I reached a very low perigee (~180 km) and a FFT analysis revealed that the tether lateral modes had been excited to hundreds of meters. Once the skip-rope modulated by the Delta rotation is estimated, the amplitude can be computed by geometrical considerations. This part of the effort is still under study. The modeling of the process and measurement errors affect the calculation of the covariance. A normal distribution of the measurements, though simplified, seems appropriate for the effort.

We recommend an additional test by running SAO high-fidelity code MASTER and generating a magnetic field at the Delta stage due to the current cycle.

The estimated components of the bias are shown in Figure 47 and the estimated vs. measured magnetometer component (Y direction) is shown in Figure 48.

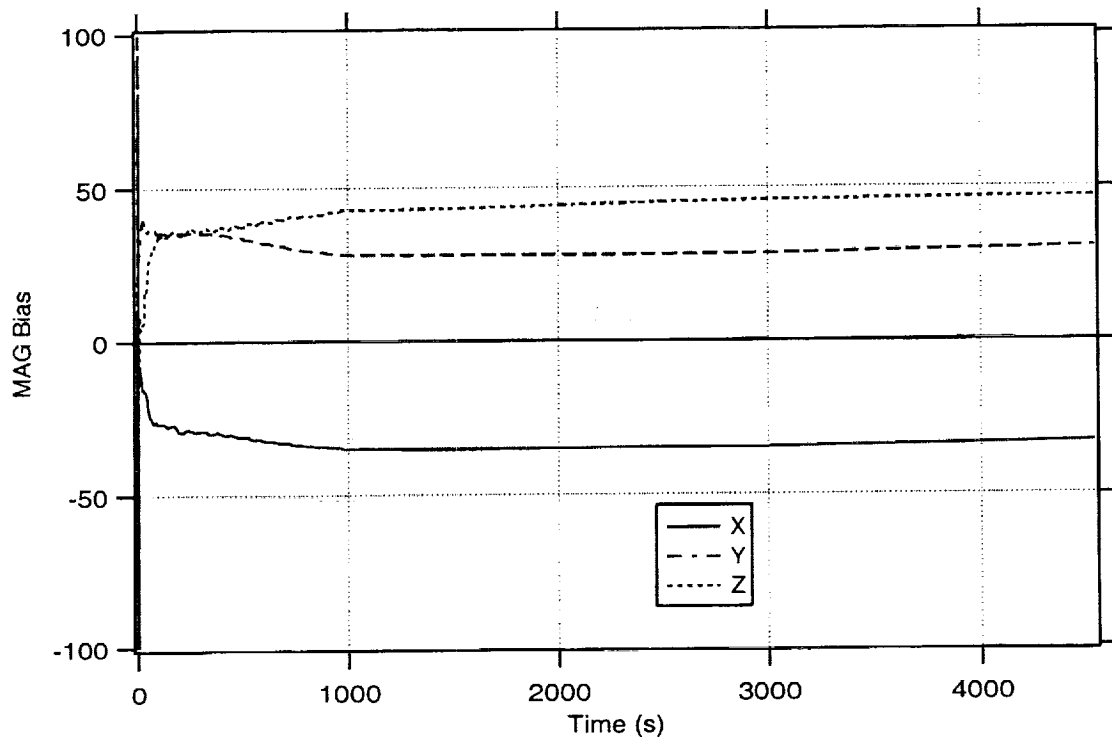


**Figure 47** Estimated Bias Components (SEDS-1 Flight Data)

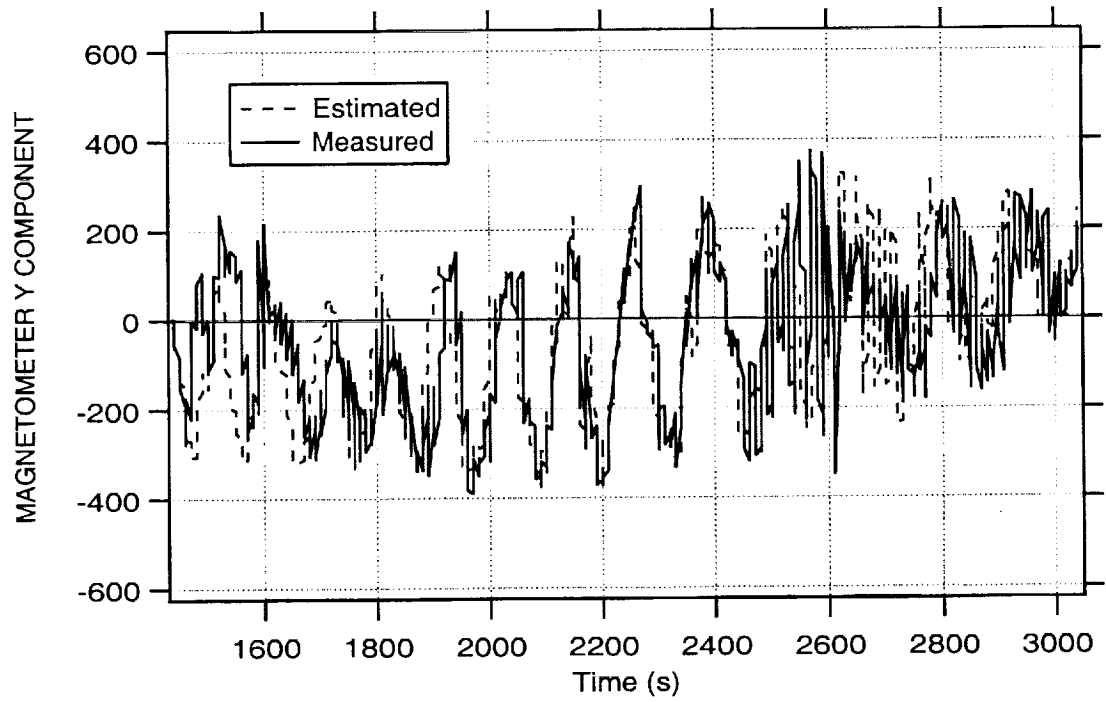


**Figure 48** Magnetometer Y Component - Estimated vs. Measured (SEDS-I Flight Data)

### 5.3 Position/current data Kalman filter

KAL\_Pos - Uses measured emf, current, position and velocity of Delta Stage to estimate:

- e. Semi-major axis and decay rate
- f. Average current
- g. Angle between local vertical and magnetic field.

GPS continuous observations of positions and velocity have been assumed during this phase. Ground-based tracking can also be used though the data would be sparsely distributed and the software should be modified accordingly. Another alternative is to check whether position-only information yield acceptable results. This possibility, however, has been briefly explored and needs further refinement.

The angle between the local vertical and the Earth's magnetic field is also estimated, because being part of the Lorentz force term, can yield information on the librations of the tether with respect to the local vertical.

The software assumes that the average current is a known fraction of the current measured at the Delta stage plus a small linear correction estimated by the filter.

All the parameters to be estimated are modeled as random-walk processes. An estimate of the magnitude of the magnetic field must be provided in input.

This software also runs on a Power Mac with a G3 processor and IGOR software for display and data analysis. Though robust, this filter needs an accurate set of initial conditions. The measurement and process errors are very sensitive to parameters' correlation so a more accurate modeling of the process could be necessary.

Data produced by MASTER simulations were used to test KAL\_Pos.

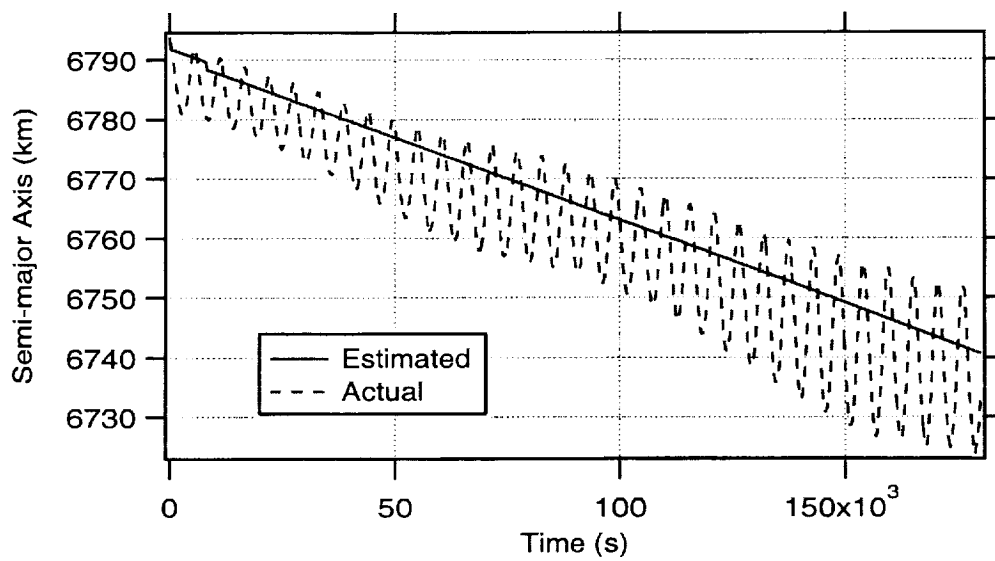


**Figure 49** Estimated vs. Actual Proseds Semi-major Axis (MASTER simulation)

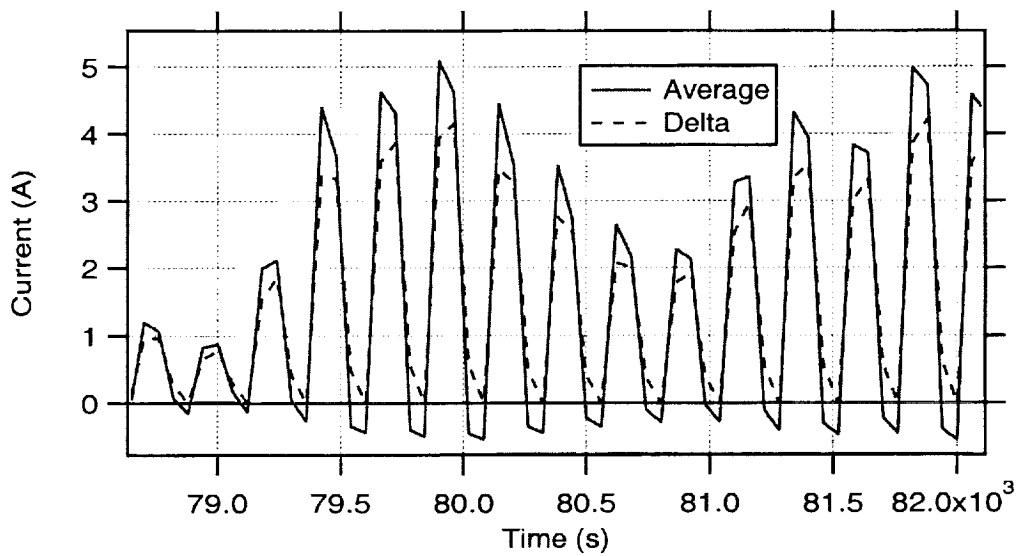


**Figure 50** Estimated Average vs. Current Measured at Delta (MASTER simulation)

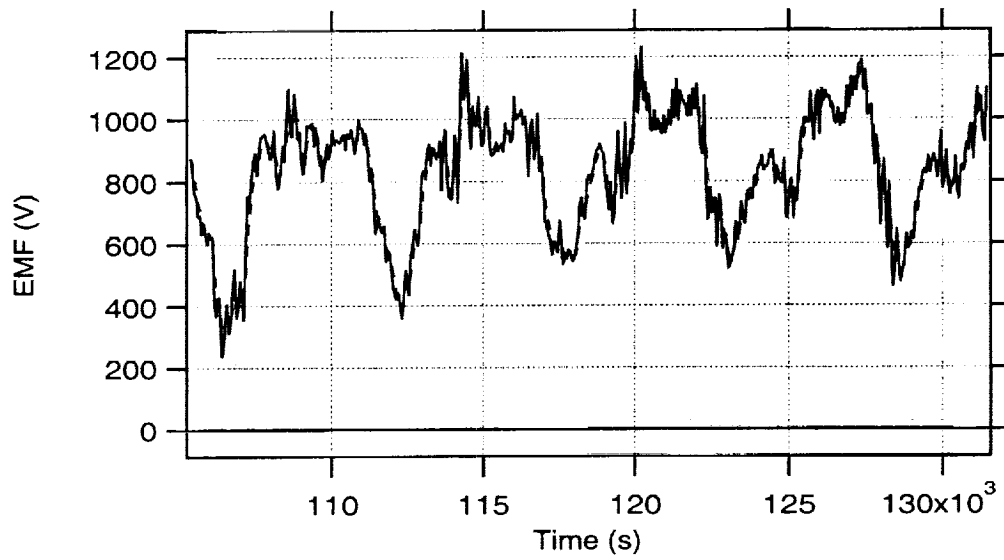


**Figure 51** Estimated Proseds EMF (MASTER simulation)

## 6. COMPARISON OF ED TETHERS AND ELECTRICAL THRUSTERS

### 6.1 Introduction

The basic figure of merit for a thruster is the ratio  $M_d/F\tau$ , which is the inverse of a velocity, and should be as small as possible<sup>9</sup>. Here,  $F$  is thrust,  $\tau$  is duration of thrusting, and  $M_d$  is dedicated mass. For electrical thrusters, which would be natural competitors of tethers,  $M_d$  is made of propellant mass  $\dot{m}_p\tau$  ( $\dot{m}_p \equiv$  propellant flow rate) and tankage and plumbing mass ( $\alpha\dot{m}_p\tau$ ); and from hardware related to the required electrical power  $W_e$ ,

$$M_d = \dot{m}_p\tau(1+\alpha) + \beta W_e. \quad (2)$$

Typically,  $\alpha$  is about 0.2, and  $\beta$  is about 6 kg/kW if just power processing unit and thruster need be considered and one order of magnitude greater if dedicated solar panels are required (Martinez-Sanchez and Pollard, 1998; Estes et al, 2000).

Introducing the specific velocity  $v_{sp}$  (specific impulse in velocity units, about 16 and 28 km/s for Hall and Ion thrusters respectively), one has  $\dot{m}_p = F/v_{sp}$  and  $W_e = Fv_{sp}/2\eta$  ( $\eta =$  thruster efficiency = 0.5-0.65), and arrives at

$$\frac{M_d}{F\tau} = \frac{1+\alpha}{v_{sp}} + \frac{\beta v_{sp}/2}{\tau\eta}. \quad (3)$$

Given a specific velocity, the ratio  $M_d/F\tau$  approaches a limit minimum for long thrust durations, with a characteristic time  $\tau \propto v_{sp}^2$ . Duration, however, may need be restricted by a number of reasons. For each maximum allowed  $\tau$ , there is an optimal specific velocity yielding a minimum in eqn. (3); as  $\tau$  is allowed to increase,  $v_{sp}(\text{opt})$  increases, resulting in a lower  $M_d/F\tau$  minimum. In addition, given a total (mission) impulse  $F\tau$ , a maximum allowed duration determines a lower bound for thrust  $F$ .

## 6.2 Comparisons

Let us compare the extended-mission mass requirements of some typical electrical thrusters with that of bare-tether thrusters chosen to have equivalent average thrust. There are two cases to consider: the case where a dedicated solar power system is required, which would be the case for any kind of electrical orbit-transfer vehicle (a space “tug”); and the case where the solar power system is already in place, with power available for thruster use, which might be the case for a Space Station drag-compensation system.

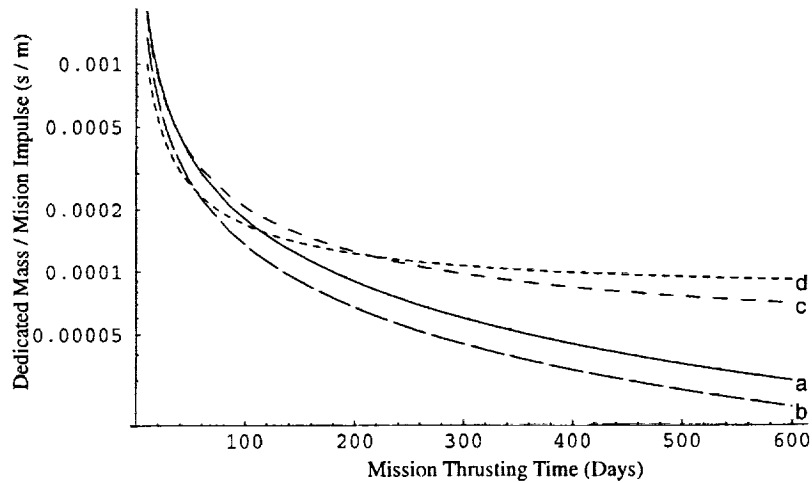


**Figure 52** Comparison of EDT (a, b) and Electrical Thrusters (c, d) With Dedicated Solar Power System

Figure 52 shows the case where a dedicated power system is required. It plots  $M_d/F\tau$  on a logarithmic scale for a range of mission (thrusting) times  $\tau$  of 10 to 600 days. All systems are taken to have  $\eta = 0.6$ . Curves c and d correspond to electrical thrusters of  $v_{sp} = 28$  and 16 km/s, respectively. The EDT systems were chosen to provide an average  $\eta$  of 0.6 over an altitude range of 300 to 800 km. Curve a is for a 30 kg tether (with  $\alpha_t = 2$ ) and  $W_e = 1$  kW. Curve b corresponds to the same tether but with  $W_e = 2$  kW; it is seen to be better than either electrical thruster for mission times of roughly 50 days or more, while the upper EDT (1 kW) curve needs a mission time of over 120 days achieve that. Both of these times are well within the time required for either type of system to boost a large payload from one low Earth orbit to another orbit several hundred kilometers higher.

Multiple orbit transfers would, of course, take proportionally longer, and the time to return to lower orbit would also have to be taken into account. We note that by only considering powered thrusting, we have, so to speak, forced the EDT to fight with one hand tied behind its back, since the EDT does not require external power to descend to a lower orbit. An orbit-transfer vehicle would need to return to a lower orbit after taking a spacecraft to a higher one, and an EDT system could, if so designed, descend more quickly than its electrical thruster counterpart. This is a topic for later development. There are implicit assumptions of system lifetimes and practicality of the systems which we note without further discussion.

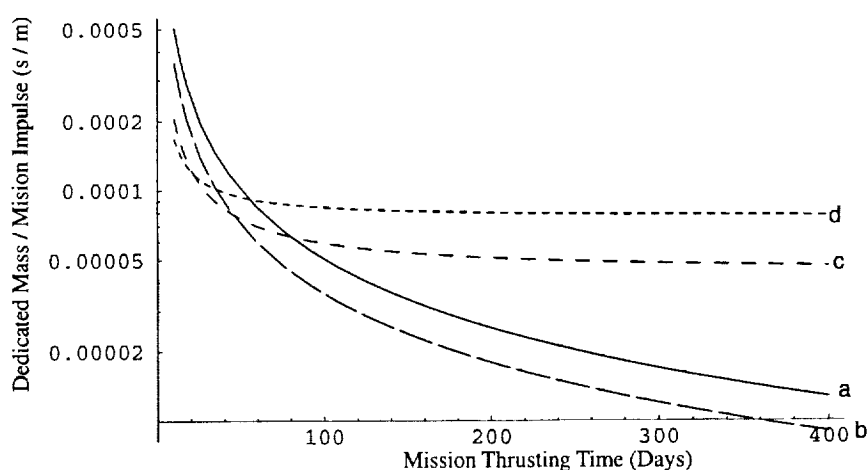


**Figure 53** Comparison of EDT (a, b) and Electrical Thrusters (c, d) Without Dedicated Solar Power System

As Figure 53 shows, for the case where abundant power is available without the need for a dedicated solar system, the EDT is clearly superior to the electrical thrusters for mission lifetimes somewhat shorter than for the case when a dedicated system is required. All parameters for the electrical thrusters c and d are the same as for Fig. 52, except for  $\beta$ . The tethers have a mass of 70 kg, and the assumed operating power is 5 kW for curve a and 10 kW for curve b. Thus, as previously noted (Estes et al., 2000), EDT would be attractive for International Space Station (ISS) reboost, assuming power were available from the Station.

### 6.3 Conclusions

In terms of total mass required for the mission, EDT thrusters are superior to electrical thrusters for mission thrusting times of 50-100 days or more both in the case of dedicated solar panels and the case when power is available without the need for a dedicated system. The advantage becomes greater as the mission time increases because of the comparatively insignificant use of gas by the EDT systems. Since an EDT tug would require no electrical power to descend, one could be designed to improve the mass to mission impulse ratio by descending at a rate faster than it ascends in the electrically powered mode, thus increasing its advantage over electrical thrusters.

## **7. DELIVERY OF INTERACTIVE SOFTWARE FOR ED TETHERS**

### **7.1 Delivered Software**

An interactive computer program for the Windows operating system that allows the user to obtain a quick estimate of the performance obtainable by bare tether propulsion systems for various applications in low Earth orbit, for both orbit raising and lowering, was delivered to NASA/MSFC in December 2001. The use of the software was demonstrated by Robert Estes to NASA/MSFC personnel in January 2001 to the satisfaction of the customer.

### **7.2 Brief Description**

The software was designed with the aim of allowing for experimentation in tether system design with quick feedback to the user on how changing various system parameters (length, collecting surface, tether material, tether geometry, available power, etc.) affect system performance under various environmental conditions. In addition, the user can use the software to get a good idea how the system would perform for different missions in which the environmental conditions vary during the mission, as, for example, the average plasma density decreases when the system moves above the F-layer of the ionosphere. The window in which the user defines the EDT system is shown below in Figure 47 for a typical deboosting operation and in Figure 48 for a typical boosting operation.

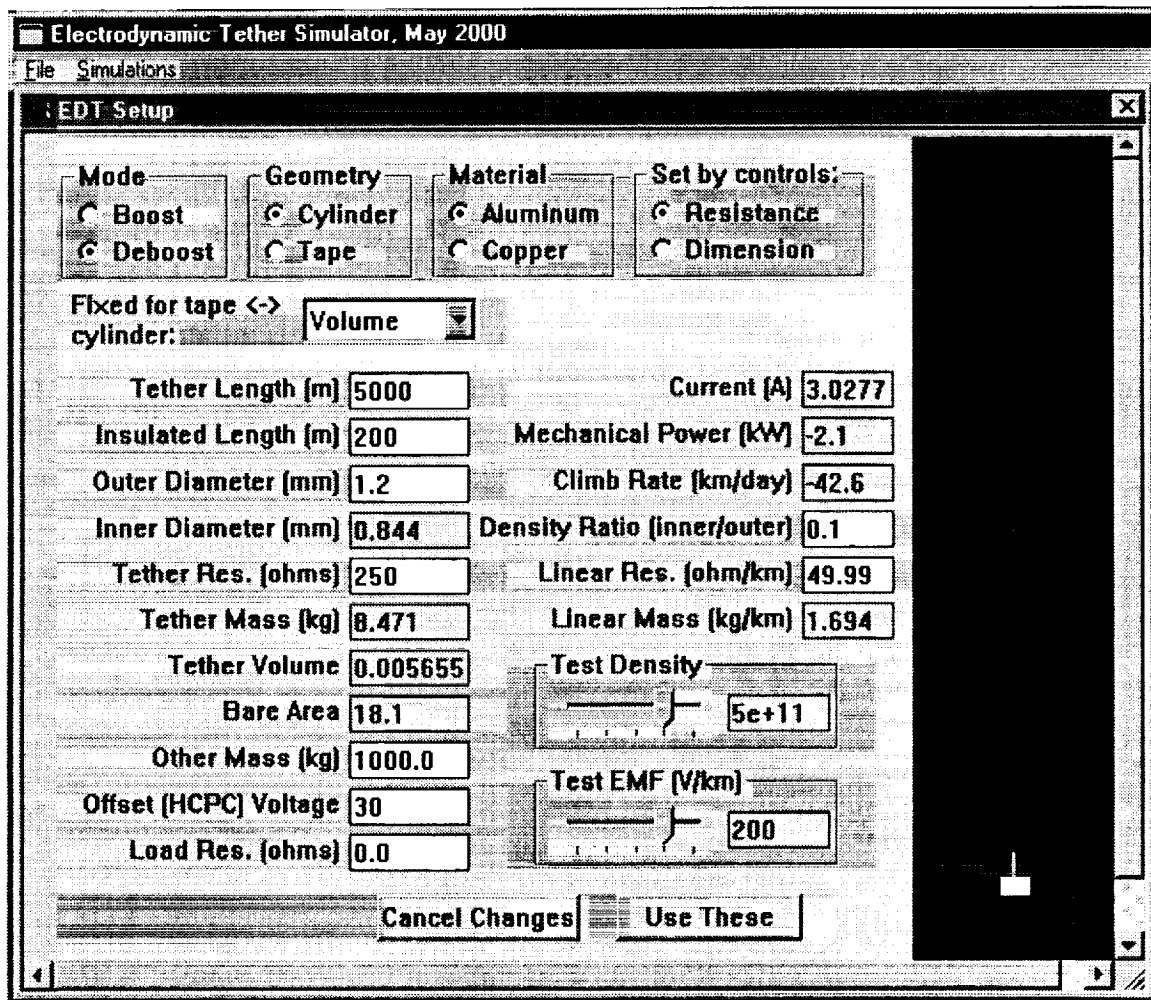


**Figure 54** The simulation setup window for defining the system.

Even taken by itself, this interactive window can be a useful tool for system design, since the test densities and motional emf values can be varied over a wide range. The user can take the simulation further, however, by actually following the progress of the system with a payload as it moves from one orbit to another. In this case, the starting orbit and date are needed, and there is another setup window that allows the user to specify these. This is shown in Figure 48. The orbital parameters may be specified in more detail (full Kepler element set) if desired, but the set shown in the figure is adequate in most cases for getting a good idea of system performance.

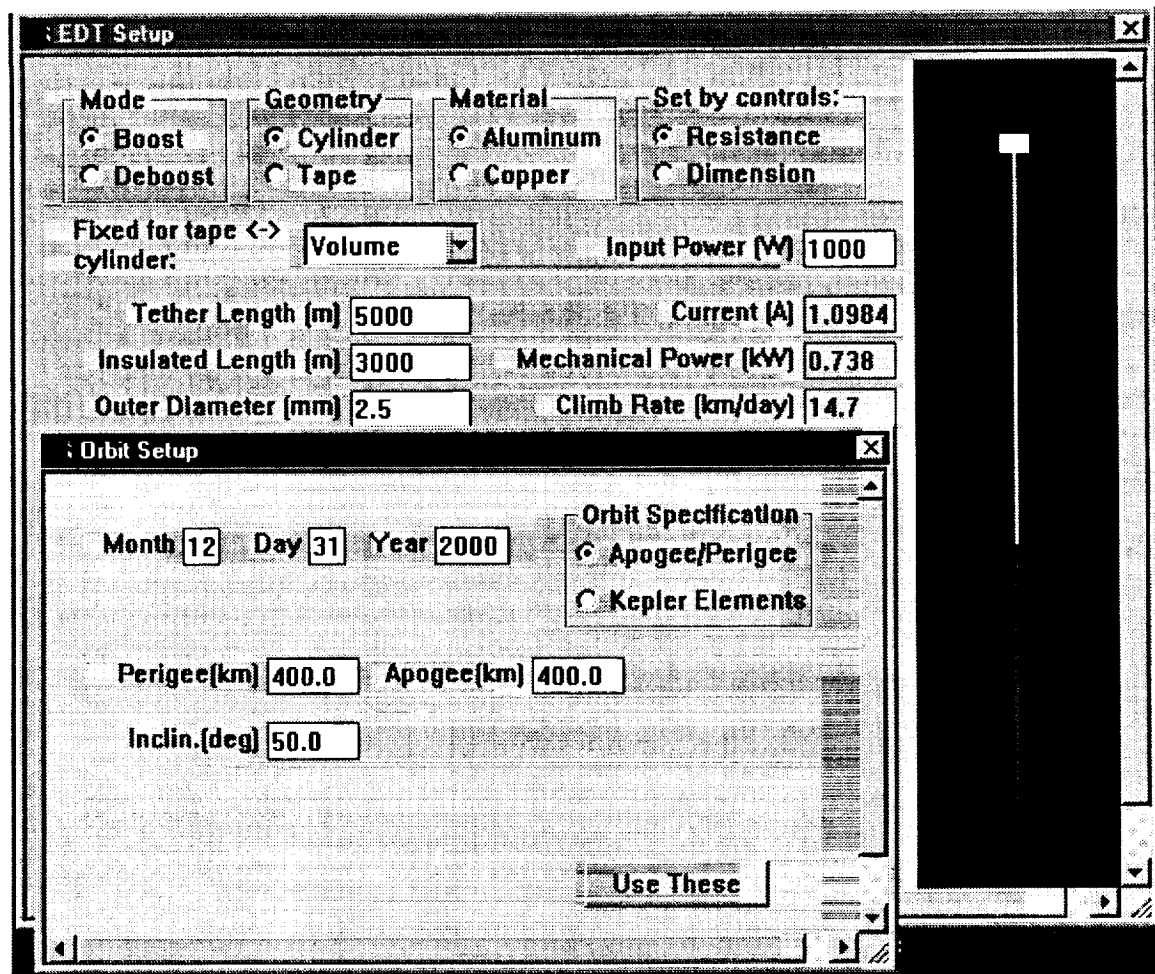


**Figure 55** Starting orbit setup window with boost system setup in background.

Based on the parameters selected the software can run simulations of an EDT (assumed aligned with the local vertical) that climbs or descend starting from a specified orbit. The simulation is done in the following way. Two complete revolutions are made starting with the input initial orbit, and the average climb rate, which varies with the plasma density and motional emf encountered along the orbit, is calculated in this period. This rate is used to advance the system to an orbit that is higher by a delta specified by the user and the process is repeated at intervals of delta-km until the desired altitude is reached. Multiple simulation runs can be made and shown on the same plot to compare different systems or the performance of the same system under different conditions (starting orbit and/or date). The results can be displayed either as the heights of the apogee and perigee vs. time or as the semi-major axis vs. time. For additional details see the Annual Report #1 of this grant.

## APPENDIX A

### Reference Table for ProSEDS deployment control law (Ref#55)

Date: June 1, 2001  
Author: E.C. Lorenzini (SAO)  
Subject: Reference table Ref#55

Note: The slowdown maneuver has been included in the reference table. The slowdown maneuver (last 205-m of tether) is controlled by the software under normal operating conditions. The slowdown maneuver is read from the reference table only for backup mode of operation.

TC	TCR	Brake Time
Turn	TC/s	BTurn s
1	3.836 0	0
31	3.828 0	8
62	3.82 0	16
92	3.814 0	24
123	3.808 0	32
153	3.802 0	40
184	3.798 0	48
214	3.793 0	56
244	3.79 0	64
275	3.787 0	72
305	3.785 0	80
335	3.783 0	88
366	3.782 0	96
396	3.782 0	104
426	3.782 0	112
456	3.783 0	120
487	3.785 0	128
517	3.787 0	136
547	3.789 0	144
578	3.793 0	152
608	3.797 0	160
638	3.801 0	168
669	3.806 0	176
699	3.812 0	184
730	3.818 0	192
760	3.825 0	200
791	3.832 0	208
822	3.84 0	216
852	3.848 0	224
883	3.857 0	232
914	3.867 0	240
945	3.877 0	248
976	3.887 0	256
1007	3.898 0	264
1038	3.91 0	272
1070	3.921 0	280
1101	3.934 0	288
1133	3.947 0	296
1164	3.96 0.002	304

## Annual Report #2, NASA Grant NAG8-1605

1196	3.973	0.008	312
1228	3.987	0.014	320
1260	4.001	0.022	328
1292	4.016	0.03	336
1324	4.03	0.038	344
1356	4.045	0.047	352
1389	4.06	0.056	360
1421	4.075	0.065	368
1454	4.091	0.074	376
1487	4.106	0.084	384
1520	4.122	0.094	392
1553	4.138	0.104	400
1586	4.154	0.114	408
1619	4.17	0.124	416
1653	4.186	0.135	424
1686	4.202	0.145	432
1720	4.219	0.156	440
1754	4.235	0.166	448
1788	4.251	0.177	456
1822	4.268	0.188	464
1856	4.284	0.199	472
1890	4.301	0.21	480
1925	4.317	0.221	488
1959	4.333	0.231	496
1994	4.35	0.242	504
2029	4.366	0.253	512
2064	4.382	0.265	520
2099	4.398	0.276	528
2134	4.415	0.287	536
2170	4.43	0.298	544
2205	4.446	0.309	552
2241	4.462	0.32	560
2277	4.477	0.331	568
2313	4.493	0.342	576
2349	4.508	0.353	584
2385	4.523	0.364	592
2421	4.537	0.374	600
2457	4.552	0.385	608
2494	4.566	0.396	616
2530	4.58	0.407	624
2567	4.594	0.417	632
2604	4.608	0.428	640
2641	4.621	0.439	648
2678	4.634	0.449	656
2715	4.647	0.46	664
2752	4.66	0.47	672
2790	4.672	0.48	680
2827	4.684	0.491	688
2864	4.695	0.501	696
2902	4.706	0.511	704
2940	4.717	0.521	712
2977	4.728	0.531	720
3015	4.738	0.54	728
3053	4.748	0.55	736
3091	4.757	0.56	744
3129	4.766	0.569	752
3168	4.775	0.579	760
3206	4.784	0.588	768

# Annual Report #2, NASA Grant NAG8-1605

3244	4.791	0.597	776
3283	4.799	0.606	784
3321	4.806	0.615	792
3359	4.813	0.624	800
3398	4.819	0.632	808
3436	4.825	0.641	816
3475	4.831	0.649	824
3514	4.836	0.658	832
3552	4.841	0.666	840
3591	4.845	0.674	848
3630	4.849	0.682	856
3669	4.853	0.689	864
3708	4.856	0.697	872
3747	4.859	0.704	880
3785	4.861	0.712	888
3824	4.863	0.719	896
3863	4.865	0.726	904
3902	4.866	0.732	912
3941	4.867	0.739	920
3980	4.867	0.746	928
4019	4.867	0.752	936
4058	4.866	0.758	944
4097	4.866	0.764	952
4136	4.864	0.77	960
4175	4.863	0.775	968
4214	4.861	0.781	976
4252	4.858	0.786	984
4291	4.856	0.791	992
4330	4.853	0.796	1000
4369	4.849	0.801	1008
4408	4.845	0.805	1016
4446	4.841	0.81	1024
4485	4.837	0.815	1032
4524	4.832	0.819	1040
4562	4.827	0.823	1048
4601	4.822	0.827	1056
4640	4.816	0.831	1064
4678	4.81	0.835	1072
4717	4.804	0.839	1080
4755	4.797	0.842	1088
4793	4.79	0.846	1096
4832	4.783	0.849	1104
4870	4.776	0.852	1112
4908	4.768	0.856	1120
4946	4.76	0.859	1128
4984	4.752	0.862	1136
5022	4.743	0.865	1144
5060	4.734	0.868	1152
5098	4.726	0.871	1160
5136	4.716	0.873	1168
5173	4.707	0.876	1176
5211	4.697	0.879	1184
5249	4.688	0.881	1192
5286	4.678	0.883	1200
5323	4.668	0.886	1208
5361	4.657	0.888	1216
5398	4.647	0.891	1224
5435	4.636	0.893	1232

## Annual Report #2, NASA Grant NAG8-1605

5472	4.625	0.895	1240
5509	4.614	0.897	1248
5546	4.603	0.899	1256
5583	4.592	0.901	1264
5619	4.581	0.903	1272
5656	4.569	0.906	1280
5692	4.558	0.908	1288
5729	4.546	0.91	1296
5765	4.534	0.912	1304
5801	4.522	0.914	1312
5838	4.51	0.916	1320
5874	4.498	0.918	1328
5910	4.486	0.92	1336
5945	4.474	0.922	1344
5981	4.462	0.924	1352
6017	4.45	0.925	1360
6052	4.437	0.928	1368
6088	4.425	0.93	1376
6123	4.413	0.932	1384
6158	4.401	0.934	1392
6194	4.388	0.936	1400
6229	4.376	0.938	1408
6264	4.364	0.94	1416
6298	4.351	0.942	1424
6333	4.339	0.945	1432
6368	4.327	0.947	1440
6402	4.315	0.949	1448
6437	4.303	0.952	1456
6471	4.291	0.954	1464
6506	4.278	0.957	1472
6540	4.267	0.96	1480
6574	4.255	0.962	1488
6608	4.243	0.965	1496
6642	4.231	0.968	1504
6675	4.22	0.971	1512
6709	4.208	0.974	1520
6743	4.196	0.977	1528
6776	4.185	0.98	1536
6810	4.174	0.983	1544
6843	4.163	0.987	1552
6876	4.152	0.99	1560
6909	4.141	0.994	1568
6943	4.13	0.998	1576
6976	4.12	1.001	1584
7008	4.109	1.005	1592
7041	4.099	1.009	1600
7074	4.089	1.014	1608
7107	4.079	1.018	1616
7139	4.069	1.023	1624
7172	4.06	1.027	1632
7204	4.05	1.032	1640
7237	4.041	1.037	1648
7269	4.032	1.042	1656
7301	4.023	1.046	1664
7333	4.015	1.051	1672
7365	4.006	1.056	1680
7398	3.998	1.061	1688
7429	3.99	1.066	1696

## Annual Report #2, NASA Grant NAG8-1605

7461	3.982	1.071	1704
7493	3.975	1.076	1712
7525	3.968	1.082	1720
7557	3.961	1.087	1728
7588	3.954	1.092	1736
7620	3.948	1.097	1744
7651	3.942	1.103	1752
7683	3.936	1.108	1760
7714	3.93	1.114	1768
7746	3.925	1.119	1776
7777	3.92	1.125	1784
7809	3.916	1.13	1792
7840	3.912	1.136	1800
7871	3.904	1.142	1808
7902	3.897	1.147	1816
7933	3.89	1.153	1824
7965	3.883	1.159	1832
7996	3.877	1.165	1840
8027	3.871	1.171	1848
8057	3.865	1.177	1856
8088	3.86	1.183	1864
8119	3.855	1.19	1872
8150	3.851	1.196	1880
8181	3.847	1.202	1888
8212	3.843	1.209	1896
8242	3.84	1.215	1904
8273	3.838	1.222	1912
8304	3.835	1.228	1920
8335	3.834	1.235	1928
8365	3.832	1.242	1936
8396	3.831	1.248	1944
8426	3.831	1.255	1952
8457	3.831	1.262	1960
8488	3.832	1.269	1968
8518	3.833	1.276	1976
8549	3.834	1.283	1984
8580	3.837	1.291	1992
8610	3.839	1.298	2000
8641	3.842	1.306	2008
8672	3.846	1.313	2016
8703	3.85	1.321	2024
8734	3.855	1.328	2032
8764	3.86	1.336	2040
8795	3.866	1.344	2048
8826	3.873	1.352	2056
8857	3.88	1.36	2064
8888	3.887	1.368	2072
8920	3.896	1.376	2080
8951	3.904	1.384	2088
8982	3.914	1.393	2096
9013	3.924	1.401	2104
9045	3.934	1.41	2112
9076	3.945	1.418	2120
9108	3.957	1.427	2128
9140	3.969	1.436	2136
9171	3.982	1.445	2144
9203	3.996	1.454	2152
9235	4.01	1.463	2160

# Annual Report #2, NASA Grant NAG8-1605

9267	4.025	1.472	2168
9300	4.04	1.481	2176
9332	4.056	1.491	2184
9365	4.073	1.5	2192
9397	4.09	1.51	2200
9430	4.108	1.52	2208
9463	4.127	1.529	2216
9496	4.146	1.539	2224
9529	4.165	1.549	2232
9563	4.186	1.56	2240
9596	4.207	1.57	2248
9630	4.228	1.58	2256
9664	4.25	1.591	2264
9698	4.273	1.601	2272
9732	4.296	1.612	2280
9767	4.32	1.623	2288
9801	4.344	1.634	2296
9836	4.369	1.645	2304
9871	4.395	1.657	2312
9907	4.421	1.669	2320
9942	4.447	1.682	2328
9978	4.474	1.695	2336
10014	4.502	1.709	2344
10050	4.529	1.724	2352
10086	4.557	1.738	2360
10123	4.585	1.754	2368
10160	4.613	1.77	2376
10196	4.641	1.787	2384
10234	4.67	1.804	2392
10271	4.698	1.821	2400
10309	4.727	1.839	2408
10347	4.755	1.858	2416
10385	4.783	1.877	2424
10423	4.81	1.896	2432
10462	4.838	1.916	2440
10501	4.865	1.936	2448
10540	4.892	1.957	2456
10579	4.918	1.978	2464
10618	4.944	1.999	2472
10658	4.969	2.021	2480
10698	4.993	2.043	2488
10738	5.017	2.066	2496
10778	5.04	2.089	2504
10819	5.062	2.112	2512
10859	5.084	2.136	2520
10900	5.104	2.16	2528
10941	5.123	2.184	2536
10982	5.141	2.209	2544
11023	5.158	2.234	2552
11064	5.173	2.259	2560
11106	5.188	2.285	2568
11148	5.201	2.31	2576
11189	5.212	2.336	2584
11231	5.222	2.362	2592
11273	5.23	2.389	2600
11315	5.237	2.416	2608
11357	5.242	2.442	2616
11399	5.246	2.47	2624

Annual Report #2, NASA Grant NAG8-1605

11440	5.248	2.497	2632
11482	5.247	2.524	2640
11524	5.245	2.552	2648
11566	5.241	2.58	2656
11608	5.236	2.607	2664
11650	5.228	2.635	2672
11692	5.218	2.663	2680
11733	5.206	2.692	2688
11775	5.192	2.72	2696
11817	5.176	2.748	2704
11858	5.158	2.777	2712
11899	5.137	2.805	2720
11940	5.115	2.834	2728
11981	5.09	2.862	2736
12022	5.064	2.89	2744
12062	5.035	2.919	2752
12102	5.004	2.947	2760
12142	4.971	2.976	2768
12182	4.936	3.004	2776
12221	4.899	3.032	2784
12260	4.859	3.061	2792
12299	4.818	3.089	2800
12337	4.775	3.117	2808
12375	4.73	3.144	2816
12413	4.684	3.172	2824
12450	4.635	3.2	2832
12487	4.585	3.227	2840
12523	4.534	3.254	2848
12559	4.48	3.281	2856
12595	4.426	3.308	2864
12630	4.37	3.335	2872
12665	4.312	3.361	2880
12699	4.254	3.387	2888
12733	4.194	3.413	2896
12766	4.134	3.439	2904
12799	4.072	3.464	2912
12832	4.01	3.489	2920
12863	3.947	3.514	2928
12895	3.884	3.538	2936
12926	3.821	3.562	2944
12956	3.757	3.585	2952
12986	3.693	3.609	2960
13015	3.63	3.631	2968
13044	3.566	3.654	2976
13072	3.503	3.676	2984
13100	3.44	3.698	2992
13127	3.378	3.719	3000
13154	3.317	3.741	3008
13180	3.256	3.762	3016
13206	3.196	3.782	3024
13231	3.137	3.803	3032
13256	3.079	3.823	3040
13281	3.022	3.843	3048
13304	2.966	3.863	3056
13328	2.912	3.882	3064
13351	2.859	3.901	3072
13374	2.808	3.92	3080
13396	2.758	3.938	3088

## Annual Report #2, NASA Grant NAG8-1605

13418	2.71	3.957	3096
13439	2.664	3.974	3104
13460	2.62	3.992	3112
13481	2.578	4.009	3120
13502	2.538	4.026	3128
13522	2.5	4.043	3136
13542	2.465	4.06	3144
13561	2.432	4.076	3152
13581	2.401	4.092	3160
13600	2.373	4.107	3168
13619	2.347	4.122	3176
13637	2.324	4.137	3184
13656	2.304	4.152	3192
13674	2.287	4.167	3200
13692	2.273	4.18	3208
13711	2.262	4.194	3216
13729	2.253	4.208	3224
13747	2.248	4.221	3232
13765	2.246	4.234	3240
13783	2.245	4.246	3248
13801	2.245	4.259	3256
13819	2.247	4.27	3264
13836	2.251	4.282	3272
13854	2.256	4.293	3280
13873	2.262	4.304	3288
13891	2.27	4.315	3296
13909	2.28	4.326	3304
13927	2.292	4.336	3312
13946	2.305	4.345	3320
13964	2.319	4.355	3328
13983	2.336	4.364	3336
14002	2.353	4.373	3344
14020	2.373	4.381	3352
14039	2.393	4.389	3360
14059	2.416	4.397	3368
14078	2.44	4.405	3376
14098	2.465	4.412	3384
14117	2.491	4.419	3392
14138	2.519	4.426	3400
14158	2.548	4.432	3408
14178	2.579	4.438	3416
14199	2.611	4.444	3424
14220	2.643	4.449	3432
14241	2.677	4.454	3440
14263	2.707	4.459	3448
14287	3.223	0.5	3456
14316	4.126	0.5	3464
14352	4.953	0.5	3472
14395	5.783	0.5	3480
14445	6.615	0.5	3488
14501	7.447	0.5	3496
14564	8.279	0.5	3504
14634	9.109	0.5	3512
14710	9.936	0.5	3520
14779	8.559	0.5	3528
14850	9.01	0.5	3536
14924	9.447	0.5	3544
15002	9.877	0.5	3552

## Annual Report #2, NASA Grant NAG8-1605

15083	10.292	0.5	3560
15166	10.693	0.5	3568
15253	11.079	0.5	3576
15343	11.452	0.5	3584
15436	11.811	0.5	3592
15532	12.158	0.5	3600
15630	12.488	0.5	3608
15732	12.806	0.5	3616
15836	13.109	0.5	3624
15941	13.398	0.5	3632
16050	13.676	0.5	3640
16161	13.941	0.5	3648
16272	14.19	0.5	3656
16387	14.43	0.5	3664
16504	14.659	0.5	3672
16621	14.874	0.5	3680
16742	15.081	0.5	3688
16863	15.276	0.5	3696
16985	15.461	0.5	3704
17110	15.637	0.5	3712
17237	15.806	0.5	3720
17363	15.963	0.5	3728
17491	16.112	0.5	3736
17622	16.255	0.5	3744
17752	16.388	0.5	3752
17884	16.514	0.5	3760
18015	16.632	0.5	3768
18148	16.743	0.5	3776
18283	16.85	0.5	3784
18418	16.948	0.5	3792
18554	17.042	0.5	3800
18692	17.13	0.5	3808
18830	17.211	0.5	3816
18966	17.285	0.5	3824
19104	17.355	0.5	3832
19244	17.421	0.5	3840
19383	17.479	0.5	3848
19524	17.535	0.5	3856
19664	17.583	0.5	3864
19805	17.629	0.5	3872
19948	17.671	0.5	3880
20089	17.706	0.5	3888
20230	17.736	0.5	3896
20372	17.762	0.5	3904
20515	17.785	0.5	3912
20657	17.802	0.5	3920
20800	17.817	0.5	3928
20942	17.825	0.5	3936
21086	17.831	0.5	3944
21228	17.83	0.5	3952
21371	17.827	0.5	3960
21512	17.818	0.5	3968
21655	17.806	0.5	3976
21796	17.788	0.5	3984
21939	17.768	0.5	3992
22082	17.744	0.5	4000
22224	17.715	0.5	4008
22364	17.68	0.5	4016

# Annual Report #2, NASA Grant NAG8-1605

22505	17.642	0.5	4024
22647	17.601	0.5	4032
22788	17.554	0.5	4040
22929	17.504	0.5	4048
23068	17.448	0.5	4056
23206	17.387	0.5	4064
23347	17.324	0.5	4072
23483	17.253	0.5	4080
23623	17.181	0.5	4088
23758	17.101	0.5	4096
23897	17.019	0.5	4104
24030	16.929	0.5	4112
24168	16.837	0.5	4120
24299	16.736	0.5	4128
24435	16.633	0.5	4136
24566	16.521	0.5	4144
24700	16.407	0.5	4152
24829	16.284	0.5	4160
24958	16.156	0.5	4168
25088	16.023	0.5	4176
25215	15.882	0.5	4184
25343	15.736	0.5	4192
25469	15.581	0.5	4200
25551	13.1	0.5	4208
25678	13.0625	0.5	4216
25804	14.5625	0.5	4224
25928	15.625	0.955	4232
26081	17.3125	1.5	4240
26209	17.5625	1.5	4248
26317	14.75	1.5	4256
26393	11.5	1.5	4264
26452	8.4375	1.5	4272
26503	6.875	1.5	4280
26548	6	1.5	4288
26589	5.375	1.5	4296
26627	4.9375	1.5	4304
26663	4.625	1.5	4312
26685	3.625	1.5	4320
26693	1.875	1.5	4328
26693	0.5	1.5	4336
26693	0	1.5	4344
26695	0.125	1.5	4352
26703	0.625	1.5	4360
26706	0.6875	1.5	4368
26706	0.1875	1.5	4376
26706	0	1.5	4384
26710	0.25	1.48769	4392
26718	0.75	1.44321	4400
26720	0.625	1.39873	4408
26720	0.125	1.35425	4416
26721	0.0625	1.30977	4424
26723	0.1875	1.26529	4432
26730	0.5625	1.22081	4440
26744	1.3125	1.17633	4448
26752	1.375	1.13185	4456
26760	1	1.08737	4464
26767	0.9375	1.04289	4472
26777	1.0625	0.998409	4480

# Annual Report #2, NASA Grant NAG8-1605

26791	1.5	0.953929	4488
26810	2.0625	0.909449	4496
26836	2.8125	0.864969	4504
26869	3.6875	0.820489	4512
26910	4.625	0.776009	4520
26965	6	0.731529	4528
27014	6.5	0.687049	4536
27014	6.125	0.642569	4544
27017	0.375	0.598089	4552
27017	0	0.553609	4560
27017	0	0.509129	4568
27017	0	0.464649	4576
27017	0	0.420169	4584
27017	0	0.375689	4592
27017	0	0.331209	4600
27017	0	0.286729	4608
27017	0	0.242249	4616
27017	0	0.197769	4624
27017	0	0.153289	4632
27017	0	0.108809	4640
27017	0	0.0643286	4648
27017	0	0.0198486	4656
27017	0	0	4664
27017	0	0	4672
27017	0	0	4680
27017	0	0	4688
27017	0	0	4696
27017	0	0	4704
27017	0	0	4712
27017	0	0	4720
27017	0	0	4728
27017	0	0	4736
27017	0	0	4744
27017	0	0	4752
27017	0	0	4760
27017	0	0	4768
27017	0	0	4776
27017	0	0	4784
27017	0	0	4792
27017	0	0	4800
27017	0	0	4808
27017	0	0	4816
27017	0	0	4824
27017	0	0	4832
27017	0	0	4840
27017	0	0	4848
27017	0	0	4856
27017	0	0	4864
27017	0	0	4872
27017	0	0	4880
27017	0	0	4888
27017	0	0	4896
27017	0	0	4904
27017	0	0	4912
27017	0	0	4920
27017	0	0	4928
27017	0	0	4936
27017	0	0	4944

Annual Report #2, NASA Grant NAG8-1605

27017	0	0	4952
27017	0	0	4960
27017	0	0	4968
27017	0	0	4976
27017	0	0	4984
27017	0	0	4992
27017	0	0	5000
27017	0	0	5008
27017	0	0	5016
27017	0	0	5024
27017	0	0	5032
27017	0	0	5040
27017	0	0	5048
27017	0	0	5056
27017	0	0	5064
27017	0	0	5072
27017	0	0	5080
27017	0	0	5088
27017	0	0	5096
27017	0	0	5104
27017	0	0	5112
27017	0	0	5120
27017	0	0	5128
27017	0	0	5136
27017	0	0	5144
27017	0	0	5152
27017	0	0	5160
27017	0	0	5168
27017	0	0	5176
27017	0	0	5184
27017	0	0	5192
27017	0	0	5200
27017	0	0	5208
27017	0	0	5216
27017	0	0	5224
27017	0	0	5232
27017	0	0	5240
27017	0	0	5248
27017	0	0	5256
27017	0	0	5264
27017	0	0	5272
27017	0	0	5280
27017	0	0	5288
27017	0	0	5296
27017	0	0	5304
27017	0	0	5312
27017	0	0	5320
27017	0	0	5328
27017	0	0	5336
27017	0	0	5344
27017	0	0	5352
27017	0	0	5360
27017	0	0	5368
27017	0	0	5376
27017	0	0	5384
27017	0	0	5392
27017	0	0	5400
27017	0	0	5408

Annual Report #2, NASA Grant NAG8-1605

27017	0	0	5416
27017	0	0	5424
27017	0	0	5432
27017	0	0	5440
27017	0	0	5448
27017	0	0	5456
27017	0	0	5464
27017	0	0	5472
27017	0	0	5480
27017	0	0	5488
27017	0	0	5496
27017	0	0	5504
27017	0	0	5512
27017	0	0	5520
27017	0	0	5528
27017	0	0	5536
27017	0	0	5544
27017	0	0	5552
27017	0	0	5560
27017	0	0	5568
27017	0	0	5576
27017	0	0	5584
27017	0	0	5592
27017	0	0	5600
27017	0	0	5608
27017	0	0	5616
27017	0	0	5624
27017	0	0	5632
27017	0	0	5640
27017	0	0	5648
27017	0	0	5656
27017	0	0	5664
27017	0	0	5672
27017	0	0	5680
27017	0	0	5688
27017	0	0	5696
27017	0	0	5704
27017	0	0	5712
27017	0	0	5720
27017	0	0	5728
27017	0	0	5736
27017	0	0	5744
27017	0	0	5752
27017	0	0	5760
27017	0	0	5768
27017	0	0	5776
27017	0	0	5784
27017	0	0	5792
27017	0	0	5800
27017	0	0	5808
27017	0	0	5816
27017	0	0	5824
27017	0	0	5832
27017	0	0	5840
27017	0	0	5848
27017	0	0	5856
27017	0	0	5864
27017	0	0	5872

Annual Report #2, NASA Grant NAG8-1605

27017	0	0	5880
27017	0	0	5888
27017	0	0	5896
27017	0	0	5904
27017	0	0	5912
27017	0	0	5920
27017	0	0	5928
27017	0	0	5936
27017	0	0	5944
27017	0	0	5952
27017	0	0	5960
27017	0	0	5968
27017	0	0	5976
27017	0	0	5984
27017	0	0	5992
27017	0	0	6000
27017	0	0	6008
27017	0	0	6016
27017	0	0	6024
27017	0	0	6032
27017	0	0	6040
27017	0	0	6048
27017	0	0	6056
27017	0	0	6064
27017	0	0	6072
27017	0	0	6080
27017	0	0	6088
27017	0	0	6096
27017	0	0	6104
27017	0	0	6112
27017	0	0	6120
27017	0	0	6128
27017	0	0	6136
27017	0	0	6144
27017	0	0	6152
27017	0	0	6160
27017	0	0	6168
27017	0	0	6176
27017	0	0	6184
27017	0	0	6192
27017	0	0	6200
27017	0	0	6208
27017	0	0	6216
27017	0	0	6224
27017	0	0	6232
27017	0	0	6240
27017	0	0	6248
27017	0	0	6256
27017	0	0	6264
27017	0	0	6272
27017	0	0	6280
27017	0	0	6288
27017	0	0	6296
27017	0	0	6304
27017	0	0	6312
27017	0	0	6320
27017	0	0	6328
27017	0	0	6336

Annual Report #2, NASA Grant NAG8-1605

27017	0	0	6344
27017	0	0	6352
27017	0	0	6360
27017	0	0	6368
27017	0	0	6376
27017	0	0	6384
27017	0	0	6392
27017	0	0	6400
27017	0	0	6408
27017	0	0	6416
27017	0	0	6424
27017	0	0	6432
27017	0	0	6440
27017	0	0	6448
27017	0	0	6456
27017	0	0	6464
27017	0	0	6472
27017	0	0	6480
27017	0	0	6488
27017	0	0	6496
27017	0	0	6504
27017	0	0	6512
27017	0	0	6520
27017	0	0	6528
27017	0	0	6536
27017	0	0	6544
27017	0	0	6552
27017	0	0	6560
27017	0	0	6568
27017	0	0	6576
27017	0	0	6584
27017	0	0	6592
27017	0	0	6600
27017	0	0	6608
27017	0	0	6616
27017	0	0	6624
27017	0	0	6632
27017	0	0	6640
27017	0	0	6648
27017	0	0	6656
27017	0	0	6664
27017	0	0	6672
27017	0	0	6680
27017	0	0	6688
27017	0	0	6696
27017	0	0	6704
27017	0	0	6712
27017	0	0	6720
27017	0	0	6728
27017	0	0	6736
27017	0	0	6744
27017	0	0	6752
27017	0	0	6760
27017	0	0	6768
27017	0	0	6776
27017	0	0	6784
27017	0	0	6792
27017	0	0	6800

Annual Report #2, NASA Grant NAG8-1605

27017	0	0	6808
27017	0	0	6816
27017	0	0	6824
27017	0	0	6832
27017	0	0	6840
27017	0	0	6848
27017	0	0	6856
27017	0	0	6864
27017	0	0	6872
27017	0	0	6880
27017	0	0	6888
27017	0	0	6896
27017	0	0	6904
27017	0	0	6912
27017	0	0	6920
27017	0	0	6928
27017	0	0	6936
27017	0	0	6944
27017	0	0	6952
27017	0	0	6960
27017	0	0	6968
27017	0	0	6976
27017	0	0	6984
27017	0	0	6992
27017	0	0	7000
27017	0	0	7008
27017	0	0	7016
27017	0	0	7024
27017	0	0	7032
27017	0	0	7040
27017	0	0	7048
27017	0	0	7056
27017	0	0	7064
27017	0	0	7072
27017	0	0	7080
27017	0	0	7088
27017	0	0	7096
27017	0	0	7104
27017	0	0	7112
27017	0	0	7120
27017	0	0	7128
27017	0	0	7136
27017	0	0	7144
27017	0	0	7152
27017	0	0	7160
27017	0	0	7168
27017	0	0	7176
27017	0	0	7184
27017	0	0	7192
27017	0	0	7200

\*\*\*\*\* EOF \*\*\*\*\*

## REFERENCES

---

- <sup>1</sup> J.R. Sanmartin, M. Manuel-Martinez, and E. Ahedo, "Bare Wire Anodes for Electrodynamic Tethers." *J. of Propulsion and Power*, Vol. 9, No. 3, 353-360, 1993.
- <sup>2</sup> R.D. Estes, J.R. Sanmartin, and M. Martinez-Sanchez, "Performance of Bare-Tethers Systems Under Varying magnetic and Plasma Conditions." *J. of Spacecraft and Rockets*, Vol. 37, No. 2, 197-204, 2000.
- <sup>3</sup> Estes, R.D., E.C. Lorenzini, J.R. Sanmartin, M. Martinez-Sanchez and N.A. Savich, "New High-Current Tethers: A Viable Power Source for the Space Station?," Smithsonian Astrophysical Observatory, White Paper, December 1995.
- <sup>4</sup> L. Johnson, R.D. Estes, E. Lorenzini, M. Martinez-Sanchez and J. Sanmartin "Propulsive Small Expendable Deployer System Experiment." *J. of Spacecraft and Rockets*, Vol. 37, No. 2, 173-176, 2000.
- <sup>5</sup> E.C. Lorenzini et al., "The Propulsive Small Expendable Deployer System (ProSEDS)." SAO Annual Report#1 on NASA Grant NAG8-1605, September 2001.
- <sup>6</sup> J.Smith, NASA/MSFC, email communication, May 2001.
- <sup>7</sup> E.C. Lorenzini et al., "The Propulsive Small Expendable Deployer System (ProSEDS)." Annual Report #1 on NASA Grant NAG8-1605, September 2000.
- <sup>8</sup> J. Glaese, R. Issa and P. Lakshmanan, "Comparison of SEDS-I pre-flight simulations and flight data" Paper AIAA 93-4766, Procs of AIAA Space Programs and Technology Conference, Huntsville, AL September 1993.
- <sup>9</sup> J.R. Sanmartin, R.D. Estes, and E.C. Lorenzini, "Efficiency of Different Types of ED Tether Thrusters." Procs. of the STAIF-2001 Conference, Reno, Nevada, February 2001.